

American University in Cairo

AUC Knowledge Fountain

Theses and Dissertations

6-1-2016

Tailored-design of molecularly imprinted polymers with induced cavities of high conformational stability as new platforms for chemical sensing applications

Ghada ALTaher Selim

Follow this and additional works at: <https://fount.aucegypt.edu/etds>

Recommended Citation

APA Citation

Selim, G. (2016). *Tailored-design of molecularly imprinted polymers with induced cavities of high conformational stability as new platforms for chemical sensing applications* [Master's thesis, the American University in Cairo]. AUC Knowledge Fountain.

<https://fount.aucegypt.edu/etds/341>

MLA Citation

Selim, Ghada ALTaher. *Tailored-design of molecularly imprinted polymers with induced cavities of high conformational stability as new platforms for chemical sensing applications*. 2016. American University in Cairo, Master's thesis. *AUC Knowledge Fountain*.

<https://fount.aucegypt.edu/etds/341>

This Thesis is brought to you for free and open access by AUC Knowledge Fountain. It has been accepted for inclusion in Theses and Dissertations by an authorized administrator of AUC Knowledge Fountain. For more information, please contact mark.muehlhaeusler@aucegypt.edu.



School of Sciences and Engineering

Tailored-design of molecularly imprinted polymers with induced cavities of high conformational stability as new platforms for chemical sensing applications

A Thesis Submitted to

The Nanotechnology Master's Program

In partial fulfilment of the requirements for

The degree of

Master of Science

By:

Ghada ALTaher AbdELHamed

Under the supervision of:

Prof. Tarek M. Madkour (Supervisor)

Professor of Polymer Chemistry

Department of Chemistry, The American University in Cairo

April 19, 2016

Acknowledgements

I have to admit that I would have never been able to go through this long journey without the support, encouragement and prayers of my beloved Father *ALTaher AbdELHamed* and my dear *Mother*. Even when I tried to quit, they supported me and pushed me to proceed whatever it takes. Also, I have to thank my brothers, especially *Mohamed* and *Eslam* for always being there whenever I needed them.

I am really grateful to Dr.*Tarek Madkour*, my Supervisor. Thank you for your kind support and assistance. Thank you for your love of chemistry that was inspirational to me. Thank you for respecting my working conditions, and helping me to move on. Thank you for never hesitating to work late with all of us even till very late hours after your long teaching day.

I highly appreciate the mentorship and guidance of Dr.*Nageh Allam* throughout all the nanotechnology courses that I have attended with him. Thank you for the support with your scientific and expert advices. Thank you for the different science perspectives that I learnt from your classes.

Special thanks and gratitude to Dr.*Wael Mamdouh* for his support and teachings during the nanotechnology courses and seminar. Thank you for the real life experiences that you always shared with us. Thank you for facilitating for me the use of certain equipment in your laboratory that were really essential in my experiments.

I am very grateful to Dr.*Adham Ramadan* for his fast response and kind support when we needed his assistance in an important aspect of my work. Also thank you for the nanochemistry classes that were a foundation to all our following courses.

I highly appreciate Dr.*Nahed Yacoub's* decency and assistance with the BET work.

I owe multitude of thanks to Mr.Mahmoud Moez, Mr.Ahmed Omia, Mr.Emad Raafat and Mr.Samir Nabhan. Thank you all for your assistance. Thank you Mr.Mahmoud for your aid with all the equipment and for the precious talks I had with a highly cultured and qualified chemist. Thank you Mr.Ahmed Omia for your dedication and support to me and all the students from the different departments. The chemistry department is blessed to have a decent person like you.

Also many thanks to the junior chemists AbdELAziz and Ahmed.

Great thanks to the STRC engineers, Asmaa, Ahmed Ghazaly, Eng.Ahmed Nour, and Eng.Ahmed Beltagy for their professional assistance and friendly attitudes.

My dear friends and sources of strength and inspiration, *Sara Omar*, *Ranim*, and *Ayat*. Thank you for your precious support in all the issues I faced. Thank you for giving me from your time to teach me a lot of things. Thank you for considering the sake of my work as if it was yours. Thank you for your angelic souls.

I was blessed to have my lab colleagues, Ahmed Hamdy, Worod, Salma, Samar, and Samia. Thank you Ahmed for your brotherhood and support to all the lab. Thank you Worod for helping me when I was stuck in my work at different occasions. Your advices saved me a lot of time.

Also multitude of thanks to *James, Peter Morcos, Ruaa, Nada, Raghda, and Nuha Ghuneimi* for helping me whenever I needed them.

Abstract

Molecularly imprinted polymers (MIP) are highly promising materials that have many applications in different fields such as chromatography, catalysis, chemical and biochemical sensing, or even drug delivery. These materials can be tailored to contain intrinsic nano scaled cavities within their structure. These cavities are highly interesting, because they can be made selective for an intended template.

Thus, MIP are deeply researched to replace proteins in sensing applications. Proteins are highly delicate and labile to slight changes in the surrounding media, however MIP are polymer based. Therefore, they are easy to handle and mechanically more stable. In addition, they are much cheaper. Still MIP are not fully ready to replace proteins, because their selectivities are usually lower than that of proteins.

The current study aims at controlling the physical and chemical properties of the cavities within MIP. Cavities in MIP are the template binding sites, which are the main determinants of the performance of MIP. Two parameters were selected to be studied and to reflect MIP performance; conformational stability and the binding capacity of the cavities. Conformational stability to the best of our Knowledge has never been studied in MIP. This feature was intended to be studied, in order to get information about the ability of different MIP systems to keep the conformational shape and specificity of their nanoscaled cavities.

The study began first by a theoretical investigation of a library of monomers using computational modeling, and then was followed by a practical investigation. The theoretical investigation screened a library of monomers, and the best scoring two monomers with regards to conformational stability and binding energy were selected for practical investigation.

The practical investigations aimed at validating the correlation between the theoretical performance of the selected candidates, and the practical performance of their MIP in a media containing the selected template, through measuring the MIP's binding capacities.

The study could show the significant importance of assessing the conformational stabilities of the MIP building blocks (monomers), and that they directly affected the binding capacities of the studied MIP. Thus it can be suggested that research should not only focus

on assessing the binding capacities of MIP, but also special focus should be given to studying the conformational stability of the binding sites.

Table of contents

Acknowledgements	II
Abstract.....	IV
List of abbreviations	VIII
List of tables.....	XI
List of schemes.....	1
1. Introduction:	3
1.1. Types of Imprinting:.....	4
1.1.1. Covalent imprinting	4
1.1.2. Non-covalent imprinting	4
2. Literature review	7
2.1. Stages of MIP formation	7
2.1.1. Preorganiston (Pre-polymerization)	7
2.1.2. Crosslinking	7
2.1.3. Initiation of polymerization.....	7
2.1.4. Extraction of the template	8
2.2. Factors affecting the performance of MIPs.....	9
2.2.1. Role of monomers	9
2.2.2. Role of crosslinkers.....	11
2.2.3. Role of solvent	12
2.3. Molecularly imprinted polymers (MIP) for glucose.....	14
2.4. Monomer selection strategies.....	15
2.4.1. Spectroscopy based selection.....	15
2.4.2. Combinatorial approaches.....	16
2.4.3. Chemometrics	18
2.4.4. Computational simulation investigation.....	18
2.4.4.1. Virtual screening of a library of monomers	20
2.4.4.2. Simulation of the pre-polymerization mixture.....	20
2.4.4.3. Simulation of a modeled molecular imprinting process	22
2.4.4.4. Conformational analysis	24
3. Materials & methods	28
3.1. Computational investigations	28
3.1.1. Primary screening	29
3.1.1.1. Conformational analysis	29

3.1.1.2. Molecular dynamics MD	31
3.1.2. Secondary analyses	31
3.1.2.1. Conformational analysis	32
3.1.2.2. Molecular dynamics MD	32
3.2. Experimental procedures	33
3.2.1. Chemicals and reagents	33
3.2.2. Synthesis of polymers	33
3.2.3. Template rebinding studies	35
3.2.3.1. Construction of calibration curves	35
3.2.3.2. Template rebinding studies at room temperature	36
3.2.3.3. Template rebinding studies at 50°C	36
3.2.4. Characterization	37
3.2.4.1. Fourier Transform Infra-Red Spectroscopy (FT-IR)	37
3.2.3.2. Scanning Electron Microscopy (SEM)	37
3.2.3.3. Thermogravimetric analysis (TGA)	38
3.2.3.4. Porosity analysis (BET)	38
4. Results and discussion	40
4.1. Computational investigation	40
4.1.1. Primary screening:	40
4.1.1.1. Conformational analysis	40
4.1.1.2. Molecular dynamics MD	46
4.1.2. The selection of best four candidates	48
4.1.3. Secondary analyses	50
4.2. Experimental investigation	51
4.2.1. Template rebinding studies	51
4.2.1.1. Template rebinding studies at room temperature	51
4.2.1.2. Template rebinding studies at 50°C	53
4.2.1.3. Template rebinding studies at room temperature for MIPs 3,4,5	57
4.2.2. Fourier Transform Infra-Red Spectroscopy (FT-IR)	59
4.2.2.1. AA based polymers (MIP 1, NIP 1, P 1)	59
4.2.2.2. AMPSA based polymers (MIP 2, NIP 2, P 2)	59
4.2.2.3. BHPEA based polymers (MIP 3, NIP 3, P 3 before template extraction)	60
4.2.3. Scanning Electron Microscopy (SEM)	64
4.2.3.1. SEM of MIPs 1,2,3 and NIPs 1,2,3	64
4.2.3.2. SEM of MIPs 3,4,5 and NIPs 3,4,5	64
4.2.4. Thermogravimetric Analysis (TGA)	67
4.2.5. BET porosity analysis	70
5. Conclusion and future outlook	80
5.1. Conclusion	80
5.2. Future outlook	81
6. References	83

List of abbreviations

2-HEMA: 2-Hydroxyethylmethacrylate
4-VP: 4-vinylpyridine
AA: Acrylic acid
AAm: Acrylamide
AMPSA: Acrylamido-2-methyl-1-propanesulfonic acid
APMA-HCl: N-(3-aminopropyl) methacrylamide hydrochloride
BHPEA: 2-(4-Benzoyl-3-hydroxyphenoxy)ethyl acrylate
CE: Cohesive energy
DDI: Distilled deionized water
DEAEM: N,N- Diethylaminoethylmethacrylate
DFT: Density functional theory
DMSO: Dimethyl sulfoxide
DVB: Divinyl benzene
EGMP: Ethyleneglycol methacrylate phosphate
EGDMA: Ethyleneglycoldimethacrylate
FT-IR: Fourier Transform Infra-Red Spectroscopy
IF: Imprinting factor
MAA: Methacrylic acid
MAH-Cu(II): Methacrylamidohistidine copper
MBAA: N,N'-methylene bisacrylamide
MD: Molecular dynamics
MIP: Molecularly imprinted polymer
NIP: Non imprinted polymer
NMR: Nuclear magnetic resonance
PEGDMA: polyethylene glycol dimethacrylate
<r>: End to end distance
RDF: Radial Distribution Function
Rg: Radius of gyration
RT: Room temperature
SEM: Scanning Electron Microscopy
T_B: Boltzmann temperature
TEGDMA: Triethylene glycol dimethacrylate
TGA: Thermogravimetric analysis
THF: Tetrahydrofuran
T_{onset} : Onset decomposition temperature
TRIM: Trimethyloxypropanetrimethacrylate
UV: Ultraviolet

List of figures

Figure 1.1 A Schematic representation showing the steps of molecular imprinting; monomer-template interaction, crosslinking, then initiation of polymerization, and finally template removal [1].	3
Figure 1.2 Schematic representation of the types of imprinting. Non-covalent imprinting (top) and covalent imprinting (bottom) [3].	5
Figure 2.1 Schematic representation of glucose template chelated to methacryloylamidohistidine–Cu(II) monomer [8].	10
Figure 2.2 The relationship between imprinting factors (IF) and dielectric constants of the solvents; acetonitrile (37.5), acetone (20.7), THF (7.58), Dioxane (2.25) [18].	13
Figure 2.3 Chemical structure of glucose.	14
Figure 2.4 The binding percentage of MIP1, MIP2 and MIP3 for abcavir (template) in water and different buffers [36].	21
Figure 2.5 Schematic representation of the modeling stages.	23
A: Pre-polymerization mixture (functional monomer (red circle), template (rod), crosslinker (blue circle))	23
B: Intact cavities formed from the monomers and crosslinkers, after the removal of the template.	23
C: Rebinding of a structurally related analogue (rod) [34].	23
Figure 2.6 Chemical structures of pyrimidine and pyrazine.	23
Figure 2.7 A polymer constituting a spherical space with R representing its end to end distance.	26
Figure 2.8 A polymer constituting a spherical space with R _g representing its radius of gyration.	26
Figure 3.1 A cubic amorphous cell containing acrylic acid monomers interacting with glucose. Dashed lines signify the intermolecular interactions.	31
Figure 3.2A Chemical structures of the selected monomers, Acrylic acid, Acrylamido-2-methyl-1-propanesulfonic acid, and 2-(4-Benzoyl-3-hydroxyphenoxy)ethyl acrylate respectively.	35
3.2B Chemical structure of the crosslinker EGDMA.	35
3.2C Chemical structure of glucose.	35
Figure 3.3 The constructed calibration curve for the stock solutions using DDI	37
Figure 4.1 A graphical representation of the calculated $\langle s \rangle$ and $\langle r \rangle$ in Å ⁰ at T=45,000K for polymers 1 to 29.	45
Figure 4.2a Atomistic structure of polymer 29 with the calculated $\langle r \rangle = 34.35 \text{ Å}^0$ at 45,000 K.	45
Figure 4.2b Atomistic structure of polymer 25 with the calculated $\langle r \rangle = 27.45 \text{ Å}^0$ at 45,000 K.	45
Figures 4.3 The strategy of selection of the four monomers for secondary analysis.	49
4.3a Cohesive energy values for polymers 1. To 30.	49
4.3b T _B values for polymers without the presence of aromatic rings.	49
4.3c T _B values for polymers bearing aromatic rings.	49
Figure 4.4 Graphical representation of the amount of glucose bound mg/gm for the polymers	52
Figure 4.5 Specific H-bond interactions (Red) between glucose and the monomeric units inside the cavities of MIP 2.	53
Non-specific H-bond interactions (Red) between glucose and the monomeric units outside the cavities of MIP 2.	53
Figure 4.6 The amount of glucose bound by each MIP at Room temperature and 50°C respectively.	55
Figure 4.7 A schematic representation of MIP 1 cavity showing H-bond (Red) interactions.	55
Figure 4.8 A schematic representation of MIP 3 cavity showing H-bond (Red) and hydrophobic ring-ring interactions (Brown).	56
Figure 4.9 Schematic representation of crosslinked networks of MIPs 1, 2, 3.	56
Figure 4.10 The amount of glucose bound for MIPs 3, 4, 5 at RT.	58
Figure 4.11A Loose polymeric network at low crosslinking density.	58

4.11B Compact polymeric network at high crosslinking density	58
Figure 4.12 FT-IR charts of P 1, MIP 1, and NIP 1.	61
Figure 4.13 FT-IR charts of P 2, MIP 2, and NIP 2.	62
Figure 4.14 FT-IR charts of P 3, MIP 3, and NIP 3.	63
Figure 4.15 SEM micrographs at 22,000 magnifications.	65
Figure 4.16 SEM micrographs at 48,000 magnifications.	66
Figure 4.17 TGA thermograms of MIP 1 and NIP 1.	68
Figure 4.18 TGA thermograms of MIP 2 and NIP 2.	68
Figure 4.19 TGA thermograms of MIP 3 and NIP 3.	69
Figure 4.20 TGA thermograms of MIP 1, MIP 2 and MIP 3.	69
Figure 4.21 Linear isotherm plot of MIP 1.	72
Figure 4.22 Linear isotherm plot of NIP 1.	72
Figure 4.23 Linear isotherm plot of MIP 2.	73
Figure 4.24 Linear isotherm plot of NIP 2.	73
Figure 4.25 Linear isotherm plot of MIP 3.	74
Figure 4.26 Linear isotherm plot of NIP 3.	74
Figure 4.27 BJH Desorption pore distribution plot of MIP 1.	75
Figure 4.28 BJH Desorption pore distribution plot of NIP 1.	75
Figure 4.29 BJH Desorption pore distribution plot of MIP 2.	76
Figure 4.30 BJH Desorption pore distribution plot of NIP 2.	76
Figure 4.31 BJH Desorption pore distribution plot of MIP 3.	77
Figure 4.32 BJH Desorption pore distribution plot of NIP 3.	77
Figure 4.33 BJH desorption pore diameter volume distribution for MIP 1(aqua), NIP 1(orange), MIP 2(green), NIP 2(purple), MIP 3(blue), NIP 3(red).	78
Figures 5.1 AA micro particles at low and high magnifications respectively.	82
Figures 5.2 BHPEA micro particles at low and high magnifications respectively.	82

List of tables

Table 2.1 The chemical structures of the common monomers used in molecular imprinting.....	17
Table 3.1 Molecular representations of the thirty investigated monomers.....	30
Table 3.2 The compositions of the synthesized polymers.....	34
Table 4.1 The simulated values for the $\langle s \rangle$ and $\langle r \rangle$ for the modeled polymers (polymers 1 To 29 at 45,000 K, while polymer 30. T 200,000 K).....	44
Table 4.2 The calculated cohesive energies CE of the modeled ensembles containing a mixture of monomer units and the template molecule.....	47
Table 4.3 The new calculated values of $\langle s \rangle$, $\langle r \rangle$ and CE for the five selected monomers.....	50
Table 4.4 The onset decomposition temperature T_{onset} for the polymers.....	67
Table 4.5 The BET surface areas, BJH adsorption and desorption pore volumes and areas for the polymers.....	71

List of schemes

Scheme 3.1 A flow chart showing the stages of the employed computational investigations..28

Scheme 4.1 The atomistic structures of the twenty monomers used to build their modeled polymers whose respective T_B values ranged from 1200 K to 5000 K.....41

Scheme 4.2 The atomistic structures of the ten monomers used to build their modeled polymers whose respective T_B values ranged from 1200 K to 5000 K.....42

Chapter 1

General Introduction

1. Introduction:

Nature has been always a source of inspiration for developing current and new technologies. The immune system has two main role players; antigens and antibodies. Our bodies are full of numerous types of antigens. Each antigen recognizes a specific antibody by means of complimentary interactions. Research on how antigens recognize antibodies found that antigens are proteins with molecular architectures that act as recognitive sites for binding to the antibodies. The binding takes place by means of complimentary interactions between functional groups on both the antigen and the antibody.

The technology of "*MolecularImprinting*" is based on the same concept. Molecular imprinting is a recent approach that has been researched in polymeric scaffolds in the last few decades. Polymers are long chains of repeating units of monomers, in which the monomers bind together covalently to form polymers.

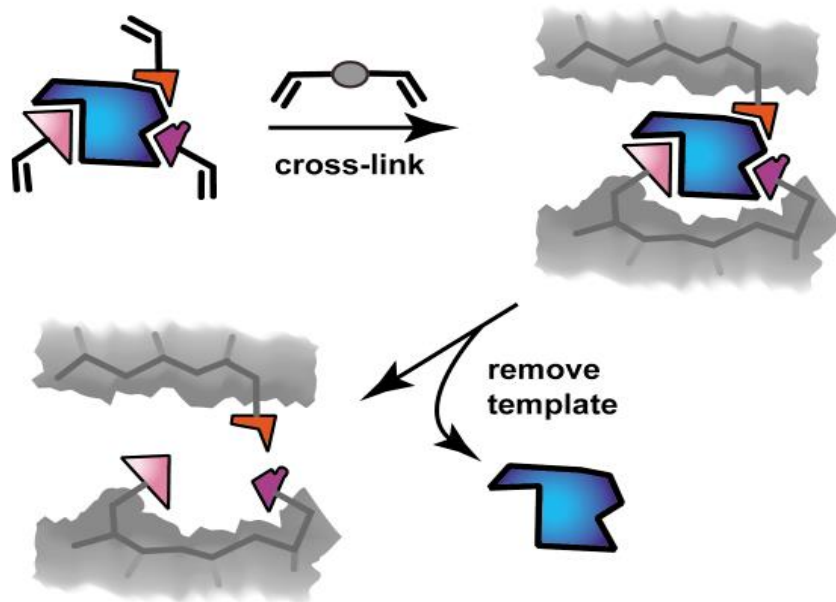


Figure 1.1 A Schematic representation showing the steps of molecular imprinting; monomer-template interaction, crosslinking, then initiation of polymerization, and finally template removal [1].

MIP are formed when monomers are allowed to complex or interact with a template (here the template resembles the antibody) in the pre-polymerization mixture, then crosslinkers are added, followed by the initiation of polymerization. Monomers polymerize forming polymeric chains around the template. Finally the template is removed leaving a cavity within the MIP (here the MIP resembles the antigen). The cavity is structurally complimentary to the template and can selectively recognize it, **Figure 1.1** [1]. Molecular imprinting is currently a hot area of research because it was postulated that the template presence alters the kinetics of polymerization and alters the structure of the final polymeric network [2].

1.1. Types of imprinting:

There are two types of molecular imprinting:

1.1.1. Covalent imprinting

Covalent imprinting is an approach of imprinting in which the monomers interact by means of covalent bonds with the template, **Figure 1.2**. This approach results in very strong complexes between the monomers and the template, and consequently very stable cavities that are homogeneously distributed across the polymer chains to a relatively good extent. However, template removal in this approach is very difficult and requires harsh conditions because of the strong nature of the bonds between the monomers and the template. Such harsh conditions are highly detrimental to the binding sites. In addition, the types of templates that can interact covalently with the monomers are not very common.

1.1.2. Non-covalent imprinting

In this approach, monomers and the template bind non-covalently or by self-assembly (i.e by Vander Waals interactions, Hydrogen bonds, ionic bonds, hydrophobic interactions, etc), **Figure 1.2**. These types of interactions are much weaker than covalent interactions and thus they produce weaker complexes than those produced in covalent imprinting, consequently less homogeneity of the binding sites. However, template removal is much easier. The approach can be employed to a wide range of monomers and templates because of the diverse

nature of the types of non-covalent interactions that can be applied [1]. Although this is an important asset in non-covalent imprinting, a lot of work needs to be done in order to establish a basic understanding of which types mainly govern the interactions in a binding pocket.

It is very interesting and essential to emphasize that non-covalent interactions are the driving forces of recognition in natural receptors. They control the nature of the interactions and recognitions in the body's complex systems such as DNA, proteins, and carbohydrates. Recognition in these systems is mainly based on the harmonization of more than one type of non-covalent interaction. Thus, these types of interactions are highly promising in developing stable molecular imprinting systems that could mimic the body's biorecognition systems.

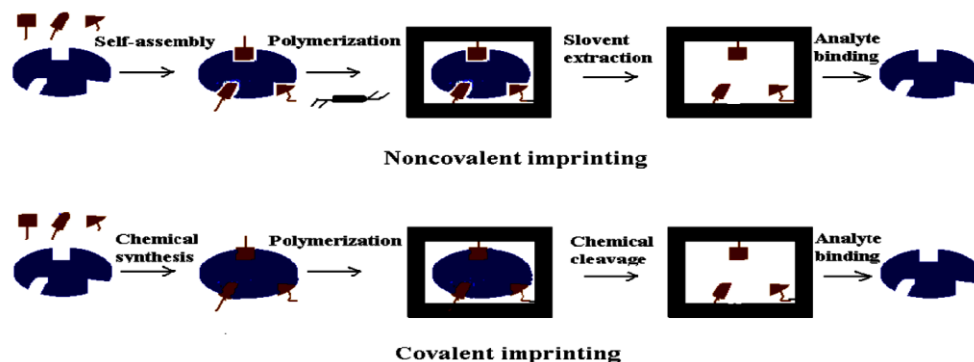


Figure 1.2 Schematic representation of the types of imprinting. Non-covalent imprinting (top) and covalent imprinting (bottom) [3].

The non-covalent approach proved to be successful and widely applicable to many types of templates. The main focus of this thesis will be the non-covalent approach and how to increase the understanding of the nature and the stability of the complexes formed in the pre-polymerization mixture in molecular imprinting systems.

The current study has an important and new objective, which is to investigate the conformational stability of the MIP building blocks (monomers). The study will be considering the influence of this novel feature on a commonly theoretically studied feature in MIP systems (which is cohesive energy), and its final projection on the actual performance of MIP systems.

Chapter 2

Literature Review

2. Literature review

2.1. Stages of MIP formation

2.1.1. Preorganization (Pre-polymerization)

This is the initial stage where complexation between the monomer and the template takes place. It is a very important stage because the strength of complexation would determine the stability of the resulting binding sites. Extremely strong complexations (like in covalent bonds) are not favorable, because template extraction by simple hydrolysis would not be feasible. When molecular imprinting is based on non-covalent interactions, it is advisable to increase the strength of complexation, by means of relying on the interactions between many functionalities on the monomer and their complimentary ones on the template.

The preorganization stage could be sometimes enhanced if employed at low temperatures (by immersion in cold baths for example), because H-bonds are highly stabilized at low temperatures. However, good care should be taken because the monomers or solvent could be unstable at low temperatures.

2.1.2. Crosslinking

Addition of the crosslinker would incur high stability to the resulting MIP, because it serves to fix the complexes formed in place in a porous network. Crosslinkers are used in high concentrations exceeding 70%, which usually has the disadvantage of making more than 60%-80% of the synthesized cavities inaccessible to the template because of the rigid network. This shortcoming could be alleviated by using tri- or tetra- functional crosslinkers, or by using crosslinkers that have functionalities that could interact with the template [4]. However, the latter solution would increase template binding by non-specific interactions.

2.1.3. Initiation of polymerization

Polymerization is initiated thermally (usually at 60°C to 70°C) by the addition of the initiator. The polymerizations result in a bulk polymer block, that require downsizing into small

suitable sized polymer particles. It should be noted that the downsizing process, by grinding or cutting for example, partially destroys partially many binding sites and thus decreases the binding capacity.

2.1.4. Extraction of the template

This is a tedious and time consuming process, because template should be extracted efficiently to avoid any false results when using the resulting MIP in any intended application, especially for analytical purposes. Ideally, the washing system should apply a solvent that could disrupt passively the interactions taking place in the binding site, at the same time the process should allow fast diffusion of the template out of the MIP [5] (for example using high temperature, microwaves, soxhlet apparatuses or even strong shaking).

Unfortunately, the extraction process is a destructive process to many of the binding sites because of the nature of the organic solvents used, and/or the longevity of the extraction process. Both either alter the functionality of the MIP cavities or cause them to collapse. Simple batch extractions have been commonly reported. Also, soxhlet extraction have been widely employed as a common mode of extraction. Another sophisticated modes of extractions have also been reported such as microwave assisted extraction and supercritical fluid assisted extractions [6]. Both have resulted in faster extractions and better results regarding the maintenance of the MIP structure and integrity, but they require specific expensive equipment, and qualified labor [6].

A common problem associated with MIP when used in their intended application is template bleeding. Template bleeding is the leaching of residual templates within the MIP during their use in an intended application. Template bleeding occurs because usually the template is not 100% extracted from the MIP during the extraction process, owing to the highly crosslinked networks created that impede the flow of templates out of the MIP from the deep binding sites inside the MIP. Common strategies employ the use of solvents where the polymers can swell well, usually they are the solvents, which were used initially during the synthesis process. For example, chlorinated solvents are good solvents for methacrylates and methylmethacrylates [5]. Also, acids and bases could be used to disrupt the electrostatic interactions between the template and the monomer within the MIP. The extraction process is a benefit risk process,

because different modes of extractions could guarantee better template removals, but at the same time there could be a risk of compromising the recognition abilities of the MIP according to the type of extraction used.

2.2. Factors affecting the performance of MIPs

There are many contributors in the molecular imprinting process; template, monomers, crosslinkers, solvents, and initiators. An ideal MIP network should be structurally rigid to maintain the structures of the synthesized nanoscaled cavities and also should be flexible enough to allow the facile diffusion of the template through the network to its complimentary binding site. In fact, the two aforementioned features contradict each other [7], and that's why optimization of the molecular imprinting process is a hard and time consuming process.

Optimization of the performance of MIPs can be attained through controlling and optimizing the different contributors involved in the molecular imprinting process.

2.2.1. Role of monomers

Monomers and crosslinkers are the building blocks of the MIP network with the monomers being responsible for binding with the template. Thus careful selection of the monomers is very essential in non-covalent imprinting. A monomer should possess functional groups that are capable of binding with other functional groups on the template. They should be complimentary to each other. For example, a H-bond donor on the monomer and a H-bond acceptor on the template [7], or a metal chelating agent and a chelator on either the monomer or the template. A study [8] synthesized the methacrylamidohistidine copper (MAH-Cu(II)) monomer in order to make use of its ability to chelate to the hydroxyl groups on the glucose template, **Figure 2.1** [8]. The study showed that the MIP synthesized using this monomer had a high binding capacity and showed higher binding affinity than a naturally existing glucose binding protein known as concanavalin A.

Non-covalent imprinting is not stoichiometrically driven as in covalent imprinting. However, it is driven by Le Chatelier principle [7], meaning that high concentrations of the monomers

with respect to the template should be used to direct the reaction towards the formation of more and more complexes in the pre-polymerization mixture and consequently more binding sites. The optimum concentration ratios of the monomer to that of the template differ from one MIP system to another. For example 2,4-dichlorophenoxyacetic acid (Herbicide) was imprinted non-covalently using 4-vinylpyridine (4-VP) as the monomer and ethyleneglycoldimethacrylate (EGDMA) as the crosslinking agent [9].

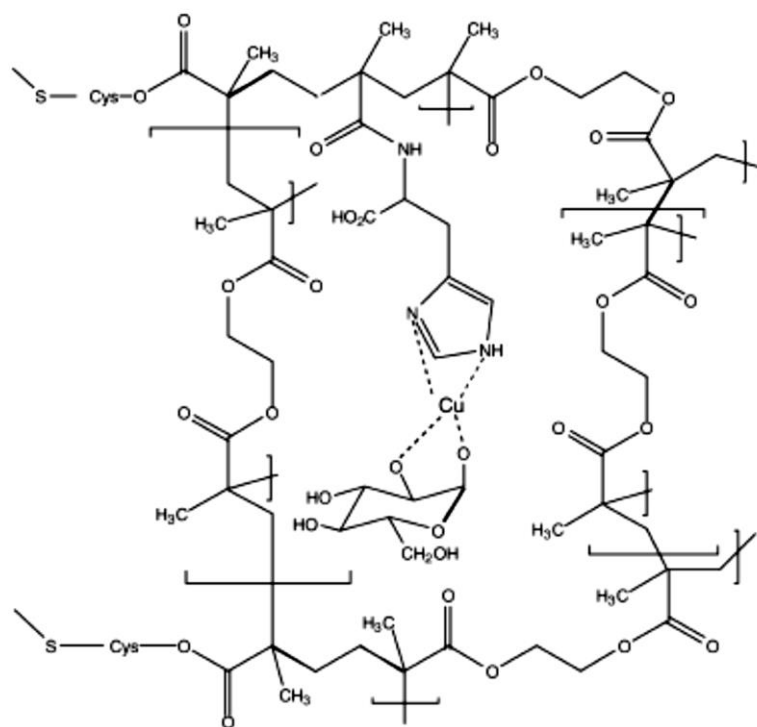


Figure 2.1 Schematic representation of glucose template chelated to methacryloylamidohistidine–Cu(II) monomer [8].

The study [9] investigated the performance of three different MIPs with three different ratios of template to monomer 1:1, 1:2, 1:4. All the MIPs showed good selectivity to the template over other structural analogues, but the 1:4 MIP showed the highest selectivity to the template, showing that an excess of monomers with respect to the template is essential for optimum binding capacities.

However, excess monomers could pose risks of monomer associations that compromise the quality of the created binding sites. This drawback could be tackled by using more than one type of monomer, and reactivity ratios should be taken into account. Ideally, reactivity ratios should be considered even when using one type of monomer (in relation to that of the

crosslinker) because of the alteration of the electronic states of the monomer together with the steric effects caused by the complexation with the template [4]. Acrylates and methacrylates are the most commonly used monomers because of their functional group that can interact non-covalently with a wide range of templates. Methacrylic acid (MAA), for example, can interact by ionic or H-bond interactions. It interacts with amides and carboxylates via H-bonds, and with amines via ionic interactions [10].

2.2.2. Role of crosslinkers

Crosslinkers serve to stabilize the structure of the cavities, and to build the mechanical integrity of the whole MIP. Usually they are used in high percentages up to 80 % of the whole MIP network in order to effectively stabilize it. Ideally the reactivity ratio of the crosslinker should be in coherence with that of the monomer, and depending on the designed MIP system, it should or should not interact with the template. The most commonly used crosslinker is EGDMA [4] because of its straightforward polymerization with free radical polymerization, in addition to its well established success in the production of rigid networks. Also, divinyl benzene is a commonly used hydrophobic crosslinker in styrene-based MIP [11].

Crosslinkers play an important role in controlling the physical properties of the resulting MIP. Crosslinkers control whether the resulting MIP is macroporous, gel, or microporous. For example, a study [12] used a common protocol to synthesize two dopamine MIP systems using EGDMA as the crosslinker in one system and N,N'-methylene bisacrylamide (MBAA) as the crosslinker in the second one. The study concluded that the pore volumes and specific surface areas for both systems were significantly different, with the MBAA MIP system having larger values. Also, the study [12] concluded that under the conditions of the studied protocol, MBAA MIP system possessed higher flexibility and consequently better binding to dopamine compared to the highly rigid EGDMA MIP system. The crosslinker's chain length/number of units could also alter the morphology and behavior of the resulting MIP. A study [13] prepared two MIP systems based on EGDMA in one system and triethylene glycol dimethacrylate (TEGDMA) in the second system. Both crosslinkers are known to produce rigid MIPs, but TEGDMA produces much more rigid MIPs owing to its trifunctionality. This was reflected in the study [13] by concluding that EGDMA MIPs have higher binding capacities to the template compared to TEGDMA MIPs.

2.2.3. Role of solvent

Solvents serve to solubilize the templates and the monomers, and serve to bring them together in the pre-polymerization mixture. Also, they control the resulting swellability and porosity of the produced MIP [14]. They are commonly referred to as porogens because they are responsible for the production of porous morphologies within the MIP. Usually as the volume of the porogen used increases, the size distribution of the pores also increases. The pores act as channels through which the template diffuse inside the MIP.

Therefore it can be possibly postulated that highly porous MIP are highly performing ones. Pores are formed within MIP due to the phase separation of the porogens from the network during polymer synthesis. A study [15] reported a mechanism for pore formation in crosslinked polymers using trimethylolpropanetriacrylate TRIM. The study reported that using good solvents led to the formation of a homogeneous network of intermolecular crosslinks. Swollen gel particles phase separate and then form grains by coagulation. Such grains build up the porous network. However poor solvents cause early phase separation of crosslinked microspheres, which aggregate forming the porous network. An interesting study [16] compared the effect of addition of linear polymer porogens to two different porogenic solvents (diglyme vs. toluene) on the porosity and consequently the performance of the synthesized MIP. The diglyme system produced MIP with higher porosity and better binding. This was attributed to diglyme being a low volatility solvent and to the linear polymers that acted to thermodynamically enhance the driving force for phase separation. This resulted in balancing the rate of the latter process (normally slower) with the rate of polymerization in these MIP, in order to avoid early domain coarsening [16]. A porogen should stabilize the non-covalent interactions, that's why apolar non protic solvents (as toluene) are good candidates [3]. However, many have reported sufficiently stable non-covalent interactions between the monomers and the template in polar solvents e.g methanol/water mixtures [12,9]. The latter finding was used by a study [17] to investigate the solvency effect of different solvents on the morphology and porous structure of the resulting MIP. The study reported that methanol:water (non-porogenic) produced larger macropores and lower BET surface areas due to the solvation of the growing microparticle clusters with resulting irregular voids in between. On the other hand acetonitrile (porogenic) produced smaller macropores and larger

BET surface areas due to being a poorly solvating medium that caused the formation of a more regular channel network.

It is not only the type of the solvent used that influence MIP behavior, but also the amount of solvent used. A study [18] prepared quercetin MIP using four solvents of differing polarities; 1,4-dioxane<tetrahydrofuran THF<acetone<acetonitrile with increasing dielectric constants. The study showed that the moderately polar THF provided the optimum stabilization of the quercetin within the polymer network as shown in **Figure 2.2**, where THF had the highest imprinting factor (IF= amount of template bound to the MIP/amount of template bound to the NIP) compared to the other solvents. Higher polarity solvents interfered with such stabilization by competing with the interactions between the monomer and the template. The study also investigated the effects of the amount of THF on the MIP behavior. At certain amounts of monomer, template and crosslinker, there is an optimum amount of porogen that produces the optimum MIP. Higher amounts causes extra dilution of the system resulting in poor binding sites, and lower amounts cause early precipitation of the polymer without adequately creating the binding cavities [18].

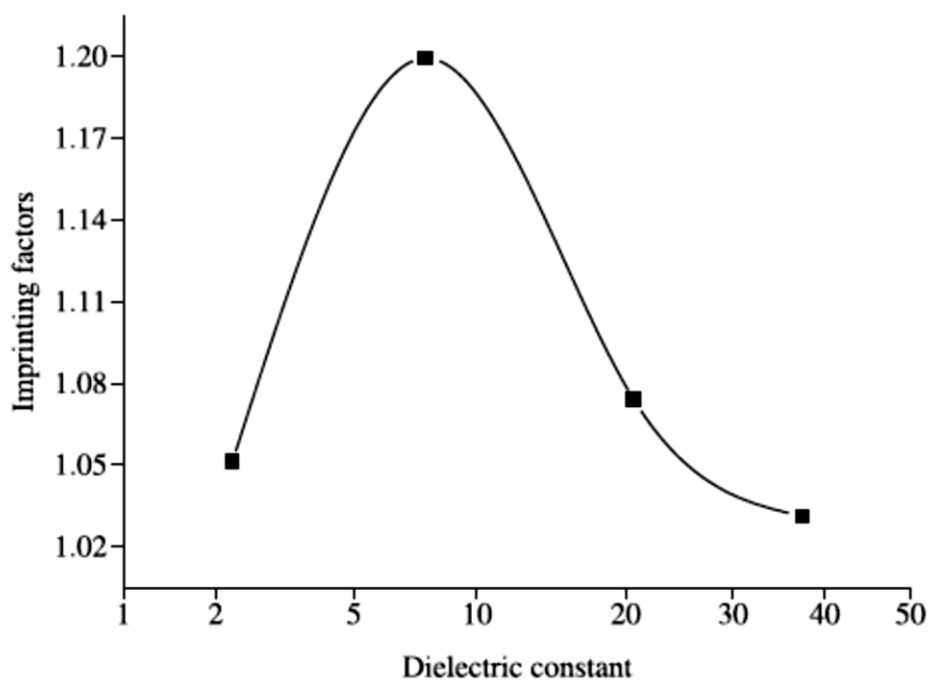


Figure 2.2 The relationship between IF and dielectric constants of the solvents; acetonitrile (37.5), acetone (20.7), THF (7.58), Dioxane (2.25) [18].

2.3. Molecularly imprinted polymers (MIP) for glucose

In this thesis, D-glucose **Figure 2.3** was selected to be the role model template to investigate our proposed hypothesis. Glucose has an average size relative to the templates that were reported in the literature to be used in molecular imprinting, and also because of its ability to interact non-covalently with various monomers [19,20].

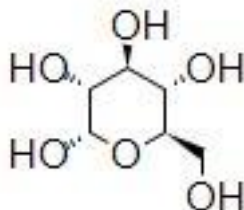


Figure 2.3 Chemical structure of glucose.

Glucose MIP was usually successfully developed making use of the ability of the hydroxyl groups on glucose molecules **Figure 2.3** to interact by H-bondings with the monomers' functionalities. For example, a study [2] synthesized three different glucose MIPs using three monomers acrylic acid (AA), hydroxyethylmethacrylate (HEMA), and acrylamide (AAm) together with poly ethylene glycol dimethacrylate (PEGDMA) as a crosslinker. Each MIP was synthesized in a polar protic solvent (water) and in a polar nonprotic solvent (dimethyl sulfoxide DMSO). The study showed that hydrogen interactions and hydrophobic or ionic interactions directed the glucose recognition process. All MIPs showed higher binding capacities compared to the corresponding control (Non imprinted polymers NIP). This study revealed that DMSO could be used as the porogen because of being polar aprotic solvent, so it would not interfere with the template monomer complexation. Also it revealed that with increasing PEGDMA content, the binding capacity increased in the HEMA network. This could be attributed to PEGDMA being a long and flexible crosslinker (14 ethylene glycol units compared to 1 in EDMA) [2]. Another study [21] investigated the effect of glucose concentration on the release dynamics of MIP gels. They prepared two MIP hydrogels with two different glucose concentrations. The study showed that the MIPs synthesized with the higher glucose concentration produced higher binding and higher release. This was attributed to the disturbance of the crosslinking network caused by the higher glucose concentration

[21]. Glucose MIPs were also synthesized using copolymers of 2-hydroxyethyl methacrylate (HEMA) and methacrylic acid (MAA) [22,23]. Another interesting study [24] analyzed the types of specific interactions between five natural glucose binding proteins. From the analysis they concluded that the most important types of specific interactions between glucose and the amino acids in the investigated proteins are H-bonding and to a lesser but important extent hydrophobic ring-ring interactions. Thus the study [24] reported the synthesis of four MIP using 4 different monomers that mimic the amino acids in the previously analyzed proteins and that can possess the same types of specific interactions. It was concluded that the resulting MIPs had high glucose binding affinities that exceeded the binding affinity of Concanavalin A (a naturally existing carbohydrate binding protein).

2.4. Monomer selection strategies

As previously mentioned in section 2.1.1, monomers determine the types of non-covalent interactions taking place with the template. As the strength of complexation between monomers and templates in the pre-polymerization mixture increases, the stability of the resulting binding sites also increases. The library of functional monomers that are commonly reported in MIP literature and that could be matched with a certain template is big **Table 2.1**. The previously reported attempts relied greatly on “intuition” or “sense” stemming from theoretical and practical experiences. However, such strategy is time consuming and caused many of the research to follow a single trend in the selection of monomer combinations and the processing of MIP.

Thus recent trends began to emerge in order to narrow down the list of selected monomers, and to accurately choose the best performing monomers in reasonable timings, and with the exertion of reasonable efforts.

2.4.1. Spectroscopy based selection


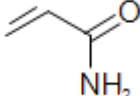
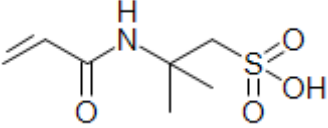
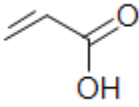
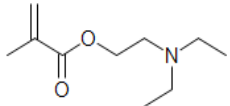
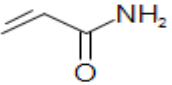
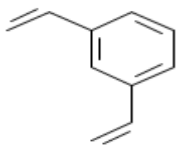
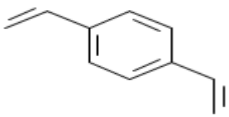
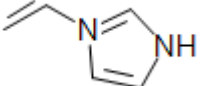
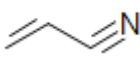
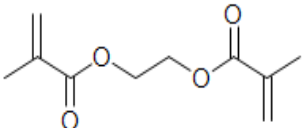
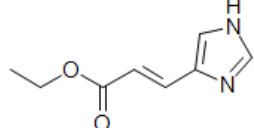
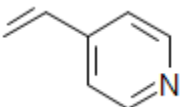
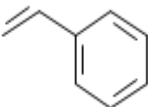
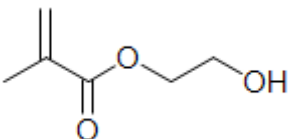
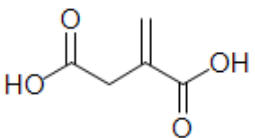
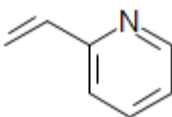
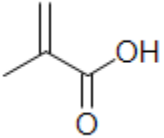
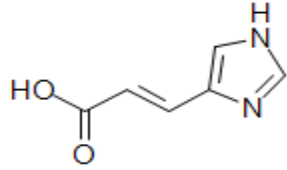
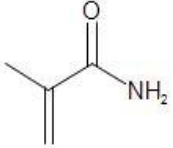
Some studies reported the application of Nuclear Magnetic Resonance NMR studies in order to aid in the determination of the types of interactions taking place. However, some template self

associations were reported to take place which complicated the NMR study results. Other studies reported the application of Fourier Transform Infra-Red Spectroscopy (FT-IR) to study the changes in the (FT-IR) band wavenumbers in the pre-polymerization mixture. However, the presence of the solvent interfered with these interactions by competing with either the template or the monomer. UV spectroscopic titrations have been reported also to screen a list of monomers based on the types of interactions taking place between the monomers and the template in pre-polymerization mixtures. These approaches are considered time and labor consuming. In addition, the process could be further complicated by taking into consideration the different ratios that could be tested, and the different parameters that can affect the resulting MIP [25].

2.4.2. Combinatorial approaches

This approach relies on the synthesis of over 50 MIPs for a certain template with different monomer combinations and ratios on small scales [25]. Combinatorial approaches necessitate the testing of a big library of monomers to synthesize large numbers of polymers. This approach requires the employment of automated pipetting machines and microtiter plates. Automation would save time and would facilitate the direct transfer of the synthesized polymers into the subsequent washing and binding procedures. Usually the evaluation of binding is done by fluorescent or UV spectroscopy in order to accelerate the analysis process. However, these template assay methods are not applicable to all kinds of templates [26].

Table 2.1 The chemical structures of the common monomers used in molecular imprinting

			
Acrolein	Acrylamide	Acrylamido-2-methyl-1-propanesulfonic acid	Acrylic acid
			
N-Diethylamino[methyl methacrylate]	Acrylamide	m-Divinyl benzene	p-Divinyl benzene
			
1-vinylimidazole	Acrylonitrile	Ethyleneglycoldimethacrylate	Urocanic acid ethyl ester
			
4-vinylpyridine	Vinylbenzene	2-Hydroxyethyl[methacrylate]	Itaconic acid
			
2-vinylpyridine	Methacrylic acid	Urocanic acid	Methacrylamide

2.4.3. Chemometrics

This approach utilizes statistical methods and mathematical models in order to analyze chemical data. The strategy allows the optimization of MIP synthesis and the prediction of the most important variables influencing MIP behavior, because in this strategy, multiple factors are varied and studied simultaneously, then data are analysed in certain matrices that allow the prediction of the most significant factors [25,26]. For example a study [27] used chemometrics to investigate the effect of the crosslinker on the physical properties of MIP beads using fluoroquinolone anti microbials as the template. The investigation was conducted on three crosslinkers; divinyl benzene DVB, EGDMA, and TRIM. The study concluded that there are synergistic crosslinker blends that enhanced the performance of MIPs. Also, there are antagonistic crosslinker blends that reduced the performance of MIPs.

2.4.4. Computational simulation investigation

Molecular simulation studies are highly effective in modeling the different variables that influence the behavior of the resulting MIP network. They became highly popular especially with the continuous advancements in computational power and speed. It is difficult to control the variations in secondary parameters (operation parameters e.g: temperature and pressure) during synthesis within different samples of the same MIP. However, molecular simulations made it feasible to adequately minimize the errors and the variations in secondary parameters, in order to accurately study the effects of the primary parameters (section 2.1) on the heterogeneity phenomena commonly reported in MIP. Also, molecular simulations proved to be more efficient than conventional methods in optimizing the conditions for expensive templates [28].

The attempts varied in which some utilized a virtual library of monomers and screened a template against them to select the best monomer interacting with the template [29,30]. Others used molecular dynamics MD, or simulated annealing techniques to compute energy differences, total energies, and closest approach distances between the templates and monomers. MD simulation is a powerful tool to analyze complex systems in reasonable time and with reasonable costs [31]. MD employs the integration of Newtonian laws of motion

($F_i = m_i a_i$) to study and predict changes in atomic positions (neglecting electronic positions [32]) with time at a certain temperature and pressure. The integration process employs algorithms such as Verlet or Leapfrog algorithms. The potential energy of a molecular system in MD is described by a force field, from which the interactions (mainly electrostatic and Van der Waals forces) between molecules can be analyzed accurately [33]. The appropriate choice of the correct force field enables the investigation of the effects of the surrounding environment on the properties of different elements of a system [34]. Different force fields (AMBER, CHARMM, GAFF) have been developed to be accurately specific for certain molecules and biomolecules. MD simulations produce trajectories defining the velocities and positions of the simulated particles [32].

Simulated annealing is a highly popular MD technique in studying (MIP). During simulated annealing, the system goes through a temperature cycle, in order to make sure that the whole system conformational space is sampled over time. The mechanism involves successive cooling and heating cycles, that yields a local minimum of potential energy for each conformation. This is very essential to make sure that complexes are not trapped in some local minima [34]. In MIP systems, simulated annealing could be employed in order to study their low energy conformations, the types of interactions taking place, and the possible effects of any other additives, like solvents or crosslinker.

Also, density functional theory (DFT) was reported to study the types of interactions in the pre-polymerization mixture, and to calculate the binding energies between different monomers and templates. The resulting scores from such calculations could help to select the best candidates for the polymerization process [29].

The events taking place in the pre polymerization mixture direct the properties of the resulting MIP. And although many studies focused on simulating the interactions between the monomer and the template, in order to understand and predict the properties of the resulting MIP, recently many studies have outlined that the roles of the solvent, and crosslinker cannot be ignored, and that they can significantly affect the properties of the resulting MIP. Thus the reported attempts could be grouped into three categories; virtual screening of a library of monomers, simulation of the pre-polymerization mixture, and simulation of the molecular imprinting process.

2.4.4.1. Virtual screening of a library of monomers

It is a very common and highly efficient approach. The template is screened against a library of monomers and the monomers are selected based on their binding scores with the template. A study [29] utilized ab initio quantum mechanical calculations to calculate the binding energies of benzo[a]pyrene template with a library of monomers. It was reported that the adopted strategy could efficiently predict that MAA would produce efficient benzo[a]pyrene MIP based on its highest binding scores. Also the theoretical results were validated experimentally. The same strategy was employed by another study [30] in order to calculate the interaction energies of chlorogenic acid template. The adopted strategy was also effective in studying the simulated stable monomer template complexes, in order to investigate the types of functional groups involved during the preorganization stage.

2.4.4.2. Simulation of the pre-polymerization mixture

A study [35] was interested to investigate the heterogeneity of binding sites in MIPs, so they employed MD studies on two systems. The first was a complete pre polymerization system containing all the system components (monomer, template, cross linker, initiator, and explicit solvent) and the second was a simplified system (without crosslinker and initiator. Then they applied RDF (Radial Distribution Function) to study the density of the monomers around the template. The study showed that the crosslinker interacted with templates and altered the homogeneity of the interactions between monomers and templates, and is thus one of the main drivers for the heterogeneity of binding sites in the resulting MIP.

A different study used molecular simulation (LEAPFROG algorithm) [36] to measure the binding energies between different monomers and the template in water. The study showed that the experimental binding in water didn't follow the same order measured from the molecular simulation process (MIP1>MIP3>MIP2) **Figure 2.4** . In this study, the simulations modeled a single monomer-template complex which translates into a single binding site [37]. This ignored the conformational structure of the rest of binding sites.

MIPs are well known to possess a heterogeneous combination of different binding sites whose affinities range from high to low affinity binding sites.

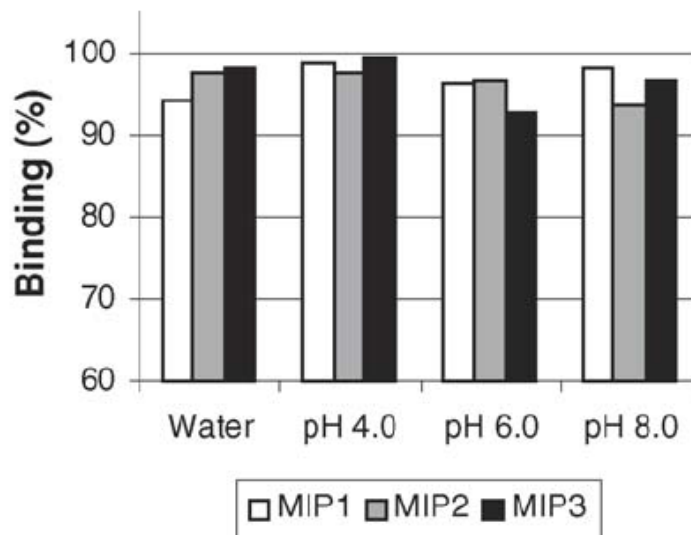


Figure 2.4 The binding percentage of MIP1, MIP2 and MIP3 for abcavir (template) in water and different buffers [36].

A different third study [38] constructed a virtual library of the commonly used functional monomers in cholate MIP synthesis. The monomers were capable of interacting by electrostatic and hydrophobic forces. Interaction energies between the templates and monomers were calculated by docking. The system was minimized using the dielectric constant of DMSO because it was the porogen intended to be used for the preparation of the polymers. Three monomers were selected based on their high interaction energies and their feasible practical implementation during the synthesis process; N-(3-aminopropyl) methacrylamide hydrochloride (APMA·HCl), ethyleneglycol methacrylate phosphate (EGMP), and N,N- Diethylaminoethylmethacrylate (DEAEM). However practically only APMA showed high binding affinities for cholate in aqueous media because binding was based on hydrophobic and ionic interactions, While DEAEM and EGMP showed high binding (according to modeling) based on H-bonds which are normally disrupted in aqueous media. These results could not be highlighted by modeling only, because screening of the monomers was done in their neutral form. This study showed that APMA.HCl NIP did not show significant lower binding than the corresponding MIP, suggesting that the monomer had high affinity for cholate, and thus computational modeling aided in the preparation of high affinity networks for cholate that need not be a MIP network.

Finally a study [39] initially screened ephedrine against a virtual library of monomers by measuring the binding scores. Also MD was used to study and calculate the closest approach

distances between the functional groups on the monomers and the templates in the pre-polymerization mixture. Then the authors selected the monomers scoring high binding energies to test them experimentally by applying them in the chromatographic separation of the template. The study showed that all the selected monomers showed high chromatographic separation except one which was hydroxyl ethyl methacrylate HEMA. It was postulated that HEMA being hydrophobic could have been embedded within the inner core of the stationary phase. This shows that not only the strength of the interactions between the monomers and the template is essential, but also the expression of the right selective functional groups on the exposed binding sites of the MIP is highly essential.

2.4.4.3. Simulation of a modeled molecular imprinting process

An interesting study [34] proposed a model in order to simulate the whole stages of MIP synthesis for MAA EGDMA MIP with pyrazine and pyrimidine templates. The study modeled the pre-polymerization mixture (functional monomer, template, and crosslinker). Then, the study modeled the polymerization step by employing a simplified strategy; First the molecules were frozen in place to create intact configurations of the template monomer complexes **Figure 2.5A**. Then the templates were removed leaving behind the intact cavities formed from the monomers and crosslinkers **Figure 2.5B**. Finally, rebinding of structurally related analogues to the simulated cavities was employed **Figure 2.5C**. The model had its limitations of being simple compared to the real situation, because of the fixation of the complexes during stage B (polymerization), which ignored the detrimental effect of the polymerization process on the formed complexes. In spite of that, the proposed model could predict the types of functional groups involved in the complexation process between the template, MAA, and EGDMA. The study showed that although both pyrazine and pyrimidine are structurally analogous to each other, only pyrazine could form specific interactions during the precomplexation process. And that's why pyrazine MIP were selective for pyrazine over pyrimidine, but pyrimidine MIP was not selective for pyrimidine over pyrazine. Based on the proposed model, this could be explained based on the steric effects caused by the close proximity of the functional groups on pyrimidine compared to pyrazine **Figure 2.6** that hindered the formation of stable complexes with MAA and EGDMA.

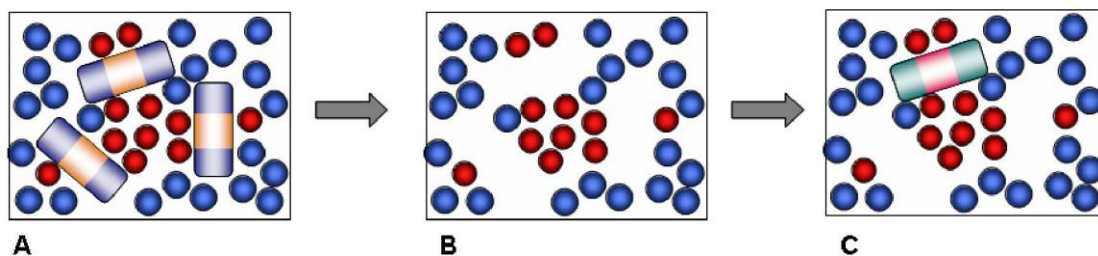


Figure 2.5 Schematic representation of the modeling stages.

A: Pre-polymerization mixture (functional monomer (red circle), template (rod), crosslinker (blue circle)).

B: Intact cavities formed from the monomers and crosslinkers, after the removal of the template.

C: Rebinding of a structurally related analogue (rod) [34].

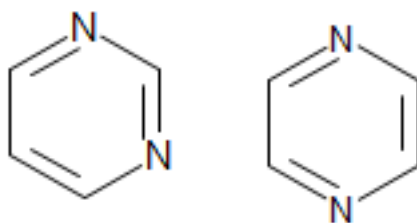


Figure 2.6 Chemical structures of pyrimidine and pyrazine.

Another study [40] used MD simulations between theophylline and polymeric chains in order to determine the interaction energies and the functional groups actively participating in creating the complexes. The authors applied MD simulations on energy minimized polymeric chains, then they added theophylline to the chains, and applied another equilibration by MD. Finally, theophylline was removed leaving behind fixed configurations of the polymeric chains, and a final MD simulation was employed on the chains in the presence of theophylline and other structurally similar ligands. In this study, the authors demonstrated that interaction energies with fixed polymer chains differed from those obtained with the chains in motion [41], and the resultant interaction energies showed no preferential binding for theophylline over other structurally similar ligands. A study [42] used the "kinetic gelation mode" to simulate by MD the whole polymerization event taking place on a previously reported HEMA-EGDMA based MIP for glucose [43,44]. This mode enables the polymer chains to interact with solvents, templates, and crosslinker in each equilibration phase. The mode also includes the exponential decay of an initiator allowing the equilibration phase to be repeated until the final polymeric network is formed. The study could identify the functional groups contributing in the specific interaction with the HEMA in the network. The theoretical

binding energy measurements were in good correlation with the previously reported practical results [43,44]. However, this mode requires long modeling times (up to days) and high computational powers to better increase the accuracy of the calculations.

2.4.4.4. Conformational analysis

Besides measuring the binding energies between the monomers and the template, this thesis considers a new approach in the selection of monomers "Conformational analysis". To the best of our knowledge, it has been never employed in studying molecular imprinting systems. The approach relies on the selection of monomers with high conformational stability based on their calculated Boltzmann temperature T_B . Such monomers are expected to create binding cavities in MIP with high conformational stability that can withstand the detrimental effects of the polymerization and extraction process. Consequently, conformationally stable and high performance MIP can be synthesized and used in many applications.

- *The significance of T_B*

The flexibility of polymers increases with the elevation of T_B in accordance with the following Arrhenius equation:

$$\tau_m = A e^{\frac{E_a}{RT}}, \text{ where:} \quad \text{Equation 1 [45]}$$

τ_m : The orientation time, which is a measure of the ease of uncoiling of polymer coils, A: Constant related to polymer structure, T_B : Boltzmann temperature

High temperatures give molecules enough energy to move and spread. According to **Equation 1**, high temperatures give the polymer chains the required energy to overcome energetic barriers from one conformer to another. Thus, this concept was used to study the conformational stability of the different polymers with respect to each other. In order to use such high conformationally stable polymers in the design of new MIP. This was expected to be extremely useful in designing MIP with nanoscaled binding cavities that are stable and could keep the binding cavities' stable structures during the whole process of MIP synthesis (which is known to be detrimental to many binding sites at many stages). Thus, the lowest T_B

causing the polymer chains to start changing their conformation was selected as an indicator of conformational stability.

- The calculated parameters from the conformational analysis study

From the conformational analysis study, two parameters can be calculated, which are:

1.End to end distance ($\langle r \rangle$): indicates how the polymer is able to adopt a relatively relaxed structure in response to incremental increase in T_B .

2.Radius of gyration (R_g): indicates how the polymer is able to adopt a compact structure in response to the same incremental increase in T_B .

Linear polymeric chains could be imaged in their simple forms (without the side chains) as linear threads joining beads (representing monomers) **Figures 2.7, 2.8**. The R_g and $\langle r \rangle$ are used to assess the size of a polymer. Firstly by considering $\langle r \rangle$, **Figure 2.7** shows a polymeric model configuration, which constitutes a spherical space. The beads are the monomeric joints that can be denoted by $r_0, r_1, r_2, \dots, r_N$. The R (diameter of the sphere) is considered to be the end to end distance starting from r_0 and ending by r_N . Polymers can adopt several conformations with different R values, thus the average value ($\langle r \rangle$) of the different R s representing different polymeric conformations can give an accurate indication of the size of the polymer and its respective ability to adopt different and many conformational states.

Secondly, considering the R_g , it can be measured as the radius of the constituted spherical space by the polymer **Figure 2.8**. It is the distance between the center of mass of the polymer from one end and a bead from the other end. Similar to $\langle r \rangle$, a polymer can have different radii values based on its different conformations, thus also the average value ($\langle s \rangle$) of the different radii (R_g) representing different polymeric conformations can give an accurate indication of the size of the polymer and its respective ability to adopt different conformational states [45,46].

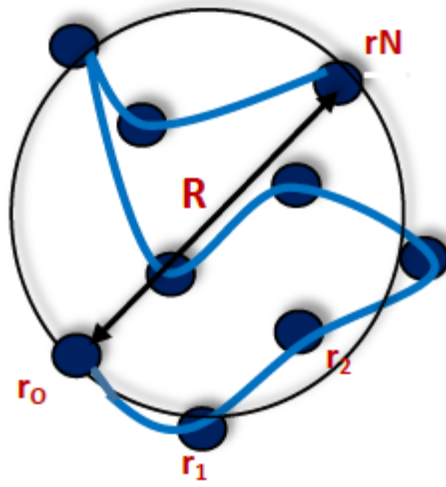


Figure 2.7 A polymer constituting a spherical space with R representing its end to end distance.

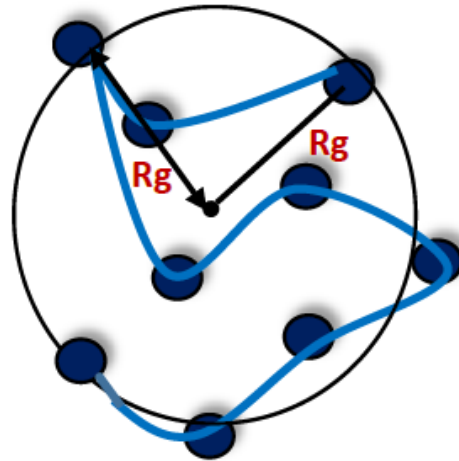


Figure 2.8 A polymer constituting a spherical space with R_g representing its radius of gyration.

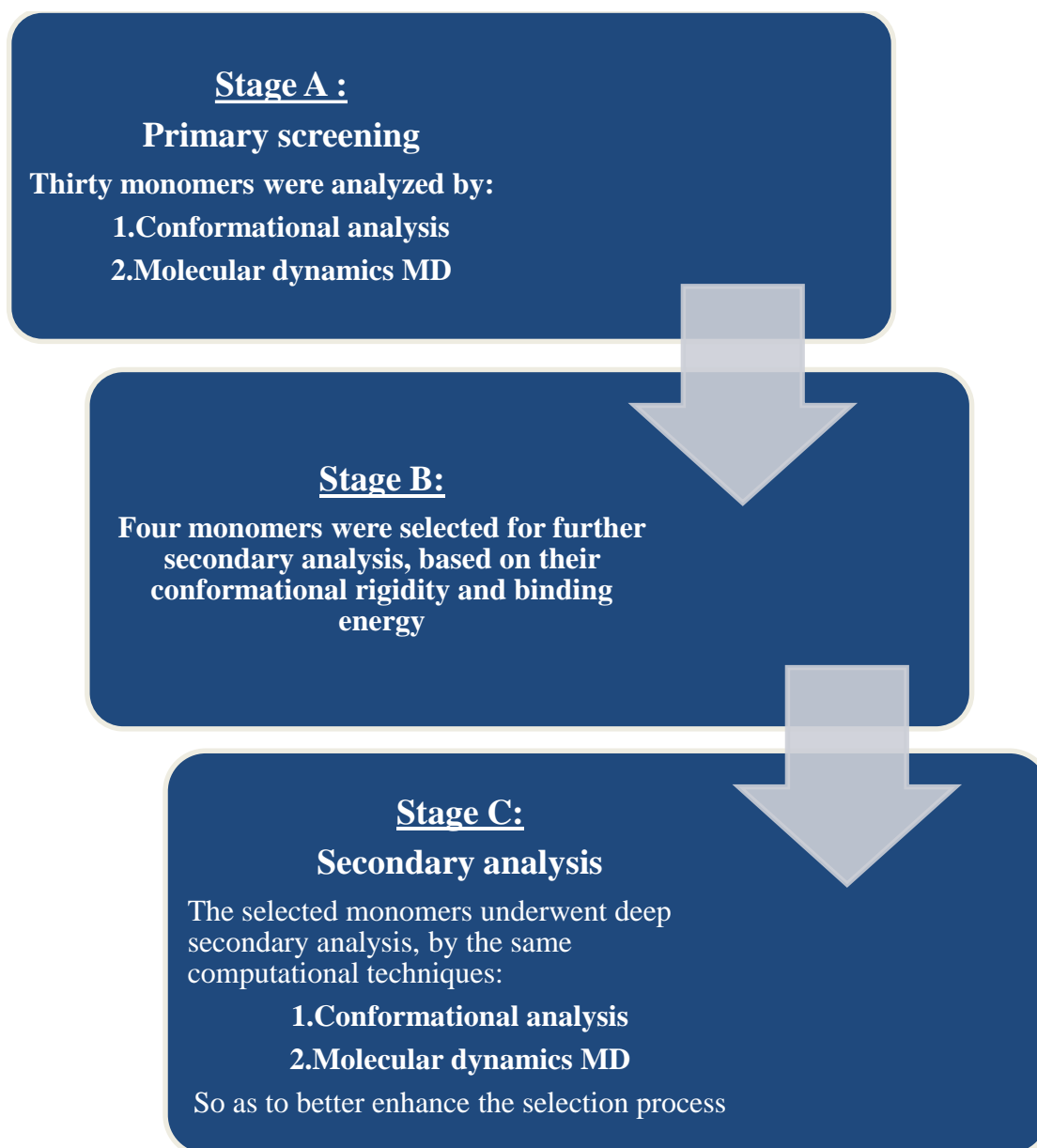
Chapter 3

Materials & Methods

3. Materials and methods

3.1. Computational investigations

Computational simulations were employed for the thirty selected monomers, using Materials Studio 5.0 (Accelrys, San Diego, CA, USA). The investigations included conformational analyses, energy minimizations, and MD calculations according to the following scheme **Scheme 3.1**. They were employed using COMPASS and Dreiding force fields.



Scheme 3.1 A flow chart showing the stages of the employed computational investigations.

3.1.1. Primary screening

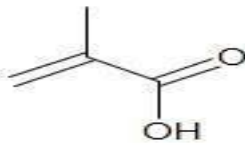
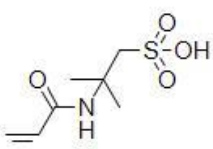
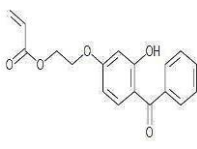
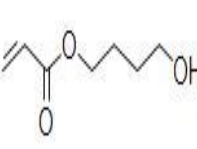
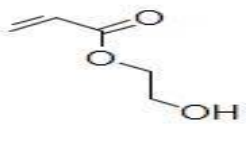
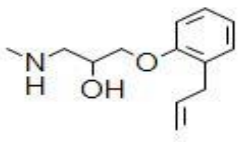
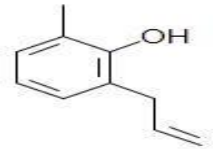
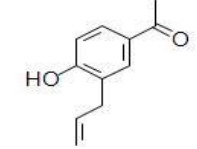
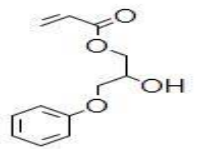
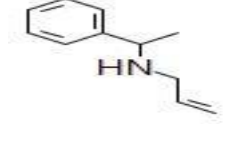
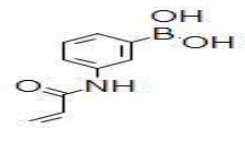
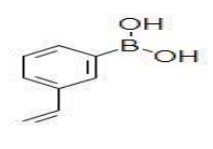
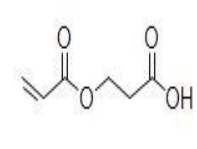
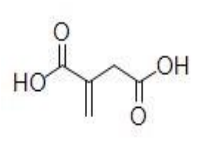
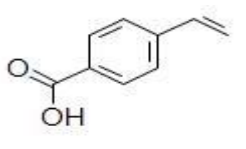
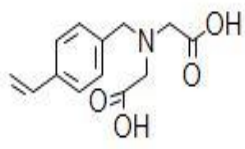
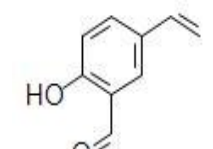
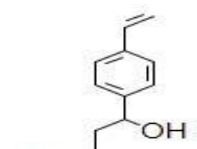
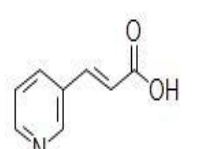
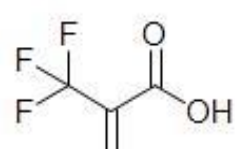
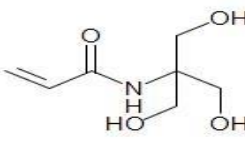
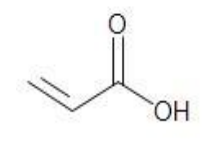
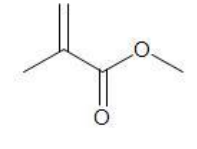
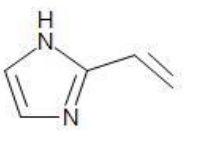
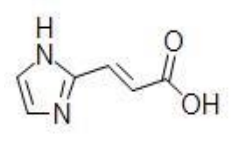
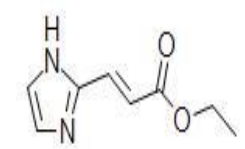
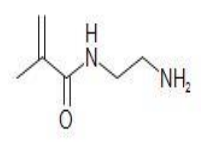
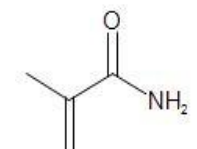
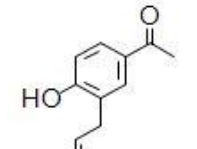
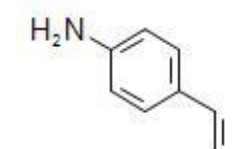
3.1.1.1. Conformational analysis

Thirty monomers were selected based on their possession of the functional groups needed to interact non-covalently with the currently studied role model template D-glucose **Table 3.1**.

The monomers were selected to possess H-bond acceptors/donors such as hydroxyl groups, amino groups, carboxylic groups and/or hydrophobic interacting aromatic rings [24]. They were expected to interact with glucose by both H-bonding and hydrophobic interactions respectively. Also, another important criteria was considered, which is to make sure that the selected monomers are affordable and commercially available.

At the onset, 3D atomistic models of the thirty monomers were created. Thereafter, linear polymers of twenty units for each monomer were built separately. Energy minimization using DISCOVER force field was applied on each individual polymeric ensemble to remove any strain energies and to optimize the geometries of the simulated molecules. Then T_B was allowed to continuously increase for each polymer, till reaching a specific T_B at which the modeled polymer began to respond to the increase in temperature through changing its conformation. Finally, both the radius of gyration $\langle s \rangle$ and the end to end distance $\langle r \rangle$ parameters were measured for each polymer at a single high T_B that exceeded all the calculated T_B values for all the modeled polymers. This was highly essential to make sure that all the modeled polymers would change their conformations in response to the same T_B , in order to investigate possible correlations between the calculated $\langle s \rangle$, $\langle r \rangle$ and polymer structure at the selected T_B . The number of conformers studied for each polymer in the preliminary screening was 200.

Table 3.1 Molecular representations of the thirty investigated monomers.

				
Methacrylic acid	Acrylamido-2-methyl-1-propanesulfonic acid	2-(4-Benzoyl-3-hydroxy phenoxy)ethyl acrylate	4-Hydroxybutyl Acrylate	2-Hydroxyethyl acrylate
				
1-(2-allyl-phenoxy)-3-Methylamino-propan-2-ol	2-Allyl-6-methylphenol	3-Allyl-4-hydroxy benzaldehyde	2-Hydroxy-3-phenoxy propyl acrylate	N-allyl-α-methylbenzyl Amine
				
3-(Acrylamido)phenyl Boronic acid	Vinyl phenyl boronic acid	2-Carboxyethyl Acrylate	Itaconic acid	4-vinyl benzoic acid
				
4-vinylbenzyl-iminodiacetic acid	2-Hydroxy-5-vinyl Benzaldehyde	2-(4-vinyl-phenyl)propan-1,3-diol	trans-3-(3-pyridyl)-acrylic acid	2-(Trifluoromethyl) acrylic acid
				
N-[Tris(hydroxymethyl) methyl] Acrylamide	Acrylic acid	Methylmethacrylate	4(5)-vinyl imidazole	Urocanic acid
				
Urocanic acid ethyl ester	N-(2-aminoethyl) Methacrylamide	Methacrylamide	3'-Allyl-4'-hydroxy Acetophenone	p-amino styrene

3.1.1.2. Molecular dynamics MD

Cubic amorphous cells with periodic boundary conditions as to simulate the model as an infinite system were created containing various monomer units and the template. The cell is modeled as a 3D cubic box, **Figure 3.2**. Then, energy minimization up to a maximum of 5000 iteration steps was applied to relax the system and remove any weak van der Waals contacts. Finally, the monomers and the template diffused and interacted in the minimized system in 100,000 MD steps for a total simulation time of 100ps utilizing a time step of 1fs and the NVT ensemble. Particle mesh Ewald algorithm was used to calculate van der Waals interactions and electrostatic interactions. The summation method for both was atom based. The FORCITE module was used to calculate the cohesive energies CE.

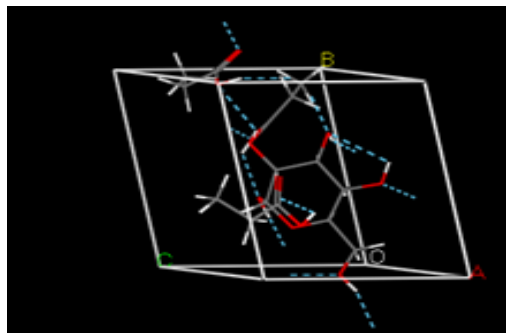


Figure 3.1 A cubic amorphous cell containing acrylic acid monomers interacting with glucose. Dashed lines signify the intermolecular interactions.

3.1.2. Secondary analyses

Out of the previous primary conformational analyses and MD simulations, five monomers were selected for further molecular analyses in order to enhance our knowledge on the nature of the template-monomer interactions. Four of these five monomers were selected based on their highest values for the Cohesive energies, Boltzmann temperatures and relatively high $\langle s \rangle$, $\langle r \rangle$. These monomers are expected to therefore show the highest conformational stability as well as the strongest interactions with glucose units. These template-monomer systems are thus expected to yield high performance MIPs. The fifth monomer was selected to be a control monomer having especially low T_B .

3.1.2.1. Conformational analysis

The number of conformers employed here were 12,000 structures. The modeled runs were repeated four times for each polymer, and the values of $\langle s \rangle$ and $\langle r \rangle$ were calculated as the average of these four runs.

3.1.2.2. Molecular dynamics MD

MD was employed as described earlier, four times for each template-monomer system. To provide better simulation results, additional equilibration and annealing tasks were performed. The simulated annealing process was attempted to the ensembles. It gives information about the locations of the monomers with respect to the template. Five annealing cycles with 5 heating and 5 cooling ramps were used for a total of 50 ps.

After minimization of the last frame, a preequilibration step was employed; The monomer units and the template molecule were then subjected to an MD run for 100 ps so as to allow the system to equilibrate. Once the system has equilibrated, a long MD run proceeded for 1 full ns (10^6 MD steps). Binding energies between the monomer units and the template were then calculated as an average of the results from four different runs as an expression of the strength of binding between the template and the monomeric units.

3.2. Experimental procedures

3.2.1. Chemicals and reagents

Acrylic acid (AA), Acrylamido-2-methyl-1-propanesulfonic acid (AMPSA) (functional monomers), and (EGDMA) (crosslinker), including D-glucose (template) were purchased from Alfa Aesar (Germany). Analytical grade phenol crystals detached were purchased from Loba Chemie (India). 2-(4-Benzoyl-3-hydroxyphenoxy)ethyl acrylate (BHPEA) (functional monomer) including B.P concentrated Sulfuric acid (95-97 %) were purchased from Sigma Aldrich (USA). Dimethyl sulfoxide (porogen) was purchased from Techno Pharmchem (India). Potassium persulfate (initiator) was purchased from Alpha Chemika (India). Methanol and glacial acetic acid were obtained from Fischer (UK). The water used was distilled and deionized (DDI) by a Milli-Q system (Millipore, Bedford, MA, USA). All chemicals were used without purifications.

3.2.2. Synthesis of polymers

Five MIPs (MIP1, MIP2, MIP3, MIP4, MIP5) and their corresponding NIP (NIP1, NIP2, NIP3, NIP4, NIP5) were synthesized by free radical polymerization using the following protocol. The template **Figure 3.2C** was dissolved with the monomer **Figure 3.2A** in DMSO. The solution was allowed to stir for 1 hour, so that the complexation process could take place. Then EGDMA (crosslinker) **Figure 3.2B** and the initiator were added. The whole mixture was finally transferred to a double neck flask, and the solution was purged with nitrogen for 10 minutes. Finally polymerization was initiated at 60°C for 20 hours in an oven or an oil bath. The resulting bulk polymers are then cut into small uniform disks.

Templates were eluted either by washing using Soxhlet apparatuses (Methanol:Acetic acid 9:1) for 24 hours or by incubating the polymers in 20ml water on a rotary shaker (Phoenix RS-10) for 2 to 3 days. The solvent was changed at regular intervals.

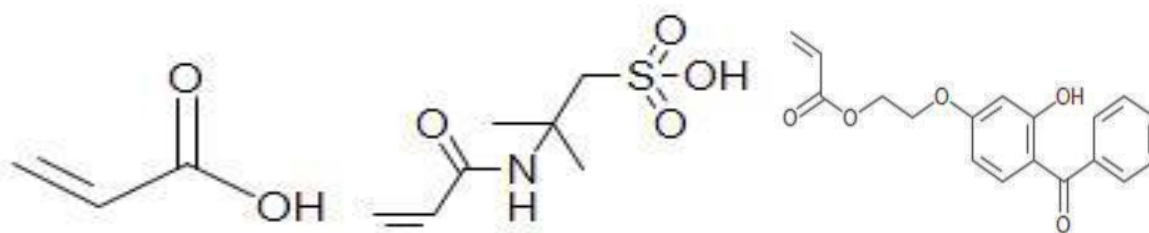
The extraction process was continued until the template could be no longer detected by UV-Visible spectrophotometry using the Phenol-Sulfuric acid assay (section 3.2.3.1) [47].

The washed polymers are then filtered from the washing solutions and allowed to dry in a vacuum oven for 24 hours.

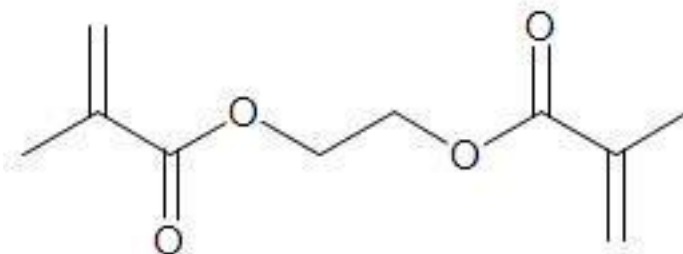
(NIP) were prepared as a control. They were synthesized using the same protocol, but in the absence of the template. **Table 3.2** shows the compositions of the synthesized polymers.

Table 3.2 The compositions of the synthesized polymers

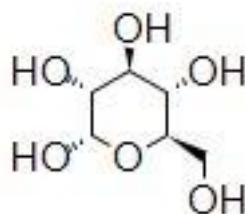
Polymer	AA (gm)	AMPSA (gm)	BHPEA (gm)	Glucose (gm)	EGDMA (gm)	Initiator (gm)	Solvent (ml)
MIP 1	0.2			0.05	0.8	0.02	10
NIP 1	0.2				0.8	0.02	10
MIP 2		0.2		0.05	0.8	0.02	10
NIP 2		0.2			0.8	0.02	10
MIP 3			0.2	0.05	0.8	0.02	10
NIP 3			0.2		0.8	0.02	10
MIP 4			0.2	0.05	0.465	0.0133	6.65
NIP 4			0.2		0.465	0.0133	6.65
MIP 5			0.2	0.05	0.2	0.004	4
NIP 5			0.2		0.2	0.004	4



A



B



C

Figure 3.2A Chemical structures of the selected monomers, Acrylic acid, Acrylamido-2-methyl-1-propanesulfonic acid, and 2-(4-Benzoyl-3-hydroxyphenoxy)ethyl acrylate respectively.

3.2B Chemical structure of the crosslinker EGDMA.

3.2C Chemical structure of glucose.

3.2.3. Template rebinding studies

3.2.3.1. Construction of calibration curves

Glucose was assayed spectrophotometrically according to a method developed by Dubois et al [48]. A stock solution of glucose was prepared. Then seven standard solutions of concentrations ranging from 0.01g/l to 0.07g/l were prepared from the stock solution. 1ml aliquot was pipetted

from each standard solution, followed by the rapid addition of 1ml phenol (5%) and 5ml concentrated sulfuric acid.

After settlement for around thirty minutes, the developed color was assayed spectrophotometrically at 490nm on UV Visible Spectrophotometer (Cary 100 Bio, Varian). Finally the calibration curve was constructed **Figure 3.3**. This method has proven great accuracy in carbohydrates measurements, and have been commonly reported in the literature [24, 19, 20].

3.2.3.2. Template rebinding studies at room temperature

50mg of MIP and NIP were weighed in glass vials containing 5ml 0.1g/100ml glucose solution in DMSO. The vials were shaken on an oscillatory shaker (Phoenix RS-10) at room temperature for 24 hours to make sure that equilibrium has been attained. Aliquots in triplicates were pipetted from each sample and the glucose concentration was assayed spectrophotometrically by the phenol-sulfuric acid assay as previously described. Each experiment was repeated at least twice.

3.2.3.3. Template rebinding studies at 50°C

Similarly, template rebinding studies were employed for MIP1, MIP2, MIP3 at 50°C on Precision Scientific shaking water bath (model 25), in order to investigate the effect of a relatively high operation temperature on the conformational stability of the constructed cavities within the MIPs. This is especially essential if the prepared MIP are intended to be used in chemical sensors that are commercialized in tropical countries.

-The amount of glucose ((mg/gm)) bound was determined using the following equation:

$$\frac{(C_i \text{ mg/ml} - C \text{ mg/ml}) \times \text{volume of solution}}{\text{grams of MIP/NIP}}$$

- IF was determined using the following equation:

$$\frac{\text{amount of glucose ((mg/gm)) bound per MIP}}{\text{amount of glucose ((mg/gm)) bound per NIP}}$$

IF reflects the efficiency of imprinting specific cavities.

-The C_i and C given in mg/gm were calculated using a calibration curve, that was previously constructed using standard solutions of glucose **Figure 3.3**. C_i and C are the initial template concentration before binding and the final template concentration after binding respectively.

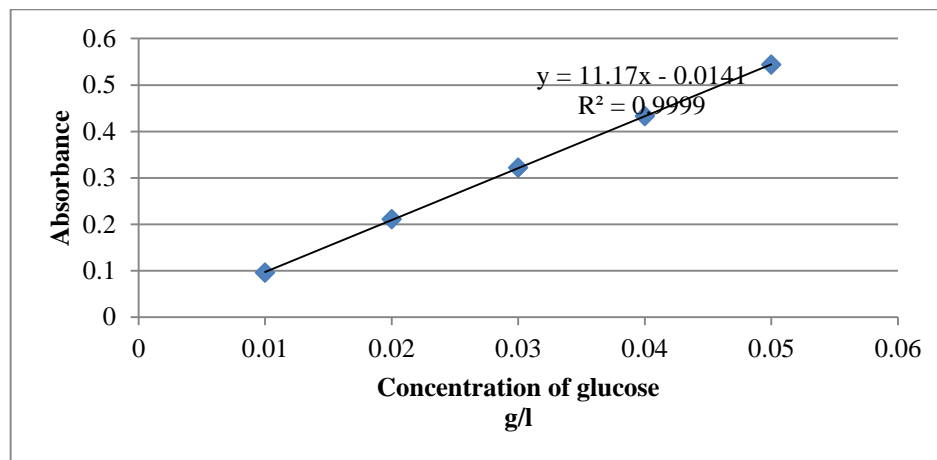


Figure 3.3 The constructed calibration curve for the stock solutions using DDI.

3.2.4. Characterization

3.2.4.1. Fourier Transform Infra-Red Spectroscopy (FT-IR)

(FT-IR) spectra for the polymers before extraction (*P 1, P 2, P 3, which represent the synthesized AA, AMPSA, BHPEA polymers before template removal*), for the polymers after extraction (MIP) and for the control polymers (NIP) were recorded using Thermo Scientific Nicolet 380 FT-IR, Waltham, MA, USA. The expression of chemical groups in general, and the expression of H-bond interactions in particular were studied in each synthesized polymer, in order to investigate the changes in relation with the type of polymer synthesized. The KBr pellet technique was employed.

3.2.3.2. Scanning Electron Microscopy (SEM)

All the polymers were gold sputtered at 15mA for two minutes, in order to render them conductive. Then, the surface morphologies were characterized using SEM (ZEISS, USA).

3.2.3.3. Thermogravimetric analysis (TGA)

The thermal stability of MIPs and NIPs 1,2,3 were determined using TA Instruments TGA (Q50, Lukens Drive, New Castle, USA). An empty aluminum crucible was used for the instrument calibration, then few mg of each polymer was weighed in the crucible. The polymers were heated from room temperature to 600 °C at heating rate of 10 °C/min. Then changes of the polymers' weights in accordance with temperature were graphically plotted.

3.2.3.4. Porosity analysis (BET)

Porosity analysis and surface area analysis were studied by nitrogen gas sorption using an ASAP 2020 analyzer (Micromeritics Instrument Corporation, Norcross, GA, USA). The dried MIP 1,2,3 and NIP 1,2,3 particles were initially treated by vacuum for four hours at 40°C. BET surface areas were evaluated using the method of Brunauer, Emmett, and Teller (BET). Adsorption and desorption isotherms were calculated at 20s equilibration intervals using 53-point pressure tables. Calculation of the distribution of mesopores and macropores was conducted using the Barrett, Joyner, and Halenda (BJH) method. Pore diameter was calculated as an average using the formula $r = 4 \times \frac{\text{total pore volume}}{\text{BET surface area}}$.

Chapter 4

Results and Discussion

4. Results and discussion

4.1. Computational investigation

The adopted MD strategy proved to be highly effective in the selection of the best candidates for MIP synthesis, as well as highly economic since it does not consume huge computational resources as compared to other reported computational strategies like DFT and quantum mechanics calculations.

4.1.1. Primary screening:


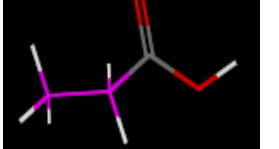
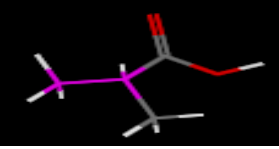

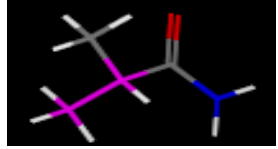
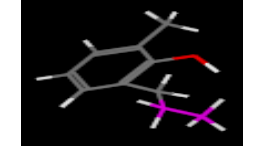
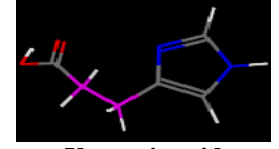
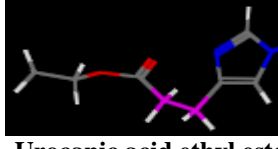
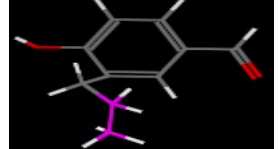
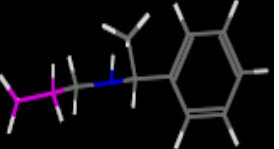
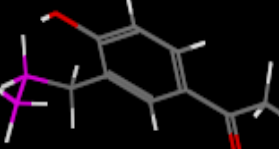
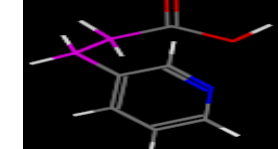
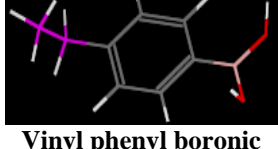

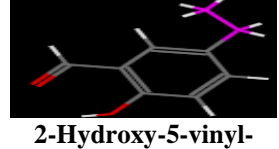
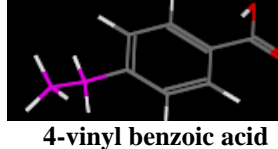
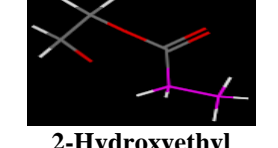
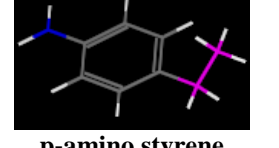
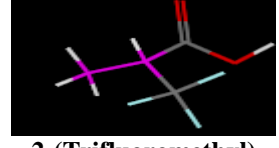
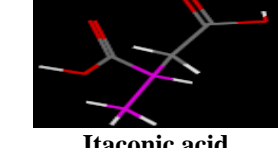
4.1.1.1. Conformational analysis

Schemes 4.1 and **4.2** list the calculated T_B (in Kelvins) for the thirty polymers in an increasing order, where **Scheme 4.1** lists group 1 which contains the polymers having T_B values between 1200 and 9000 K, while **Scheme 4.2** lists group 2 which contains the polymers having T_B values above 9000 K. It is obvious that T_B could be directly correlated to the conformational stability of the modeled polymers, i.e rigid polymers needed high T_B to overcome their conformational energy barriers and alter their conformations. Also it can be shown that the presence of aromatic rings did not always translate into high values for T_B and consequently high rigidity towards conformational changes. However, the position of the rings, the types of functional groups and their locations with respect to each other have influenced T_B the most.

By careful observation of group 1 **Scheme 4.1**, it can be noticed that most of them contained hydroxyl groups, but these hydroxyls are relatively distantly separated from other types of functional groups that if otherwise were in proximate to each other would have increased the T_B values as in group 2 **Scheme 4.2**. It can be noticed also that in group 1, the branched rings sometimes aided in such distant separation. The elevation of T_B values became much more significant in group 2. This could be attributed to the presence of polar and/or electronegative moieties such as sulfur, fluorine and hydroxyl groups in close proximity to each other. They consequently increased the resistance of the modeled polymers towards any changes in their conformation before reaching their corresponding high T_B **Scheme 4.2**.

Polymer 30 has exceptionally very high T_B . The branches contain several electronegative oxygen moieties and two aromatic rings.


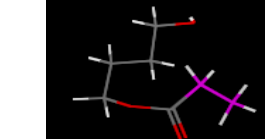
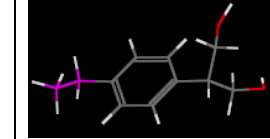
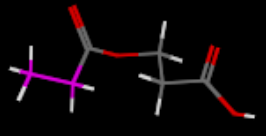

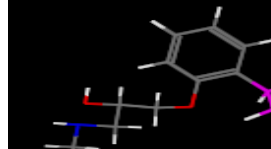
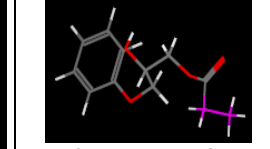
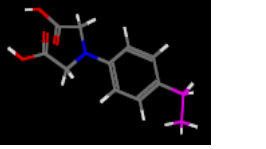
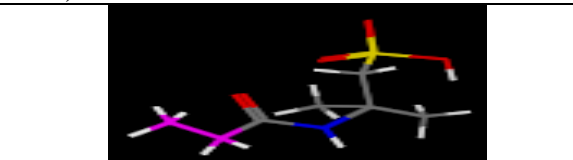
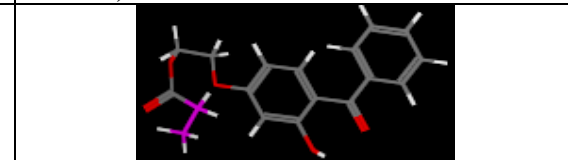
Scheme 4.1 The atomistic structures of the twenty monomers used to build their modeled polymers whose respective T_B values ranged from 1200 K to 5000 K.

1. 1200  Methylmethacrylate	2. 1500  Acrylic acid	3. 2000  Methacrylic acid	4. 2000  4(5)-vinyl imidazole
5. 3000  Methacrylamide	6. 3000  2-Allyl-6-methylphenol	7. 4000  Urocanic acid	8. 5000  Urocanic acid ethyl ester
9. 5000  3-Allyl-4-hydroxybenzaldehyde	10. 5000  N-allyl- α -methylbenzyl Amine	11. 5000  3'-Allyl-4'-hydroxy Acetophenone	12. 5000  trans-3-(3-pyridyl)-acrylic acid
13. 5000  Vinyl phenyl boronic acid	14. 5000  3-(Acrylamido) phenylboronic acid	15. 7000  2-Hydroxy-5-vinyl-Benzaldehyde	16. 7000  4-vinyl benzoic acid
17. 7000  2-Hydroxyethyl acrylate	18. 7000  p-amino styrene	19. 8000  2-(Trifluoromethyl) acrylic acid	20. 9000  Itaconic acid

Vinyl moiety, Nitrogen moiety, Oxygen moiety, Boron moiety, Fluorine moiety, Hydrogen

From **Schemes 4.1** and **4.2**, it can be noticed that a T_B value of 45,000K would be adequate to unify a single value for all the modeled polymers (except polymer 30) at which they would all change their conformations. The $\langle r \rangle$ and $\langle s \rangle$ for polymers 1 to 29 were calculated at 45,000K. The $\langle r \rangle$ and $\langle s \rangle$ for polymer 30 were calculated at 200,000K because of its exceptionally high T_B (**Scheme 4.2**).

Scheme 4.2 The atomistic structures of the ten monomers used to build their modeled polymers whose respective T_B values ranged from 1200 K to 5000 K.

21. 10,000  N-(2-aminoethyl) Methacrylamide	22. 10,000  4-Hydroxybutyl acrylate	23. 13,000  2-(4-vinyl-phenyl)propan-1,3-diol	24. 18,000  2-Carboxyethyl acrylate
25. 23,000  N-[Tris(hydroxymethyl) methyl]acrylamide	26. 25,000  1-(2-allyl-phenoxy)-3- Methylamino- propan-2-ol	27. 35,000  2-Hydroxy-3- phenoxypropyl acrylate	28. 40,000  4-vinylbenzyl- iminodiacetic acid
29. 40,000  Acrylamido-2-methyl-1-propanesulfonic acid	30. 200,000  2-(4-Benzoyl-3-hydroxy phenoxy)ethyl acrylate		

Vinyl moiety, Nitrogen moiety, Oxygen moiety, Sulfur moiety, Boron moiety, Fluorine moiety, Hydrogen

For some modeled polymers, it was difficult to correlate the values of $\langle r \rangle$ and $\langle s \rangle$ at 45,000K **Table 4.1** with their respective T_B values **Schemes 4.1** and **4.2**, because there were no trends for the calculated values of $\langle s \rangle$ and $\langle r \rangle$ as shown in **Figure 4.1**. This could be attributed to that for example a polymer could be highly rigid (high T_B) such as polymer 29, and at the same time exhibit high $\langle r \rangle$ or $\langle s \rangle$ owing to the intrinsic repulsive forces between the electronegative sulfur and oxygen moieties that caused the chain to accommodate a wider

space in vacuum *Figure 4.2a*. On the other hand, another polymer could be also highly rigid (high T_B) such as polymer 25, but at the same time exhibit relatively low $\langle r \rangle$ or $\langle s \rangle$ and consequently occupy a relatively smaller space in vacuum *Figure 4.2b*. It is worth to mention that the most rigid polymers 27 to 30 (highest T_B values) exhibited the highest $\langle r \rangle$ and $\langle s \rangle$. This could be explained based on the presence of rigid rings that occupy a relatively significant space (in vacuum) together with other polar hydroxyl groups (like in polymers 27, 28 and 30), or due to the significant contribution of polar atoms (like sulfur in polymer 29) that are present in close proximity from other electronegative polar atoms on the same or nearby branches.

Table 4.1 The simulated values for the $\langle s \rangle$ and $\langle r \rangle$ for the modeled polymers (polymers 1 To 29 at 45,000 K, while polymer 30. T 200,000 K).

Polymer model No	T_B (K)	$\langle s \rangle$ (Å°) At 45,000	$\langle r \rangle$ (Å°) At 45,000
1.Methylmethacrylate	1200	11.01376	29.4456
2.Acrylic acid	1500	9.157077	22.76835
3.Methacrylic acid	2000	9.842024	25.67065
4.4(5)-vinyl imidazole	2000	10.02773	24.9201
5.Methacrylamide	3000	10.11383	26.9151
6.2-Allyl-6-methylphenol	3000	11.32924	28.40365
7.Urocanic acid	4000	10.88075	26.4964
8.Urocanic acid ethyl ester	5000	12.28545	33.3622
9.3-Allyl-4-hydroxybenzaldehyde	5000	11.23952	28.52205
10.N-allyl- α -methyl benzylamine	5000	11.97124	29.9401
11.3'-Allyl-4'-hydroxyacetophenone	5000	11.51831	27.8261
12.trans-3-(3-pyridyl)-acrylic acid	5000	11.59624	30.4742
13.vinyl phenyl boronic acid	5000	11.44902	26.74375
14.3-(Acrylamido)phenylboronic acid	5000	12.42965	29.5821
15.2-Hydroxy-5-vinyl-benzaldehyde	7000	10.74472	25.90475
16.4-vinyl benzoic acid	7000	11.36187	29.15765
17.2-Hydroxyethyl acrylate	7000	10.37845	25.0115
18. <i>p</i> -Amino styrene	7000	10.49105	24.0781
19.2-(Trifluoromethyl) acrylic acid	8000	9.962021	26.6296
20.Itaconic acid	9000	10.32564	26.1777
21.N-(2-aminoethyl) methacrylamide	10,000	11.22559	28.77025
22.4-Hydroxybutyl acrylate	10,000	11.61669	26.5252
23.2-(4-vinyl-phenyl)propan-1,3-diol	13,000	12.37483	28.70705
24.2-Carboxyethyl acrylate	18,000	10.8001	25.26985
25.N[Tris(hydroxymethyl) methyl]acrylamide	23,000	11.75718	27.32755
26.1-(2-allyl-phenoxy)-3-methylamino-propan-2-ol	25,000	12.50491	33.6248
27.2-Hydroxy-3-phenoxypropyl acrylate	35,000	15.33941	38.2738
28.4-vinyl benzyl-iminodiacetic acid	40,000	12.82616	30.68095
29.Acrylamido-2-methyl-1-propanesulfonic acid	40,000	12.1777	35.19325
30.2-(4-Benzoyl-3-hydroxyphenoxy)ethyl acrylate	200,000	14 (at 200,000)	37.89 (at 200,000)

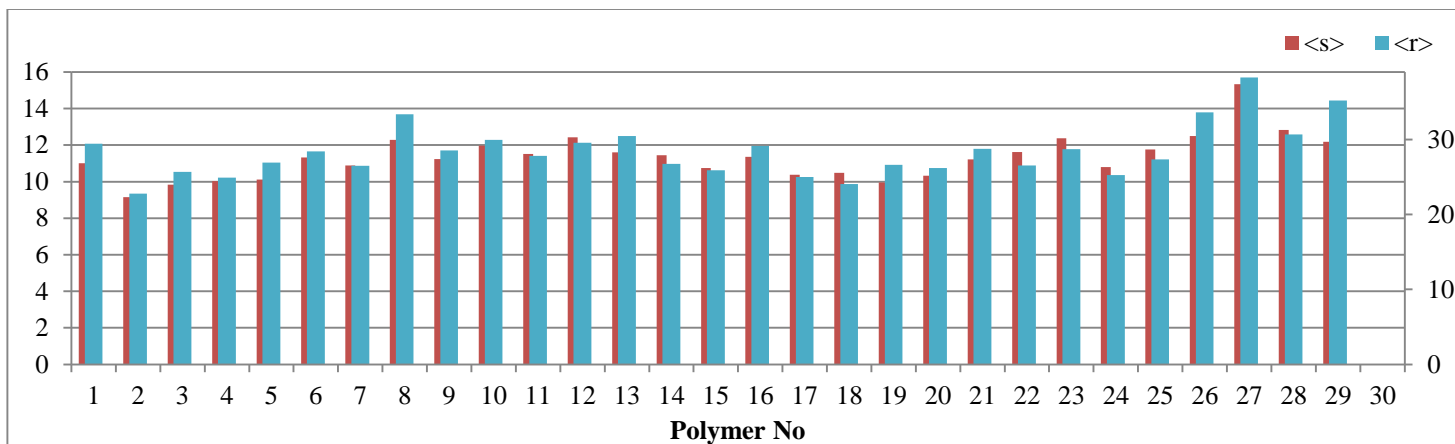
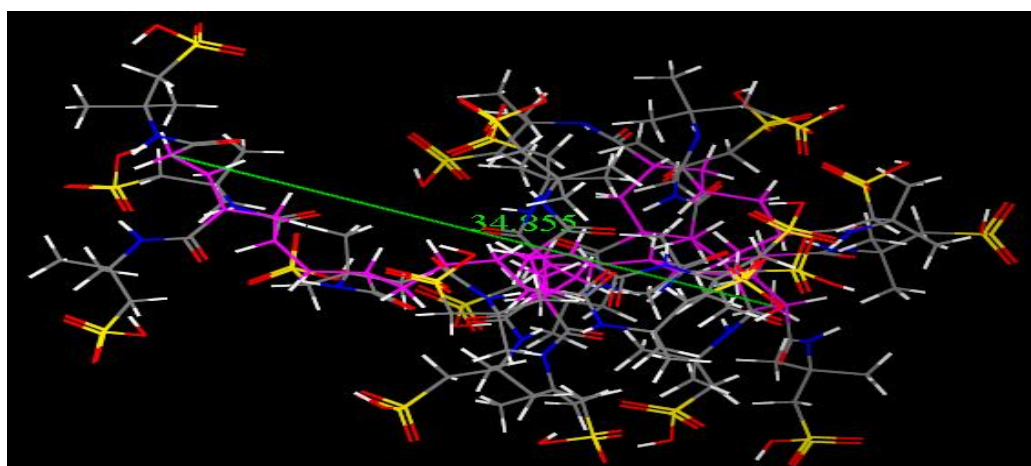
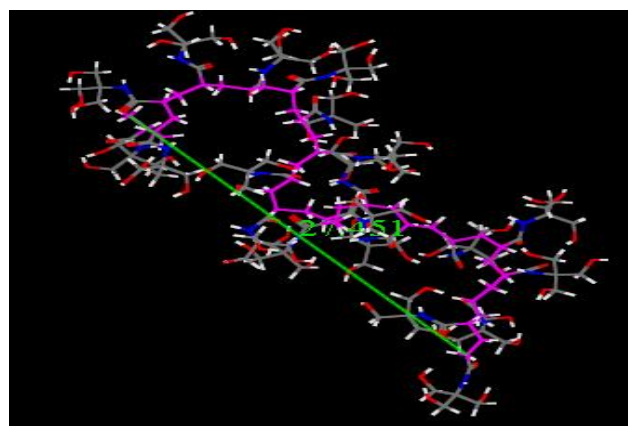


Figure 4.1 A graphical representation of the calculated $\langle s \rangle$ and $\langle r \rangle$ in Å° at $T=45,000\text{K}$ for polymers 1 to 29.



a



b

Figure 4.2a Atomistic structure of polymer 29 with the calculated $\langle r \rangle = 34.35 \text{ Å}^\circ$ at 45,000 K.

Figure 4.2b Atomistic structure of polymer 25 with the calculated $\langle r \rangle = 27.45 \text{ Å}^\circ$ at 45,000 K.

4.1.1.2. Molecular dynamics MD

Previous modeling studies [49,50] showed that the nature, strength and quantity of the interactions between the monomer units and the template determined MIP's selectivity. **Table 4.2** lists the calculated cohesive energies CE of the modeled ensembles containing a mixture of monomer units and the template molecule. It can be noticed that H-bondings are the main contributors to the CE values, and that the hydrophobic interactions are essential contributors but to a lesser extent. This can be concluded from the high CE values of polymers 25, 26, 28, and 29. They all possess many hydroxyl groups on their side chains that can interact favorably by H-bondings with the glucose hydroxyl groups. Polymers 27 and 30 have only a single hydroxyl group, but they are extremely rigid which could have forced the single hydroxyl group on the side chains to adopt an orientation that favored its interaction with glucose, moreover they could also interact by additional hydrophobic ring-ring interactions.

Table 4.2 The calculated cohesive energies CE of the modeled ensembles containing a mixture of monomer units and the template molecule.

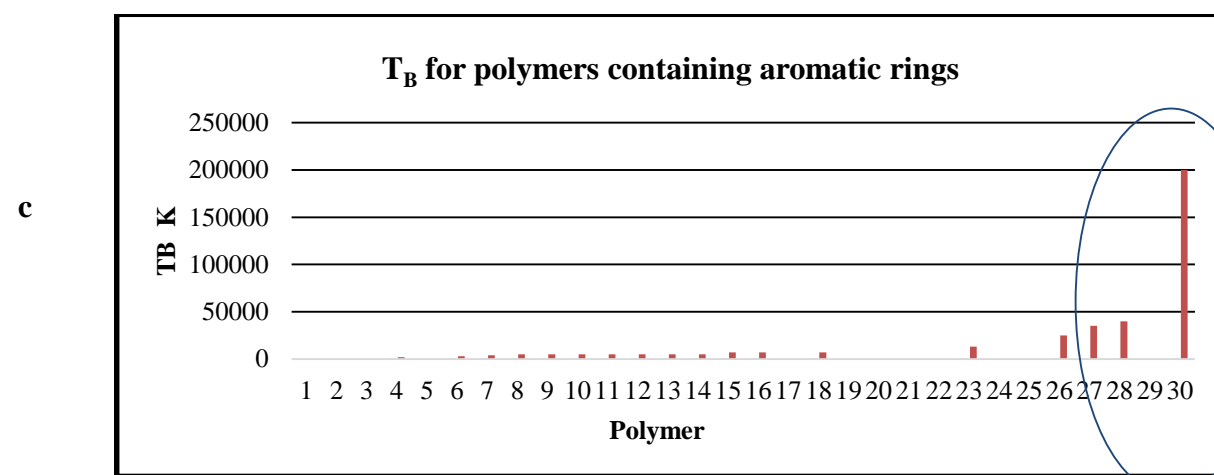
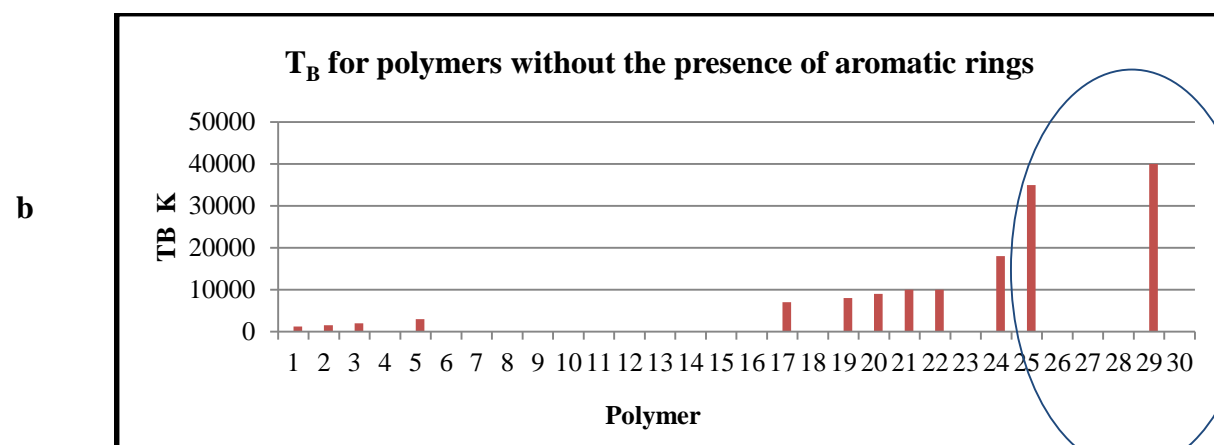
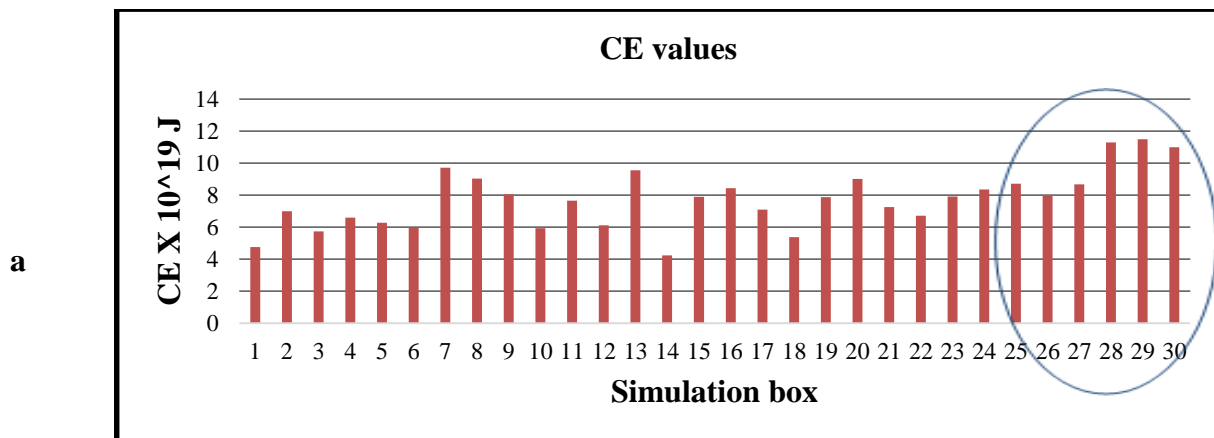
Modeled AC No.	Cohesive Energy CE (Joules) x 10¹⁹
1. Methacrylate	4.75
2. Acrylic acid	7
3. methacrylic acid	5.735
4. 4(5)-vinyl imidazole	6.6
5. Methacrylamide	6.27
6. 2-Allyl-6-methylphenol	5.95
7. Urocanic acid	9.72
8. Urocanic acid ethyl ester	9.04
9. 3-Allyl-4-hydroxybenzaldehyde	8.045
10. N-allyl- α -methyl benzylamine	5.931
11. 3'-Allyl-4'-hydroxyacetophenone	7.65
12. trans-3-(3-pyridyl)-acrylic acid	9.56
13. vinyl phenyl boronic acid	4.228
14. 3-(Acrylamido) phenylboronic acid	6.103
15. 2-Hydroxy-5-vinyl-benzaldehyde	7.889
16. 4-vinyl benzoic acid	8.431
17. 2-Hydroxyethyl acrylate	7.085
18. p-amino styrene	5.37
19. 2-(Trifluoromethyl) acrylic acid	7.867
20. Itaconic acid	9.008
21. N-(2-aminoethyl) methacrylamide	7.26
22. 4-Hydroxybutyl acrylate	6.713
23. 2-(4-vinyl-phenyl)propan-1,3-diol	7.907
24. 2-Carboxyethyl acrylate	8.36
25. N[Tris(hydroxymethyl) methyl]Acrylamide	8.71
26. 1-(2-allyl-phenoxy)-3-methylamino-propan-2-ol	8.022
27. 2-Hydroxy-3-phenoxypropyl acrylate	8.68
28. 4-vinyl benzyl-iminodiacetic acid	11.3
29. Acrylamido-2-methyl-1-propanesulfonic acid	11.5
30. 2-(4-Benzoyl-3-hydroxyphenoxy)ethyl acrylate	11

4.1.2. The selection of best four candidates

Data from the preliminary investigations were digested into 3 graphical representations as shown in **Figures 4.3 a,b,c**. It can be shown that CE values correlated well with the modeled polymers' rigidity (T_B values), especially at the higher ends.

Thus, the investigated polymers could be grouped into two categories. The first group **Figure 4.3b** contains the polymers bearing only hydroxyl groups on their side chains. These are expected to interact with the template by H-bondings only. The second group **Figure 4.3c** contains polymers bearing hydroxyl groups and aromatic rings. These are expected to interact with the template by H-bondings and hydrophobic ring-ring interactions. Consequently for the secondary conformational and MD analyses (section 4.1.3) four monomers were selected (polymers 25 & 29 **Figure 4.3b** and polymers 27 & 30 **Figure 4.3c**) based on their expression of both high CE values **Figure 4.3a** and high T_B values.

A fifth control monomer was selected based on its low T_B value **Scheme 4.1**, which is acrylic acid. Acrylic acid was also an excellent choice to represent the control polymer, because it is one of the most commonly used monomers in the literature in MIP synthesis.



Figures 4.3 The strategy of selection of the four monomers for secondary analysis.

4.3a Cohesive energy values for polymers 1. To 30.

4.3b T_B values for polymers without the presence of aromatic rings.

4.3c T_B values for polymers bearing aromatic rings.

The oval rings show the selected polymers for further secondary analyses.

4.1.3. Secondary analyses

The previously selected five monomers underwent deep secondary computational analysis. **Table 4.3** shows the updated calculated values of $\langle s \rangle$, $\langle r \rangle$ and CE of the five selected monomers resulting from the secondary analyses.

Table 4.3 The new calculated values of $\langle s \rangle$, $\langle r \rangle$ and CE for the five selected monomers.

Polymer No.	T_B Kelvins	$\langle s \rangle$	$\langle r \rangle$	CE X 10¹⁹ J
2	1500	9.083808	20.29673	3.92
25	35,000	11.61598	27.38338	8.13
29	40,000	11.60913	27.56315	8.11
27	35,000	12.67223	28.07813	6.96
30	200,000	13.96175	34.86542	8.16

From **Table 4.3**, it can be noticed that the calculated values were in good agreement with the previous assumptions. The control polymer 2 (lowest T_B) showed the lowest CE value. Polymers 25, 29, 27, and 30 had high CE values which could be directly correlated with their molecular expression of the functional groups essential for interacting with glucose, and also could be correlated with their high conformational stability and rigidity (high T_B).

Consequently, polymers 2, 29, and 30 (Acrylic acid (AA), Acrylamido-2-methyl-1-propanesulfonic acid (AMPSA), and 2-(4-Benzoyl-3-hydroxyphenoxy)ethyl acrylate (BHPEA) respectively) were selected for the practical investigations.

4.2. Experimental investigation

4.2.1. Template rebinding studies

(MIP) are known to possess a memory of the conformational structure of the binding sites created during synthesis, including also the types of interactions taking place within the cavities. This memory is best regained when the binding experiments take place in the same solvent(s) previously used during the synthesis procedure. Thus template rebinding studies were all employed in DMSO.

4.2.1.1. Template rebinding studies at room temperature

Figure 4.4 shows the amount of glucose bound per each polymer. It can be shown that all MIPs have bound certain amounts of glucose. All NIPs did not bind any glucose amounts with the exception of NIP 2. These findings could be explained as follows:

- i) All the MIPs recalled the memory of glucose binding within the glucose-monomer complexes formed during the synthesis. This memory was stored in the form of complimentary cavities within each MIP during its synthesis. However NIPs did not recall such memory, because they were synthesized in the absence of the template.
- ii) Although both MIPs and NIPs were synthesized under exactly the same conditions, with the exception of the template presence, however still MIPs could bind glucose, because they could possess complimentary binding sites within crosslinked networks that could retain such sites and could retain channels through which the template moved out during extraction, and moved in during binding. NIPs resisted the flow of glucose through its crosslinked networks due to the absence of the complimentary cavities and the absence of the channels that lead to such cavities.
- iii) NIP 2 is the only NIP that exhibited relatively small binding to glucose owing to the presence of non-specific interactions. Non-specific interactions are the interactions taking place between the monomer functionalities and the template outside the binding sites, i.e the monomer functionalities that are normally expressed on the polymer chains outside the cavities and could bind the template. These interactions are expressed to some detectable extent only in

NIP 2, because of the significant expression of H-bonding capable moieties (three polar functionalities) in the structure of each monomeric unit AMPSA *Figure 4.5* that builds up both MIP 2 and NIP 2. Such functionalities have the ability to H-bond with the hydroxyl groups on glucose molecules, and are not significantly expressed on AA and BHPEA. These non-specific interactions are also expected to be present within MIP 2, because it is built up of the same monomeric unit. Still, MIP 2 had a high (IF) of 15.63. The value of IF is directly correlated with the significant contribution of the specific interactions. Specific interactions in MIP 2 are based also on H-bonds between the polar groups in the structure of the monomeric unit AMPSA and the hydroxyl groups on glucose molecules, and they are mainly located within the complimentary binding sites *Figure 4.5*. However non-specific interactions are usually concentrated on the polymeric chains surfacing the crosslinked network, and thus they do not alter the conformational organization of the NIP.

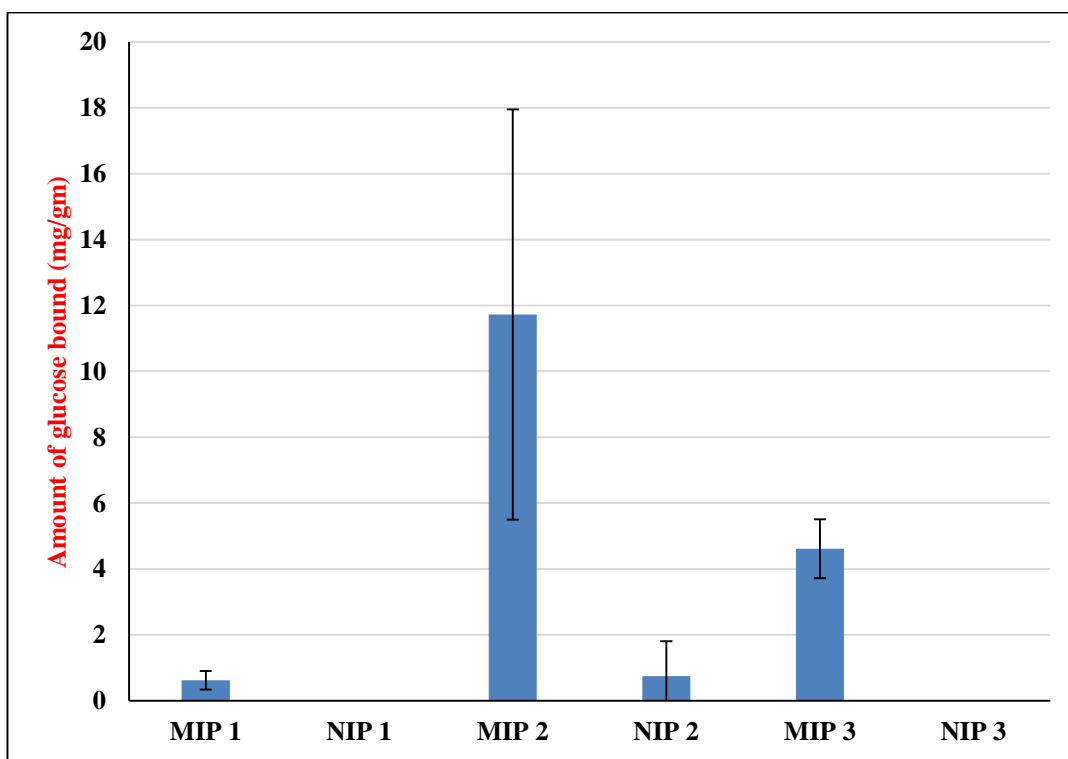


Figure 4.4 Graphical representation of the amount of glucose bound mg/gm for the polymers.

iv) It is worth mentioning that MIP 2 (polymer 29) and MIP 3 (polymer 30) had significant higher glucose bindings compared to MIP 1 (polymer 2) *Figure 4.4*. This finding is in

agreement with the previously calculated CE values shown in **Table 4.3**, where AMPSA and BHPEA monomers (building blocks of MIP 2 and MIP 3 respectively) showed higher CE than AA monomer (MIP 1 building block). For MIP 1, it can be postulated that template associations was more favorable than template monomer associations in the pre-polymerization mixture during MIP 1 synthesis.

v) It can be noticed from **Figure 4.4** that although MIP 2 had higher binding capacities (almost triple) than that of MIP 3, the error bars are also significantly bigger. This can directly validate that the high conformational stability of the cavities within MIP 3 enhanced the reproducibility and directly affected its calculated binding capacities.

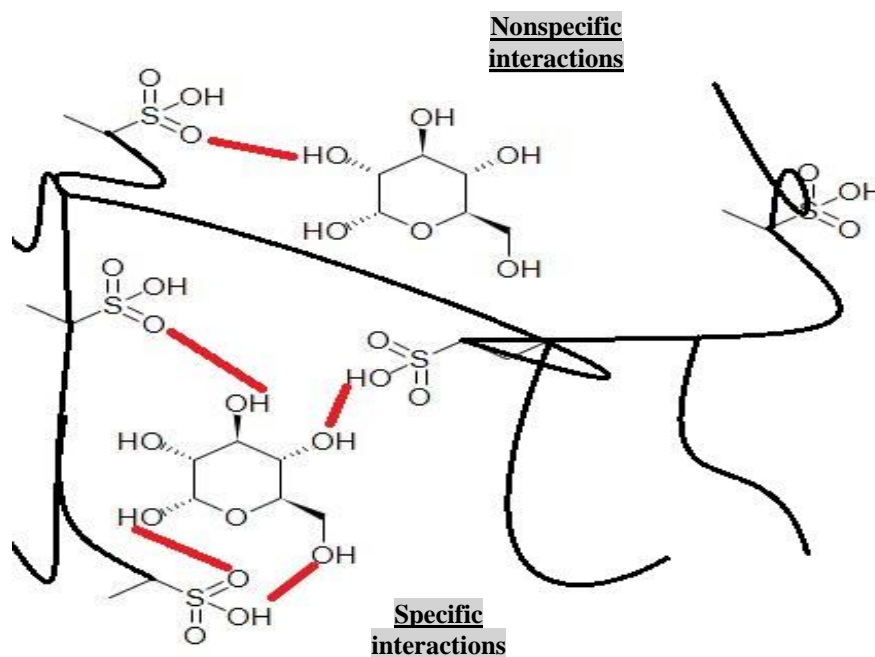


Figure 4.5 Specific H-bond interactions (Red) between glucose and the monomeric units *inside* the cavities of MIP 2. Non-specific H-bond interactions (Red) between glucose and the monomeric units *outside* the cavities of MIP 2.

4.2.1.2. Template rebinding studies at 50°C

One major drawback of proteins in biochemical sensing applications is that their binding sites are highly labile to changes in the surrounding media. It was also reported that the geometry of proteins' binding sites can be altered by the binding of its ligands [51] (ligands here mimic templates in MIPs). This could affect the reproducibility of its results after repeated use in

sensing applications. Also, it has been reported that MIPs could suffer from the same drawback to a lesser extent, in which the polymeric chains change their conformations in response to pH, solvent, or temperature [12,52]. This could be a major drawback in chemical sensing applications, especially in tropical countries. Thus template rebinding studies at 50°C was attempted for MIPs 1, 2, 3 in order to study the correlation between their calculated T_B values **Schemes 4.1, 4.2** and their conformational stability at high temperature. **Figure 4.6** shows the amount of glucose bound by each MIP at 50°C in comparison with that bound at room temperature RT of 25°C \pm 2. It can be shown that at 50°C MIP 1 exhibited a significant increase in the amount of glucose bound (8.94 mg/gm) in comparison with RT (0.62 mg/gm), but MIP 3 showed a slight increase in the amount of glucose bound (5.14 mg/gm) in comparison with RT (4.61 mg/gm). This could accurately validate the conformational stability studies in the computational modeling. MIP 1 is based on AA monomer units, whose polymeric chain exhibited low conformational stability $T_B = 1500$ K, but MIP 3 is based on BHPEA, whose polymeric chain exhibited the highest conformational stability $T_B = 200,000$ K. This showed that at high temperature AA polymeric chains within the MIP cavities **Figure 4.7** acquired enough energies to move and deform within the crosslinked network, thus allowing more and more glucose molecules to diffuse and interact non-specifically with the hydroxyl groups expressed on the polymeric chains **Figure 4.9**. However BHPEA polymeric chains are highly rigid because they contain rigid aromatic rings on the side chains that could retain the conformational shape of the binding sites **Figure 4.8** even at high temperatures.

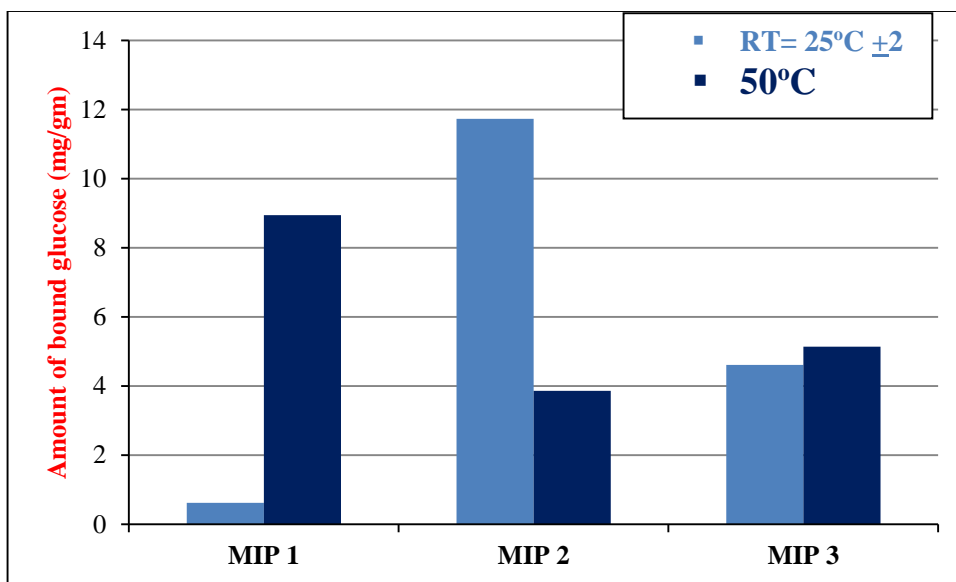


Figure 4.6 The amount of glucose bound by each MIP at Room temperature and 50°C respectively.

It was surprising that MIP 2 exhibited a completely different behavior, where the amount of bound glucose decreased significantly *Figure 4.6*. Although MIP 2 is based on AMPSA monomer units whose polymer chains showed high rigidity $T_B = 40,000$ K, which is an

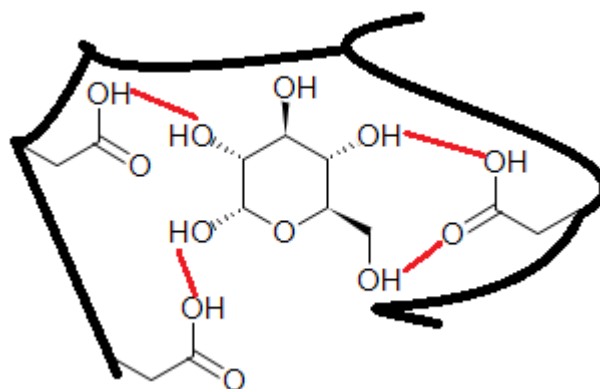


Figure 4.7 A schematic representation of MIP 1 cavity showing H-bond (Red) interactions.

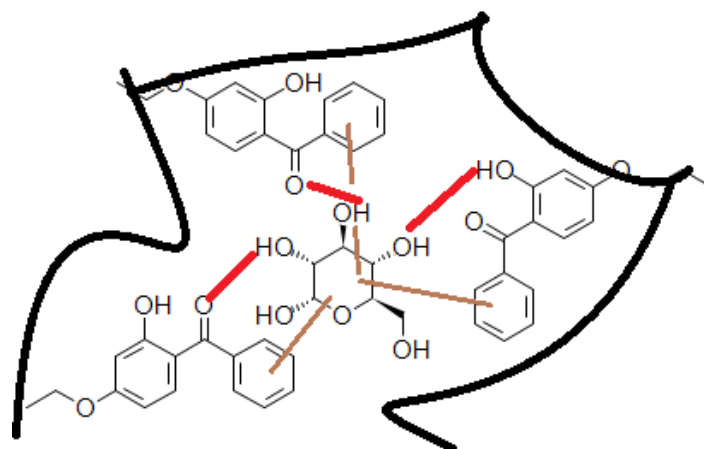


Figure 4.8 A schematic representation of MIP 3 cavity showing H-bond (Red) and hydrophobic ring-ring interactions (Brown).

intermediate value between that of AA and BHPEA polymer chains. This could be explained based on that AMPSA side chains contain several polar functionalities that interact in a concerted fashion with the hydroxyl groups on glucose molecules **Figure 4.5**. It has been reported that polar groups and H-bonds weaken at high temperatures [53], which could also have resulted in the alteration of the association geometry between the templates and the monomeric units, and consequently binding affinity decreased significantly. It should be noted that the binding affinity of BHPEA to glucose molecules is assumed to be based on the harmonization of H-bond and hydrophobic ring-ring interactions **Figure 4.9**. This could further explain the insignificant alteration in its binding capacity at high temperatures.

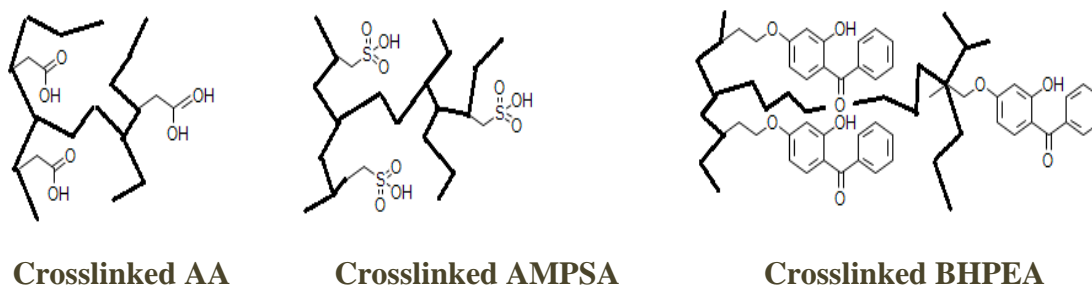


Figure 4.9 Schematic representation of crosslinked networks of MIPs 1, 2,3.

4.2.1.3. Template rebinding studies at room temperature for MIPs 3,4,5

It has been concluded in the previous section that BHPEA based MIP 3 is a highly rigid MIP and could retain the conformational stability of its binding sites at room and high temperatures. Thus it was very interesting to study how would reducing the crosslinking density affect the performance of BHPEA based MIPs. It is well established that most MIPs are synthesized with high crosslinking densities in order to maintain the physical and mechanical integrity of the network, however this has the disadvantages of limiting template removal during extraction and limiting template diffusion during binding, which consequently limit the binding capacities of the produced MIPs. Thus low crosslinking density 70% MIP 4 and 50% MIP 5 were synthesized in order to study if the high rigidity of the monomer could have the advantage of producing low crosslinking density MIPs without affecting their binding capacities. **Figure 4.10** shows the amount of glucose bound for MIPs 3,4,5. It was found that the aforementioned assumptions did not go right. **Figure 5.0** shows that still MIP 3 (80% crosslinking density) had higher binding capacities (4.61 mg/gm) than MIP 4 (0.73 mg/gm) and MIP 5 (2.68 mg/gm). This could prove that for the studied amounts of monomer and template, the high crosslinking density is still highly essential to maintain MIP integrity and consequently maintain its high binding capacity and specificity to the template, even when using highly rigid monomeric units. It can be postulated that a rigid monomer is essential for the conformational stability of the binding site, and that the high crosslinking is essential for maintaining the configurational network structure of the whole MIP. MIP 5 and NIP 5 showed significant glucose binding, with NIP 5 slightly exceeding MIP 5. This could be explained based on their low crosslinking densities that allowed uncontrolled diffusion of the template throughout the network, and also prevented the appropriate formation of a physically integral binding site **Figure 4.11**. The template diffused freely through the loose network **Figure 4.11** and could interact non specifically with the exposed functionalities on the side chains. MIP 4 still could retain to some extent good specificity to the template, but at a lower capacity. These results correlated well with the study conducted by Bodugoz et al [22] that reported the use of long crosslinkers PEG600DMA (chain length 754) in an attempt to enhance the binding capacity. However the MIP synthesized using PEG600DMA showed reduced binding capacities compared to those synthesized using the crosslinker TEGDMA (chain length 330).

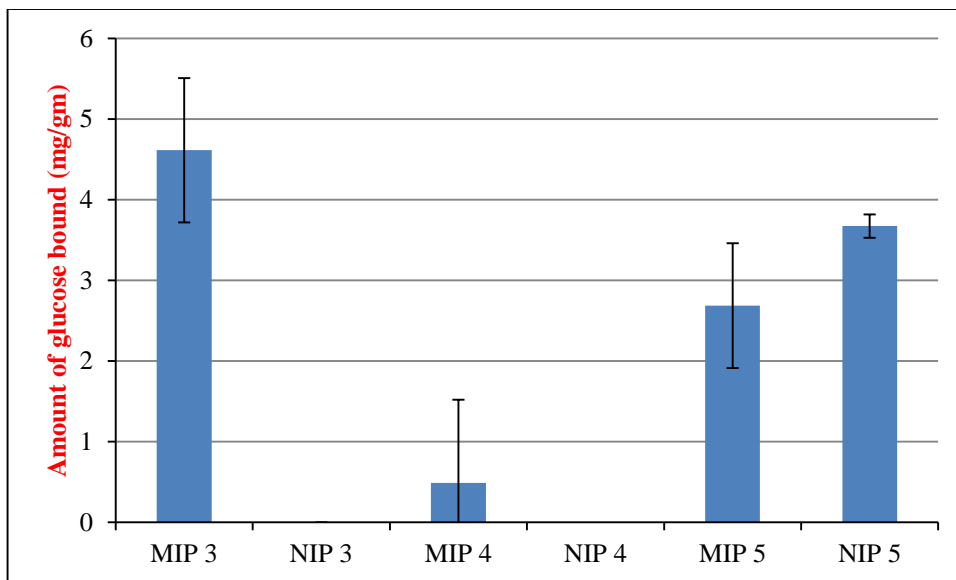


Figure 4.10 The amount of glucose bound for MIPs 3,4,5 at RT.

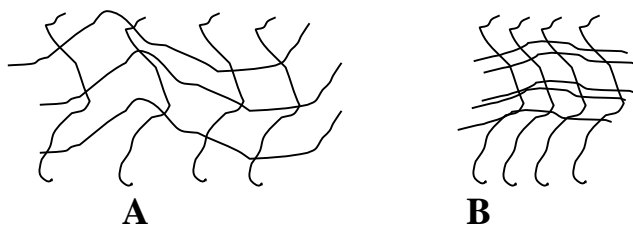


Figure 4.11A Loose polymeric network at low crosslinking density.

4.11B Compact polymeric network at high crosslinking density.

4.2.2. Fourier Transform Infra-Red Spectroscopy (FT-IR)

4.2.2.1. AA based polymers (MIP 1, NIP 1, P 1)

The successful crosslinking of the synthesized polymers was validated by the expression of the C-H bend of -CH₃ and -CH₂ in the (FT-IR) spectra. The C-H bend of -CH₃ and CH₂ bands are expressed at 1407cm⁻¹ and 1438 cm⁻¹ in P 1 (The synthesized MIP 1 before template removal) **Figure 4.12**. The same bands are expressed at 1391 cm⁻¹ and 1459 cm⁻¹ in both the MIP and NIP. This confirms the highly close resemblance of the chemical functionalities in both MIP and NIP, which are normally synthesized under the same conditions with the exception of the template presence during the synthesis of MIPs. By close observation to **Figure 4.12**, it can be observed that the C=O stretch are expressed at nearly the same wave numbers 1727 cm⁻¹, 1731cm⁻¹, 1731 cm⁻¹ for P 1, MIP 1, NIP 1 respectively.

The -OH stretch peaks at 3445 cm⁻¹ and 3449 cm⁻¹ for the NIP and MIP have nearly the same broadness and shapes. However the same -OH stretch peak in P 1 is shifted towards 3419 cm⁻¹ and showed much more broadness. This confirmed the presence of glucose molecules and their interaction by H-bond with the monomeric units in P 1, and also proved the successful removal of the template molecules during the extraction process. Based on the very close resemblance of the (FT-IR) charts for both the MIP and NIP especially at the -OH stretch region, it can be postulated that there is a direct correlation between the insignificant glucose binding to both MIP 1 and NIP 1, and their (FT-IR) charts.

4.2.2.2. AMPSA based polymers (MIP 2, NIP 2, P 2)

Similarly, the C-H bend of CH₃ and CH₂ bands are shown at 1390 cm⁻¹ and 1456 cm⁻¹ respectively in both the MIP and NIP, which confirms the highly close resemblance of the chemical functionalities in both MIP and NIP **Figure 4.13**. The same bands are expressed at 1406 cm⁻¹ and 1437 cm⁻¹ in P2 (The synthesized MIP 2 before template removal). By careful observation to **Figure 4.13**, it can be observed that the C=O stretch are expressed at nearly the same wave numbers 1724 cm⁻¹, 1731 cm⁻¹, 1728 cm⁻¹ for P 3, MIP 3, NIP 3 respectively.

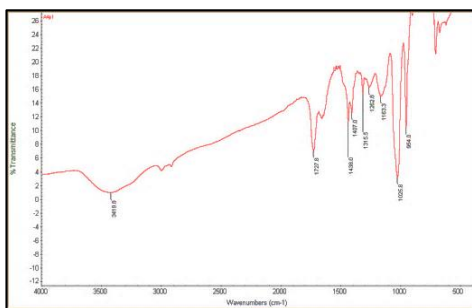
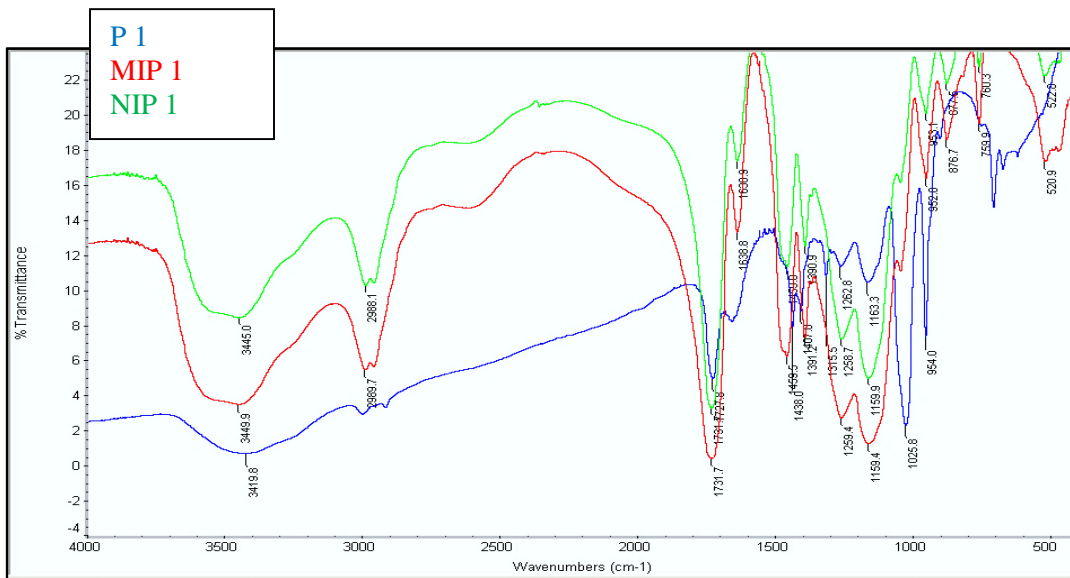
On the contrary to MIP 1 and NIP 1 **Figure 4.12**, the OH peak in MIP 2 did not resemble that in NIP 2. The OH peak is more broad in MIP 2(at 3444 cm⁻¹)than in NIP 2(at 3431 cm⁻¹),

which was due to the presence of the template during synthesis, which interacted with the expressed hydroxyl groups on the monomeric side chains, and after its removal, it left behind different orientations of OH groups that caused peak broadening. The OH peak in P 2 is the broadest peak owing to the significant interactions between the monomeric units and glucose.

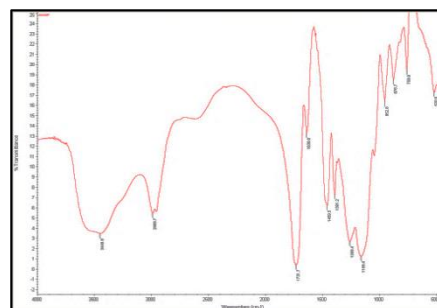
4.2.2.3. BHPEA based polymers (MIP 3, NIP 3, P 3 before template extraction)

Similarly, the C-H bend of CH₃ and CH₂ bands are expressed at 1388 cm⁻¹ and 1454 cm⁻¹ respectively in both the MIP and NIP, which again confirms the highly close resemblance of the chemical functionalities in both MIP and NIP **Figure 4.14**. The same bands are expressed at 1344 cm⁻¹ and 1439 cm⁻¹ in P 3(The synthesized MIP 3 before template removal). By careful observation to **Figure 4.14**, it can be shown that the C=O stretch are expressed at nearly the same wave numbers 1728 cm⁻¹, 1732 cm⁻¹, 1731 cm⁻¹ for P 3, MIP 3, NIP 3 respectively.

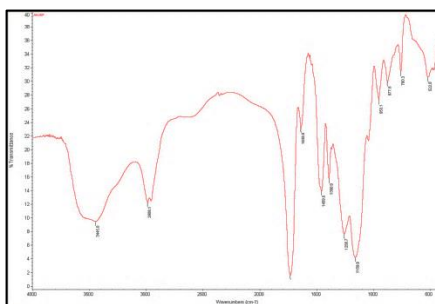
The OH peak in both the MIP and NIP had nearly the same wave numbers 3444 cm⁻¹ and 3447 cm⁻¹ respectively, but it was slightly narrower and had slightly higher transmittance in the MIP. This validates the effective template removal, and that the slightly different orientations of the hydroxyl groups are due to the creation of specific interactions in the MIP. In contrast to AMPSA and AA based polymers **Figures 4.13** and **4.13**, the OH stretch peak in P 3 was narrower than that of both MIP 3 and NIP 3, had higher transmittance, and was expressed at 3432 cm⁻¹. This confirmed that the single hydroxyl groups on the polymeric side chains are sterically hindered ones owing to the presence of 2 rigid aromatic rings in close proximity to each one. The high transmittance shows that the rings were not only sterically hindering the orientation of the hydroxyl groups, but also they were contributing to the binding interactions with the glucose molecules.



P 1

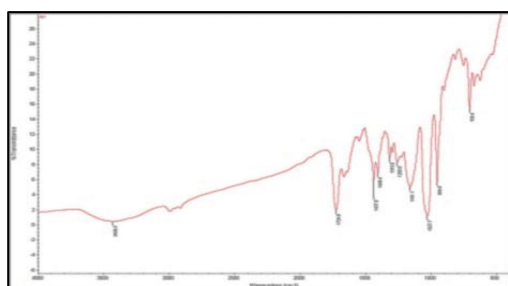
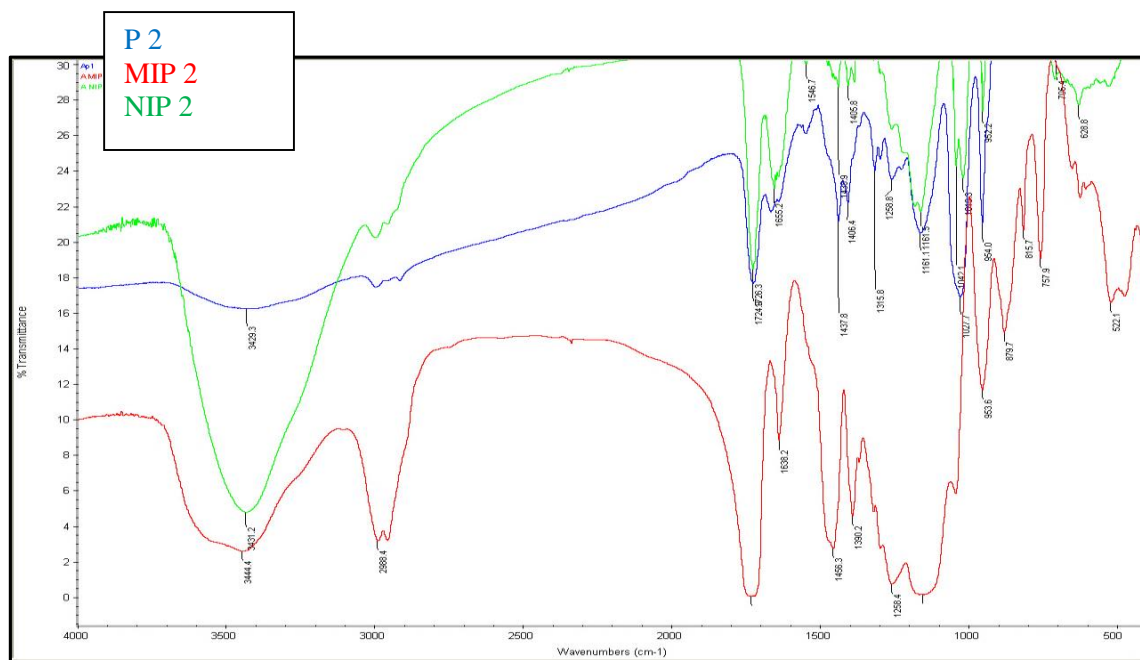


MIP 1

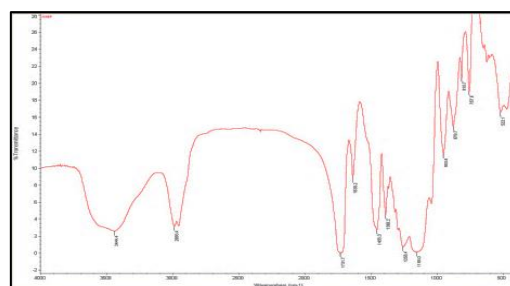


NIP 1

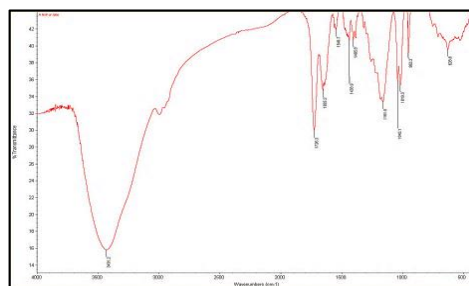
Figure 4.12 FT-IR charts of P 1, MIP 1, and NIP 1.



P 2



MIP 2



NIP 2

Figure 4.13 FT-IR charts of P 2, MIP 2, and NIP 2.

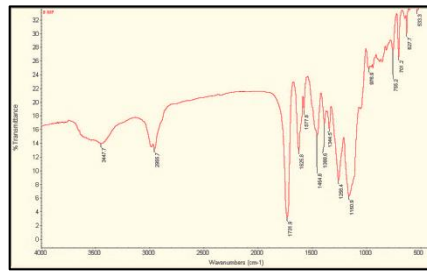
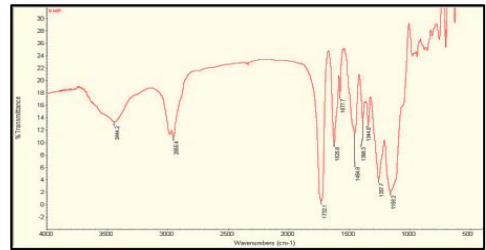
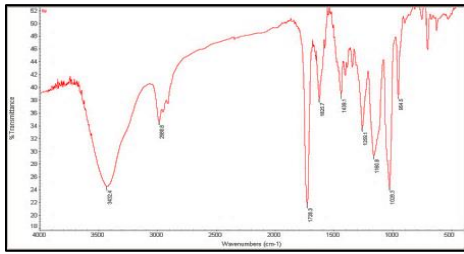
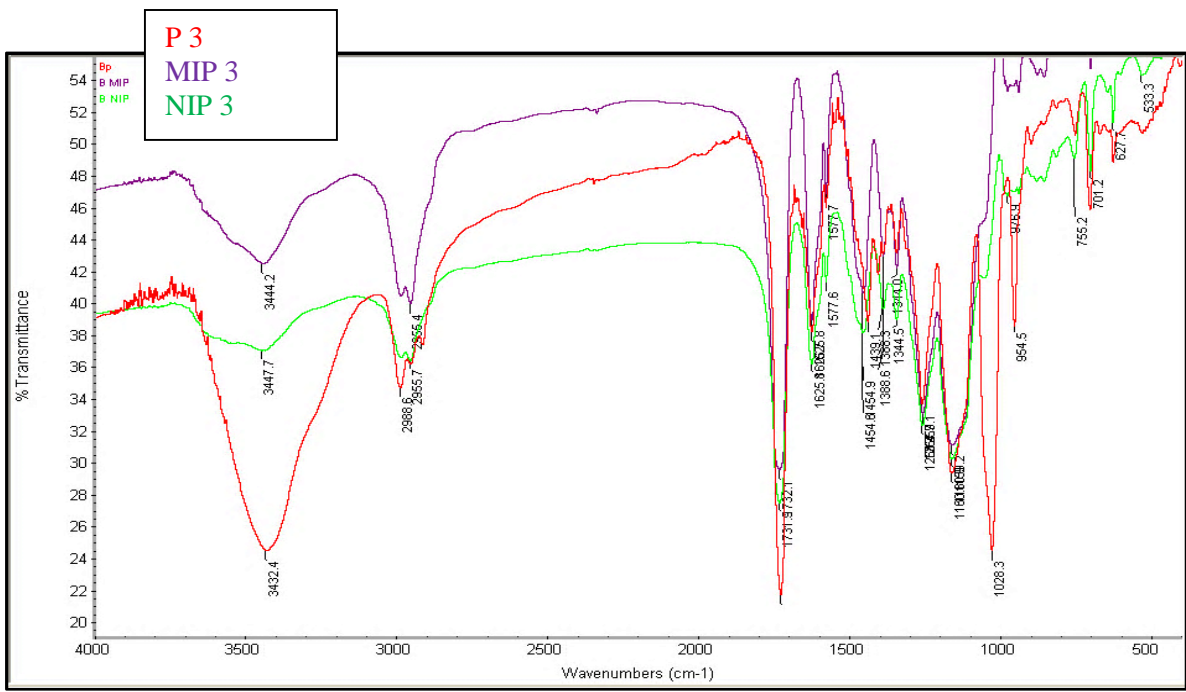


Figure 4.14 FT-IR charts of P 3, MIP 3, and NIP 3.

4.2.3. Scanning Electron Microscopy (SEM)

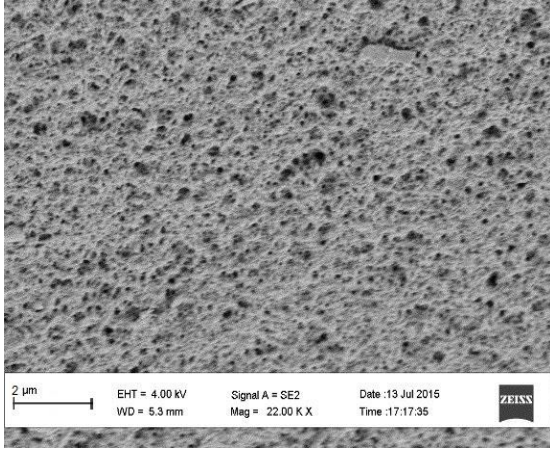
Morphological characterisation was performed by SEM. Morphological characterization can give information about the distribution of pores, pore channels and cavities greater than 50nm (which are constructed for aggregates of templates in MIPs). Such porous texture could be directly correlated to the performance of the polymers. It has been reported [13] that template presence could alter the nucleation, growth and network formation of MIPs compared to their respective NIPs.

4.2.3.1. SEM of MIPs 1,2,3 and NIPs 1,2,3

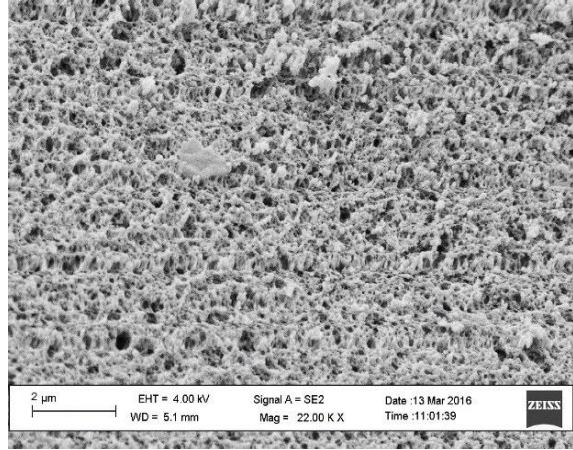
The SEM micrographs of MIPs 1,2,3 and NIPs 1,2,3 showed that all the polymers had rough surfaces **Figure 4.15**. The surface morphology of MIP 1 slightly differed from that of NIP 1, and the distribution of pore channels for both was nearly the same. And this could further validate the weak binding behavior of MIP 1 and NIP 1. However in MIP 2, the presence of the template greatly enhanced the homogeneity of distribution of the pores and pore channels in comparison with the pore channel distribution in NIP 2. Finally the SEM micrograph of MIP 3 showed significant better pore channel distribution and wider pores than those shown in NIP 3. This could further directly validate the better performances of MIP 2 and MIP 3.

4.2.3.2 SEM of MIPs 3,4,5 and NIPs 3,4,5

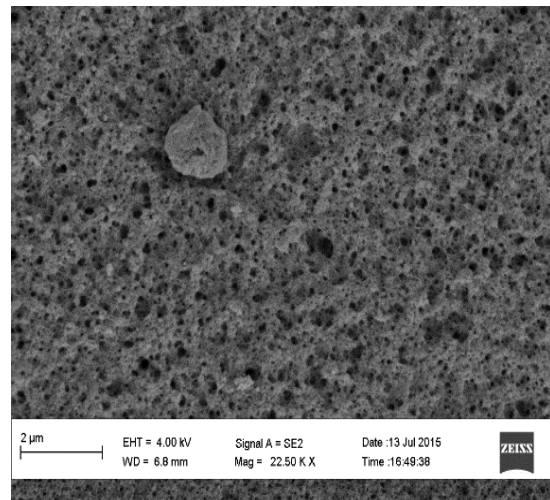
Figure 4.16 shows the morphological characterization of MIPs 3,4 and 5 and NIPs 3,4 and 5. It can be observed that MIP4, MIP 5 and their corresponding NIPs had negligible differences in their surface morphologies. In addition, MIP 5 and NIP 5 had relatively flat surfaces compared to the other polymers. Although MIP 4 and NIP 4 showed good pore channel distribution, but still they had bad performances **Figure 4.10**. Thus it can be postulated that the high crosslinking density whether in MIPs or NIPs are the main determinant of the pore channel distribution. Another finding can be postulated from the flat morphologies of MIP 5 and NIP 5, is that they exhibited unclear porosity (or may be very small undetectable nanopores), but still they showed better glucose binding than the highly crosslinked MIP 4 and NIP 4. This could be concluded in that the binding was mainly surface binding, and that's why it was highly non specific.



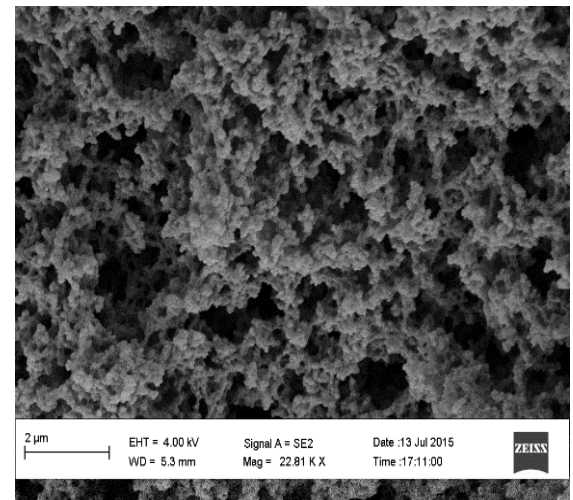
MIP 1



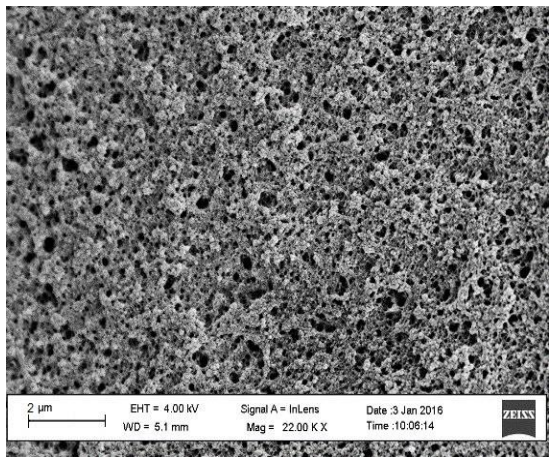
NIP 1



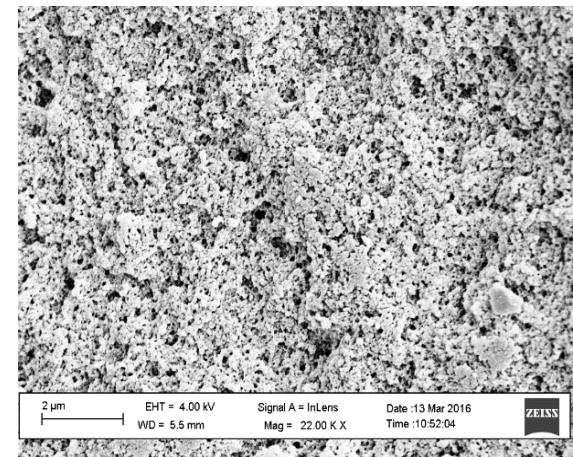
MIP 2



NIP 2

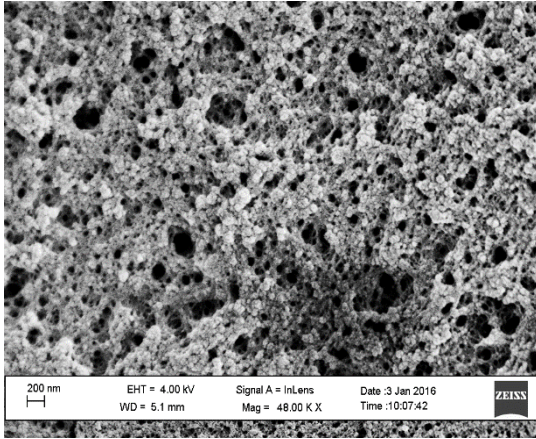


MIP 3

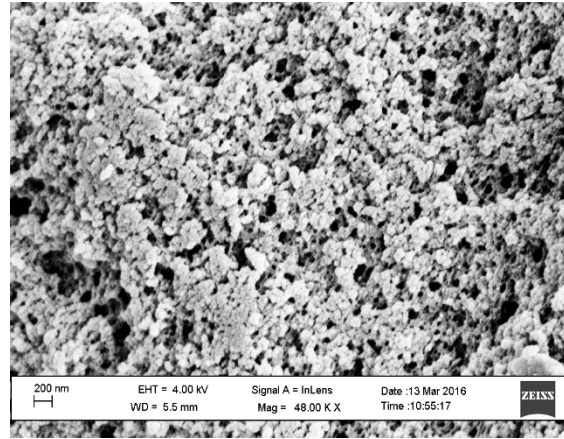


NIP 3

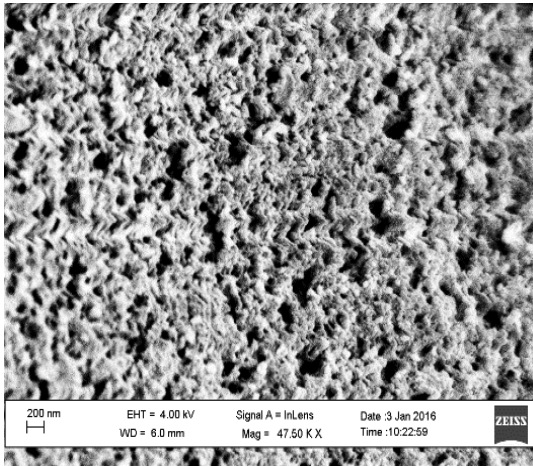
Figure 4.15 SEM micrographs at 22,000 magnifications.



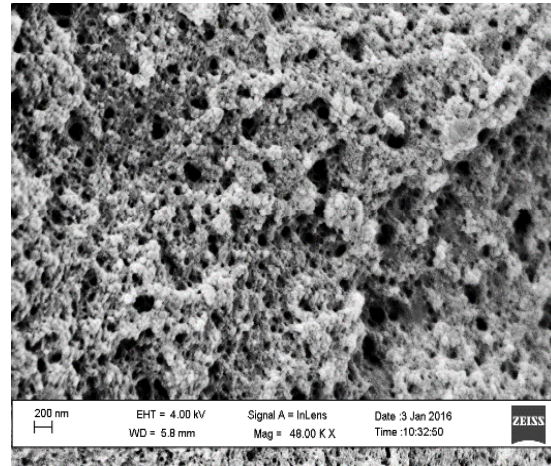
MIP 3



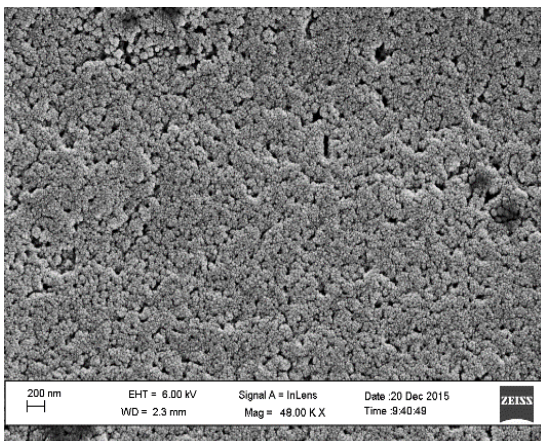
NIP 3



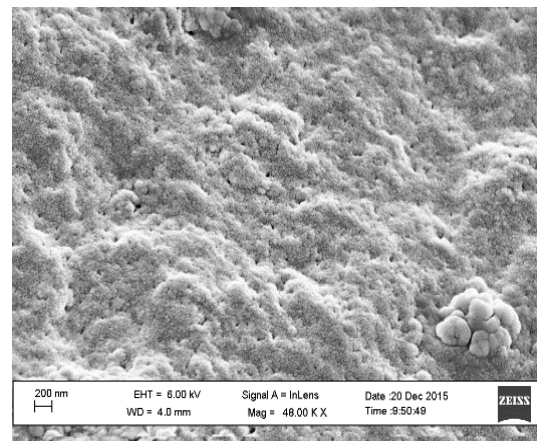
MIP 4



NIP 4



MIP 5



NIP 5

Figure 4.16 SEM micrographs at 48,000 magnifications.

4.2.4. Thermogravimetric Analysis (TGA)

TGA was successfully employed to give information about the thermal stability of MIPs 1,2,3 and NIPs 1,2,3. **Figures 4.17, 4.18, 4.19** show the thermograms of MIP 1, NIP 1, and MIP 2, NIP 2, and MIP 3, NIP 3 respectively. All the MIPs show relatively similar thermal stabilities compared to their respective NIPs, with the exception of MIP 2 and NIP 2, where NIP 2 exhibited a relatively lower thermal stability than MIP 2. This shows that the thermal stability of the synthesized polymers was not significantly affected by the presence of the template.

Table 4.4 shows the onset decomposition temperature T_{onset} of all the polymers. MIP 1 and NIP 1 were based on the least conformationally stable AA polymeric chain ($T_B=1500\text{K}$), and this could explain its relatively lower T_{onset} compared to the other polymers. NIP 2 showed a steep decline in its thermal stability following its T_{onset} .

Table 4.4 The onset decomposition temperature T_{onset} for the polymers

Polymer No	T_{onset}
MIP 1	225°C
NIP 1	225°C
MIP 2	300°C
NIP 2	100°C
MIP 3	300°C
NIP 3	300°C

Figure 4.20 shows the thermograms of MIPs 1,2,3. Although MIP 3 had the same T_{onset} as MIP 2, but still MIP 3 showed higher resistance to thermal degradation, because the weight percent at the T_{onset} was relatively higher than that of MIP 2. The thermal stability of the MIPs followed the order MIP 3 > MIP 2 > MIP 1. This order was in coherence with the T_B values of their respective polymeric chains $\text{BHPEA}_{\text{chain}}(T_B=200,000\text{K}) > \text{AMPSA}_{\text{chain}}(T_B=40,000\text{K}) > \text{AA}_{\text{chain}}(T_B=1500\text{K})$. Thus it can be concluded that the rigidity of the polymeric backbone could be directly correlated with its thermal stability, especially that MIP 1 exhibited early degradation on its thermogram.

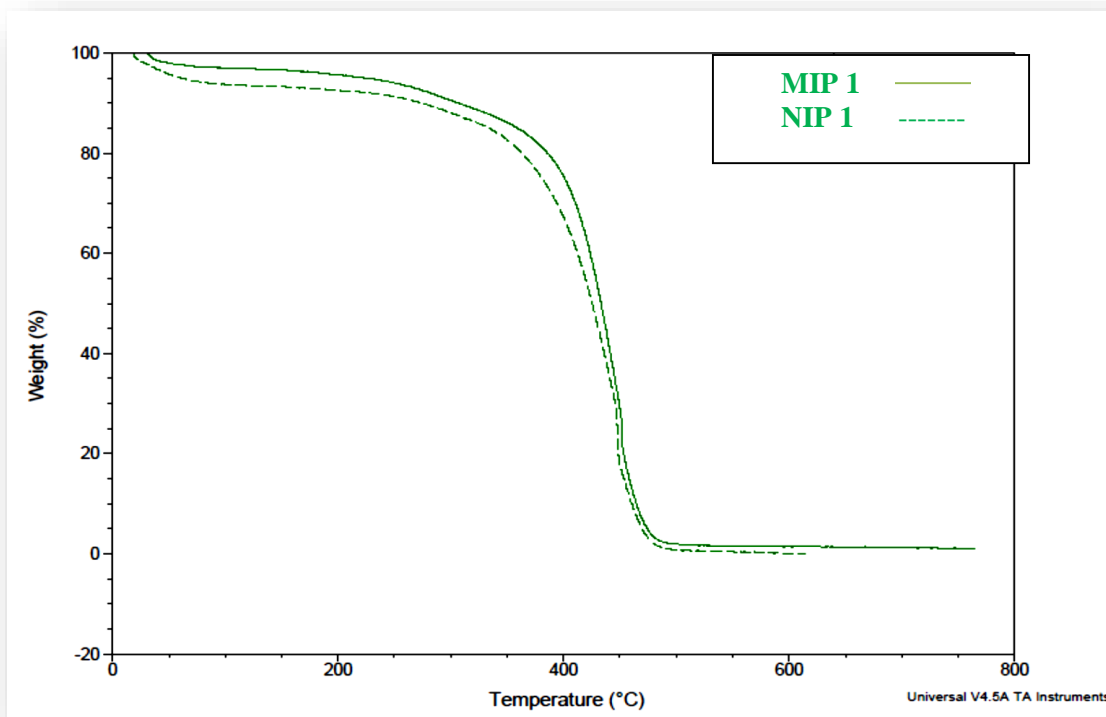


Figure 4.17 TGA thermograms of MIP 1 and NIP 1.

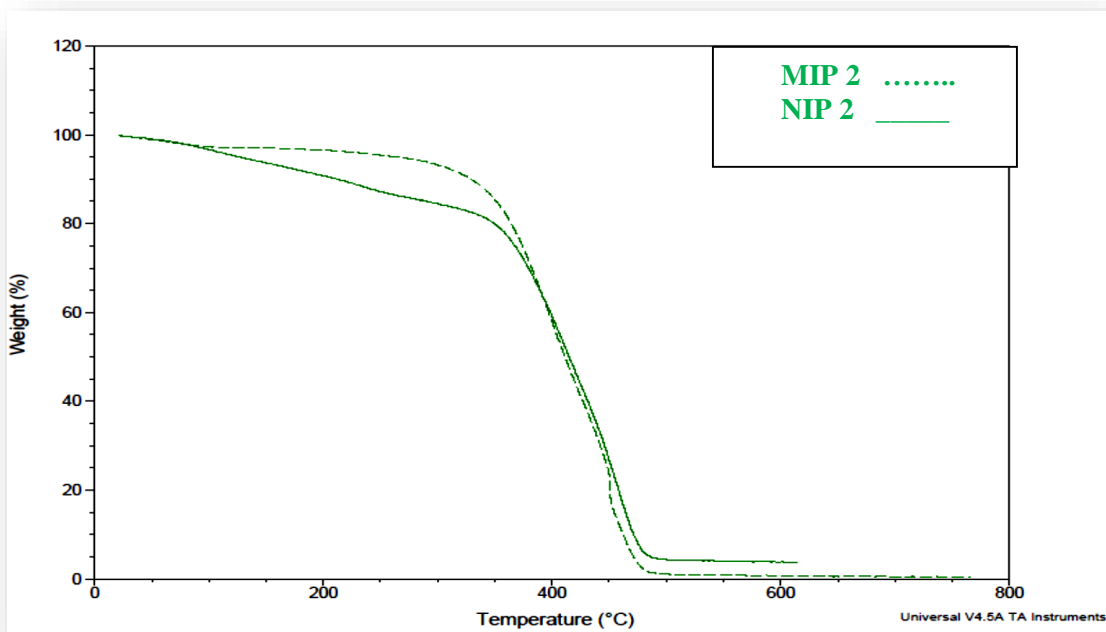


Figure 4.18 TGA thermograms of MIP 2 and NIP 2.

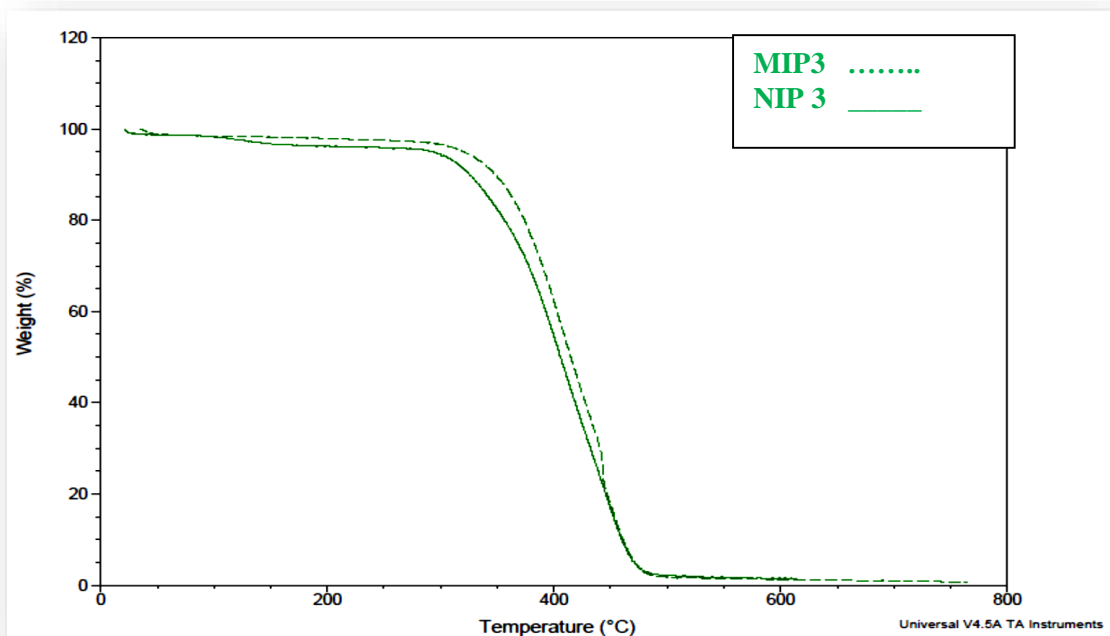


Figure 4.19 TGA thermograms of MIP 3 and NIP 3.

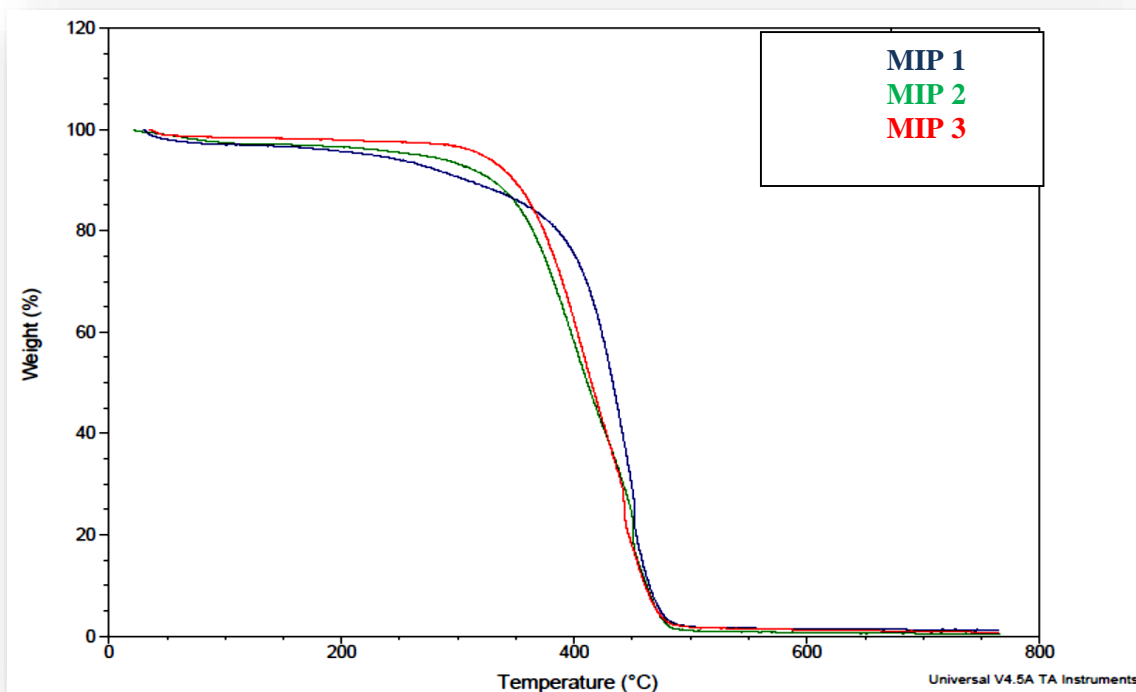


Figure 4.20 TGA thermograms of MIP 1, MIP 2 and MIP 3.

4.2.5. BET porosity analysis

The surface areas and porosity of the prepared MIPs 1,2,3 and NIPs 1,2,3 were evaluated. The nitrogen gas sorption isotherms of all the prepared polymers showed hysteresis, which was shown to be greater in MIPs as compared to their corresponding NIPs, indicating the presence of mesoporosity (pores in the range of 2-50nm) **Figures 4.21-4.26**. It can also be observed that the desorption branch never coincided with the adsorption branch at the starting point ($x=0$), i.e the loop never closed at the origin. This was commonly reported for these kinds polymeric systems, and was explained based on the entrapment of the adsorbed nitrogen molecules within narrow pores, or due to the incomplete template extraction from such narrow pores in cases of MIPs [15,54].

Table 4.5 shows the calculated BET surface areas, BJH adsorption and desorption pore volumes and areas for the polymers. The table shows that MIPs and NIPs have different BET surface areas, with the control polymers NIPs possessing higher values than their corresponding MIPs. This was explained elsewhere [12] based on the possible shrinkage of the cavities after the template extraction, due to the shift of the temperature from the polymerization temperature (60°C) to the extraction temperature (room temperature). This again validates that the template presence could affect the polymerization events resulting in different porosities [55].

Figures 4.27-4.32 show the pore distribution obtained from BJH desorption. It can be shown that the chart shapes of pore volume and pore area distributions are relatively similar for the same type of polymer (MIP 1 and NIP 1, MIP 2 and NIP 2, MIP 3 and NIP 3). MIP 1 and NIP 1 show different peak pore diameters **Figures 4.27-4.28**, MIP 1 had two peak pore diameters 10nm and 15nm, while NIP 1 had wider pore distribution with four peak diameters 4nm, 7nm, 11nm, and 15nm. MIP 3 and NIP 3 showed also different behaviors **Figures 4.31-4.32**. MIP 3 had two peak diameters at 10nm and 14nm, while NIP 3 had three peak diameters 7nm, 9nm, and 16nm. The pore areas and pore volumes in NIP 3 are distributed over a wider pore diameter range. However both MIP 2 and NIP 2 had a peak pore diameter at 14nm, but with higher incremental pore volumes and areas for the NIP compared to the MIP. Thus it can be shown that template presence homogenized the distribution of pores, and narrowed the pore diameter ranges throughout the MIP networks.

This could be directly correlated to the presence of template specific nanoscaled cavities.

The pore diameters' distributions for all the polymers showed a trend in that pore volumes decreased with increasing pore diameters *Figure 4.33*. MIPs specifically showed a narrower volume distribution for the pores compared to their corresponding NIPs. This was greatly manifested in the wider curves of NIP 1 and NIP 3 compared to their corresponding MIPs. Thus, it can be concluded that template presence could greatly affect the formation of narrowed and ordered pore diameter distributions due to the complexation between the template and the monomer functionalities, in addition to the creation of template specific cavities.

Although MIP 2 proved to have a significant higher binding capacity compared to NIP 2, however MIP 2 and NIP 2 did not have different pore distributions. This could be explained based on the significant expression of the hydroxyl group functionalities on both the MIP and NIP *Figure 4.6*, and consequently the higher MIP 2 binding capacity was due to the creation of specific template complimentary binding sites, that were absent in the NIP.

Table 4.5 The BET surface areas, BJH adsorption and desorption pore volumes and areas for the polymers.

	MIP 1	NIP 1	MIP 2	NIP 2	MIP 3	NIP 3
BET surface area (m² / g)	83.7436	132.8810	128.0026	260.3108	189.3616	208.8921
Adsorption average pore width (4V/A by BET) (nm)	8.09606	8.88374	5.29886	3.72733	6.61597	9.45418
BJH Adsorption cumulative surface area of pores*(m² / g)	71.437	112.444	103.782	155.431	160.683	182.953
BJH Desorption cumulative surface area of pores*(m² / g)	178.3636	193.3753	204.6768	231.4281	228.8783	222.2929
BJH Adsorption cumulative volume of pores*(cm³/g)	0.156421	0.311371	0.142710	0.181864	0.276478	0.461094
BJH Desorption cumulative volume of pores*(cm³/g)	0.175333	0.343850	0.183703	0.215758	0.327681	0.508303

* *Between 1.70 nm and 300.00 nm diameter (m² / g)*

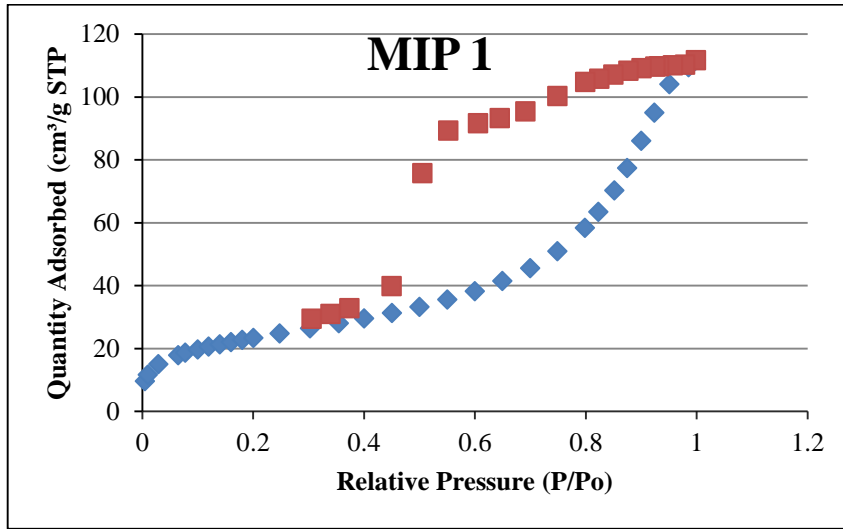


Figure 4.21 Linear isotherm plot of MIP 1.

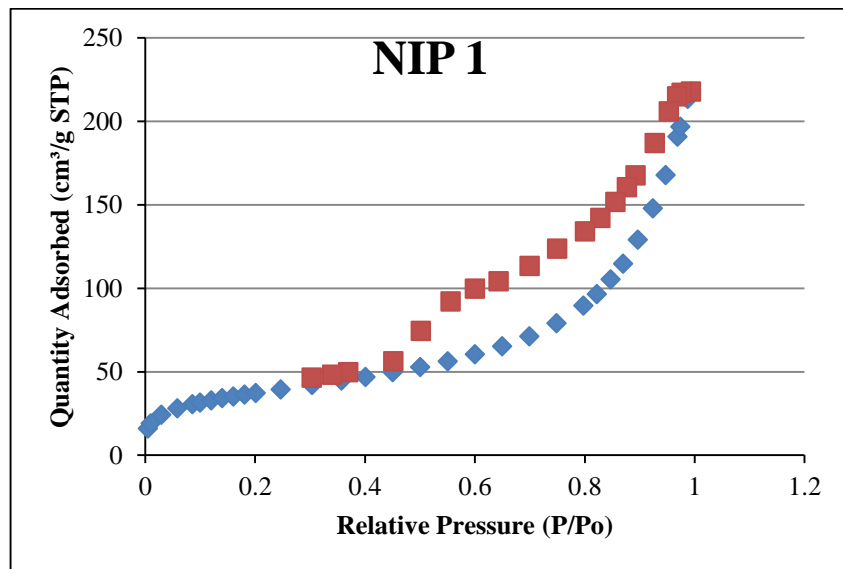


Figure 4.22 Linear isotherm plot of NIP 1.

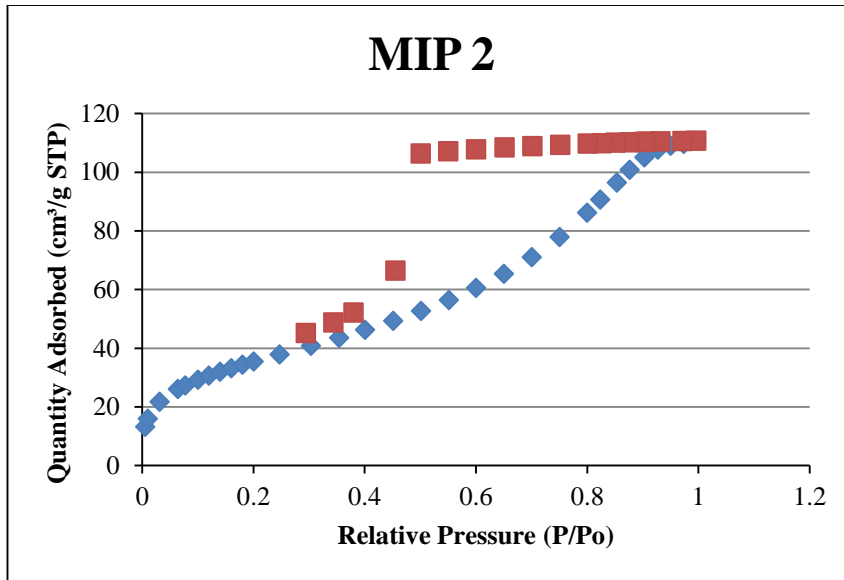


Figure 4.23 Linear isotherm plot of MIP 2.

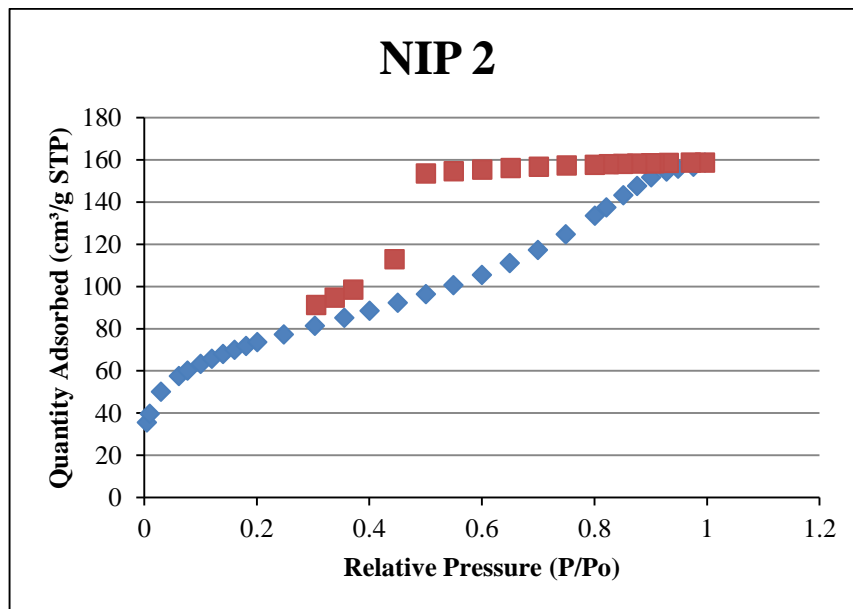


Figure 4.24 Linear isotherm plot of NIP 2.

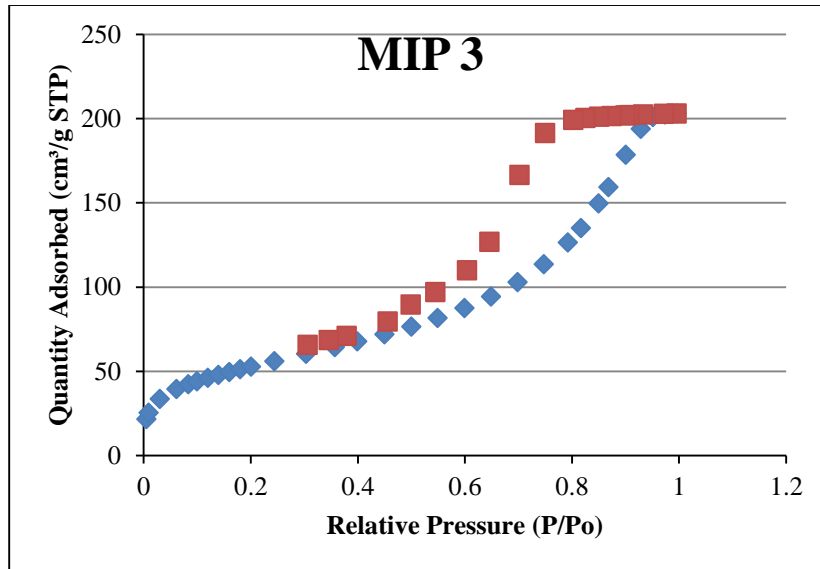


Figure 4.25 Linear isotherm plot of MIP 3.

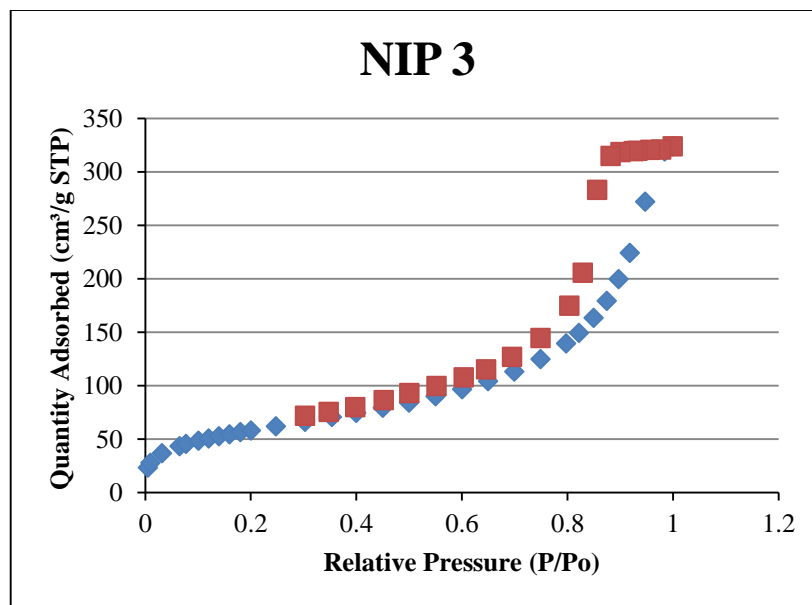


Figure 4.26 Linear isotherm plot of NIP 3.

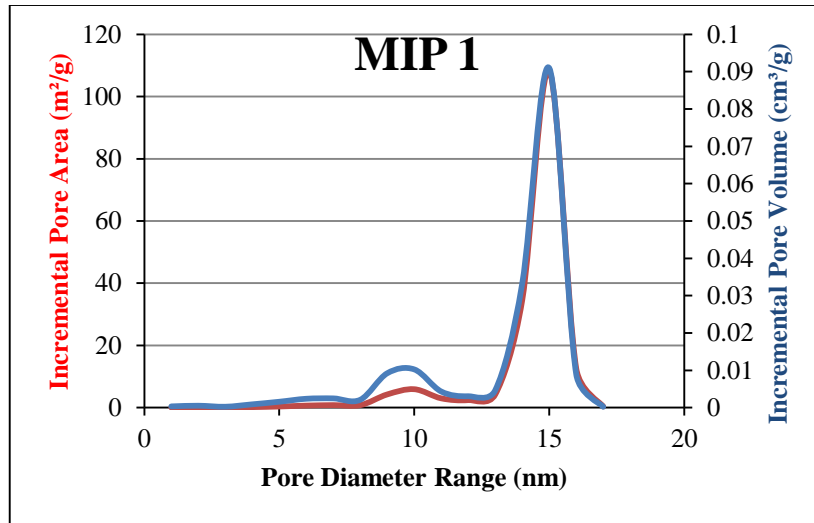


Figure 4.27 BJH Desorption pore distribution plot of MIP 1.

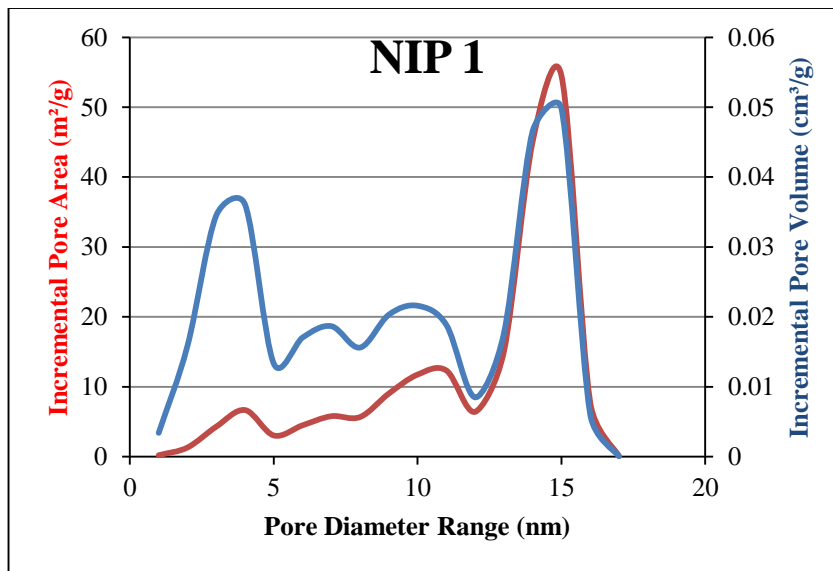


Figure 4.28 BJH Desorption pore distribution plot of NIP 1.

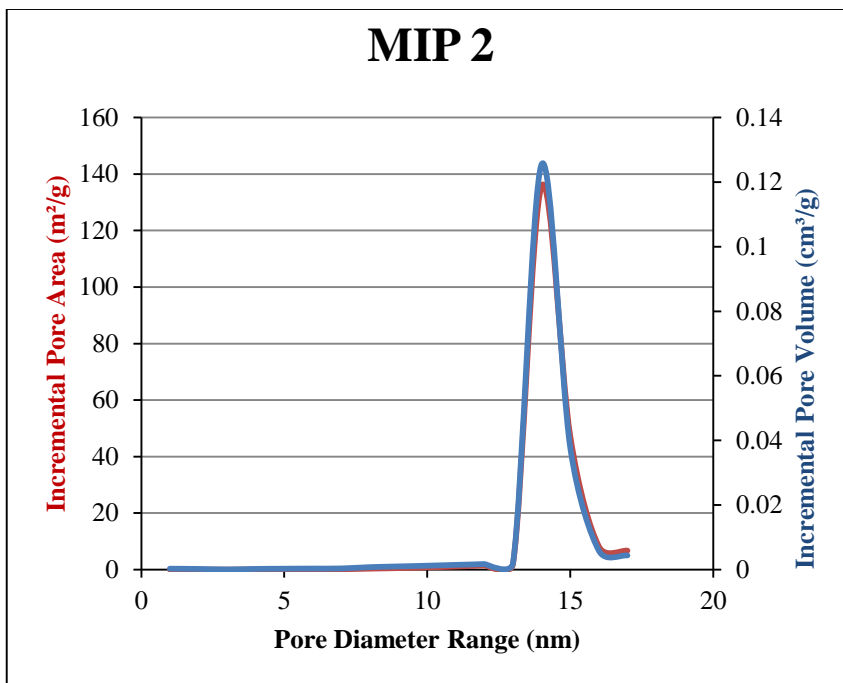


Figure 4.29 BJH Desorption pore distribution plot of MIP 2.

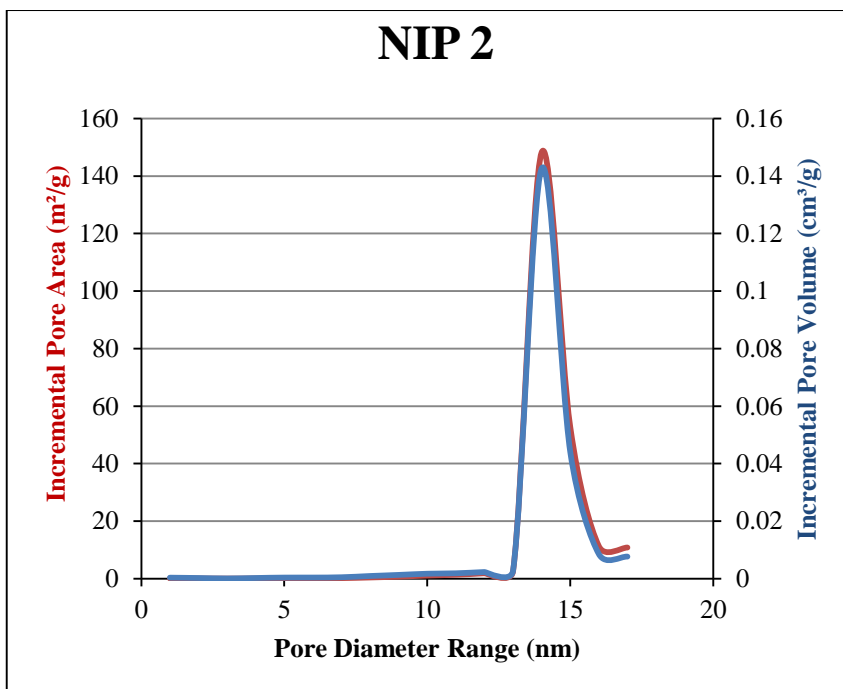


Figure 4.30 BJH Desorption pore distribution plot of NIP 2.

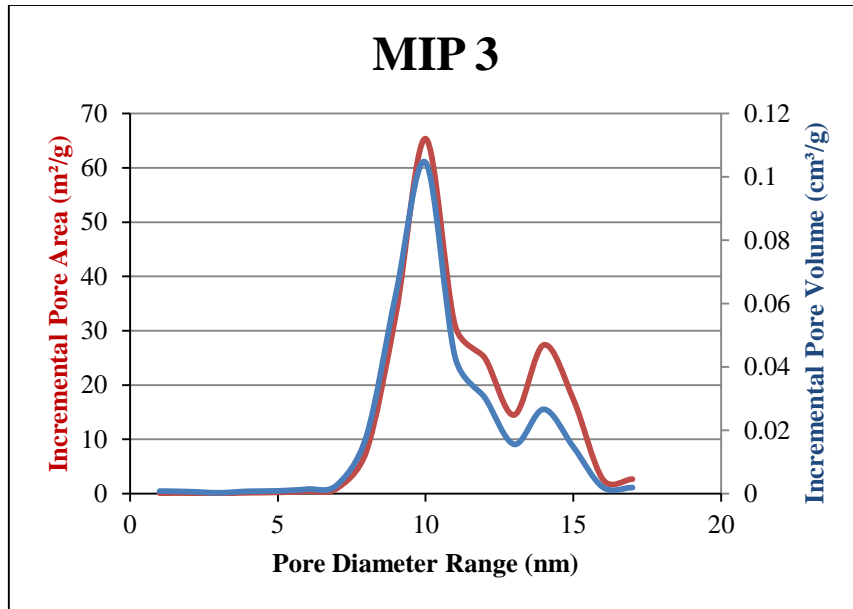


Figure 4.31 BJH Desorption pore distribution plot of MIP 3.

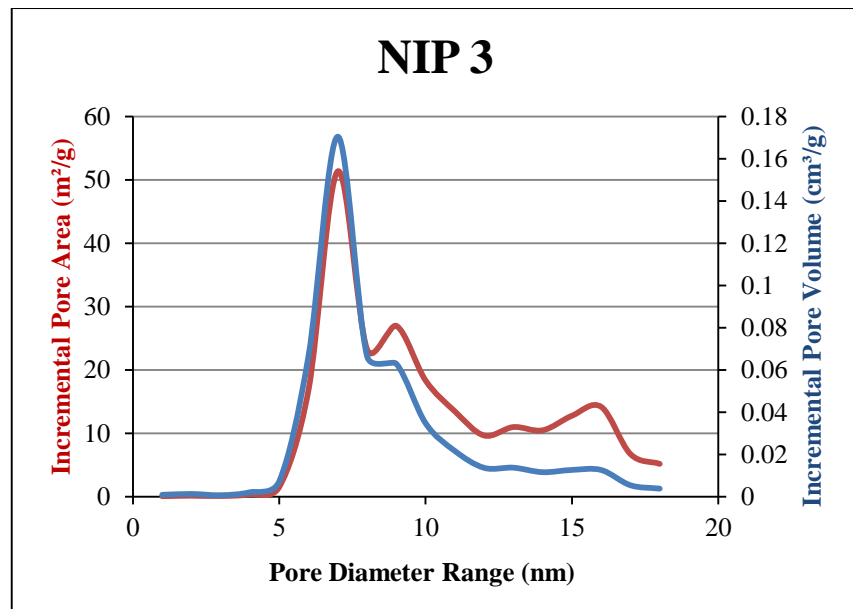


Figure 4.32 BJH Desorption pore distribution plot of NIP 3.

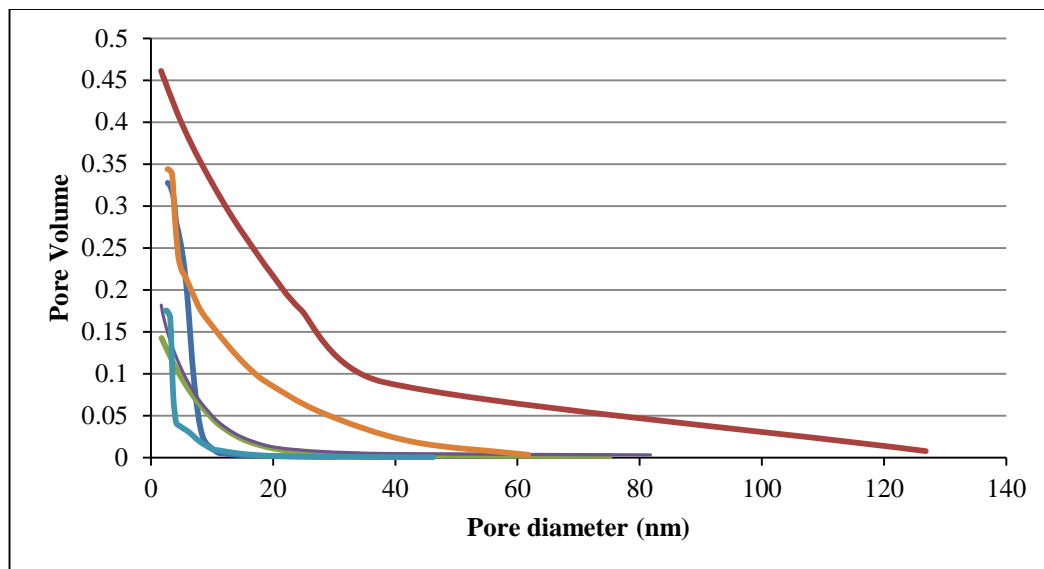


Figure 4.33 BJH desorption pore diameter volume distribution for MIP 1(aqua), NIP 1(orange), MIP 2(green), NIP 2(purple), MIP 3(blue), NIP 3(red).

Chapter 5

Conclusion and Future Perspectives

5. Conclusion and future outlook

5.1. Conclusion

This study aimed at studying a new aspect in the science of MIPs, which is the conformational stability of (MIP). To the best of our knowledge, this is the first study to address MIPs from this new perspective. The study also studied the influence of this feature on their binding capacities. Theoretical calculations were employed in order to study the conformational stability of the monomers (building blocks of these polymeric systems), and also to study the binding energies between the monomers and the template (glucose). A library of thirty monomers was constructed, they were selected based on their capabilities to interact with the role model template glucose. Then primary investigations were attempted, followed by secondary deep investigations.

The resulting calculations lead to the selection of the theoretically best two performing monomers in terms of high conformational stability and high template binding energies to be used in the synthesis of MIP.

MIPs and NIPs using the selected monomers were experimentally synthesized, and their binding capacities were measured in comparison to a control MIP (low conformational stability monomer). Interestingly the experimental results could validate that the conformational stability of the monomers can directly affect the creation of conformationally stable nanoscaled cavities that could retain their conformation throughout the detrimental events taking place during synthesis, extraction, and binding.

In addition, a thermal stability binding study was conducted in order to study the effects of high temperatures on the binding capacities of MIP. Interestingly MIP 3 showed the highest resistance towards changes in its binding capacity, however MIP 1 showed the lowest resistance towards changes in its binding capacity.

The final MIP systems together with their respective controls (non imprinted polymers NIP) were characterized by means of Fourier Transform Infra-Red Spectroscopy (FT-IR), Scanning Electron Microscopy (SEM), Thermogravimetric analysis (TGA), and porosity analysis (BET). (FT-IR) could show the significant differences in H-bond interactions between the

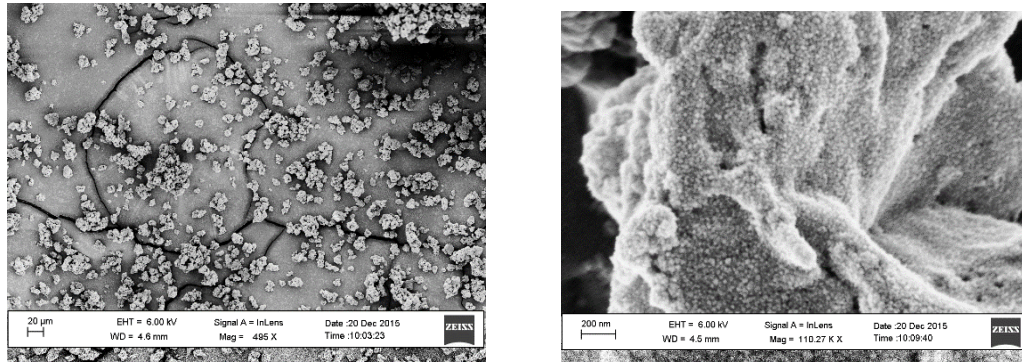
polymers before template removal and their respective MIPs or NIPs. SEM and BET could show the different pore distributions in both MIPs and NIPs, which was directly correlated to the template presence in MIPs. Finally TGA gave accurate information on the thermal degradability of the polymers, with MIP 3 and MIP 2 showing the highest resistance towards thermal degradation.

5.2. Future outlook

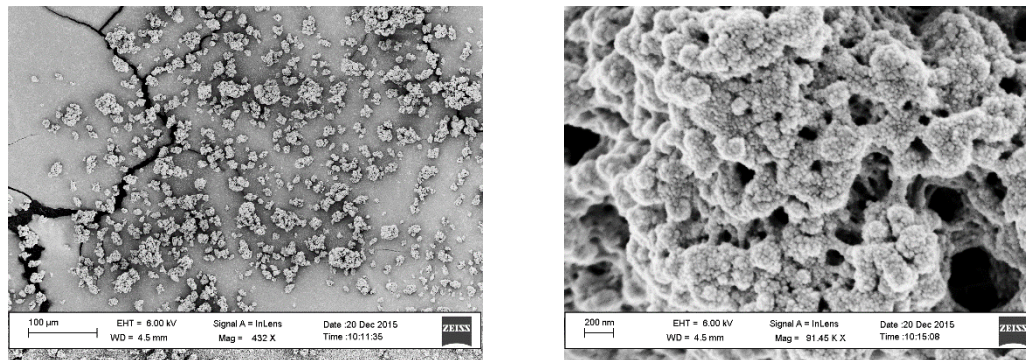
(MIP) are highly promising materials for a wide range of applications, such as biochemical sensing, food analysis, drug delivery and chromatography. Research has proven that such materials have superior specificity and selectivity over their (NIP) counterparts. They are highly stable, highly economic compared to enzymes and proteins (Most commonly employed in sensing applications), and they can be tailored to a big library of drugs and templates. However, they still suffer from some drawbacks that are hindering their commercial application widely. Research have outlined that these polymeric systems express a wide distribution of cavities and each differ in its selectivity towards the template. Such heterogeneity on the contrary is not commonly reported with biobased materials, such as enzymes and proteins. Thus some of the current research is directed towards the synthesis of MIPs as micro or nano particles, rather than bulk particles. Research have shown that micro or nano sized MIP particles exhibit higher external surface areas and consequently higher binding capacities and/or (IF) compared to their bulk counterparts. Synthesis of MIP particles in micro or nano ranges has the advantage that their sizes and porosities could be adequately homogenized during the course of their synthesis. This has a direct influence on controlling the high expression of a high density of selective cavities [56,57,58].

Thus, attempts in this study have been employed to investigate the potential synthesis of AA and BHPEA based MIP micro or nano particles. The resulting particles were highly promising in terms of their mechanical integrity and performance. *Figures 5.1-5.2* show SEM micrograph of the synthesized particles. It can be observed that the particles are randomly distributed over slightly consolidated particles (this could have taken place during the extraction process). Thus further work could be directed to investigate and optimize the synthesis of these polymeric

systems in micron or nano sizes, and to study of the effects of their sizes on their porosity distribution and binding capacities.



Figures 5.1 AA micro particles at low and high magnifications respectively.



Figures 5.2 BHPEA micro particles at low and high magnifications respectively.

6. References:

1. Zimmerman, S.; Lemcoff, G. Synthetic hosts *via* molecular imprinting—are universal synthetic antibodies realistically possible?. *Chem. Commun.*, **2004**, 5 – 14.
2. Byrne, M.; Oral, E.; Hilt, J.; Peppas, N. Networks for recognition of biomolecules: Molecular imprinting and micropatterning Poly (ethylene glycol)- containing films. *Poly. Adv. Technol.*, **2002**, 13, 798-816.
3. Yan, H.; Row, H. Characteristic and synthetic approach of molecularly imprinted polymer. *Int J Mol Sci*, **2006**, 7, 155-187.
4. Kempe, H. Advances in Separation Science: Molecular imprinting: development of spherical beads and optimization of the formulation by chemometrics. Doctoral Thesis, Stockholm University, Sweden, **2007**.
5. Ellwanger, A.; Berggren, C.; Bayouth, S.; Crecenzi, C.; Karlsson, L.; Owens, P.; Ensing, E.; Cormack, P.; Sherrington, D.; Sellergren, D. Evaluation of methods aimed at complete removal of template from molecularly imprinted polymers. *Analyst*, **2001**, 126, 784–792.
6. Lorenzo, R.; Carro, A.; Lorenzo, C.; Concheiro, A. To Remove or Not to Remove? The challenge of extracting the template to make the cavities available in molecularly imprinted polymers (MIPs). *Int. J. Mol. Sci.* **2011**, 12, 4327-4347.
7. Spivak, D.A. Optimization, evaluation, and characterization of molecularly imprinted polymers. *Adv Drug Deliv Rev.* **2005**, 57, 1779-1794.
8. Ersöz, A.; Denizli, A.; Özcan, A.; Say, R. Molecularly imprinted ligand-exchange recognition assay of glucose by quartz crystal microbalance. *Biosens Bioelectron.* **2005**, 20, 2197–2202.
9. Annamma, K.; Mathew, B. Design of 2,4-dichlorophenoxyacetic acid imprinted polymer with high specificity and selectivity. *Mater Sci Appl.* **2011**, 2, 131-140.
10. Algieri, C.; Drioli, E.; Guzzo, L.; Donato, L. Bio-Mimetic sensors based on molecularly imprinted membranes. *Sensors.* **2014**, 14, 13863-13912.
11. Sasaki, S.; Ooya, T.; Takeuchi, T. Highly selective bisphenol A—imprinted polymers prepared by atom transfer radical polymerization. *Polym Chem.* **2010**, 1, 1684–1688.
12. Suedee, R.; Seechamnaturakit, V.; Canyuk, B.; Ovatlarnporn, C.; Martin, G. Temperature sensitive dopamine-imprinted (N,N-methylene-bis-acrylamide cross-linked) polymer and its potential application to the selective extraction of adrenergic drugs from urine. *J Chromatogr A.* **2006**, 12, 1114(2), 239-49.
13. Simões, M.; Martins, N.; Cabrita, M.; Burke, A.; Garcia, R. Tailor-made molecularly imprinted polymers for dimethoate and deltamethrin recognition: synthesis, characterization and chromatographic evaluation. *J Polym Res.* **2014**, 21, 368.
14. Oral, E.; Peppas, N. Hydrophilic molecularly imprinted poly(hydroxyethyl-methacrylate) polymers. *J Biomed Mater Res A.* **2006**, 78(1), 205-210.
15. Sellergren, B.; Shea, K. Influence of polymer morphology on the ability of imprinted network polymers to resolve enantiomers. *J. Chromatogr.* **1993**, 635, 31-49.

16. Schmidt, R.; Belmont, A.; Haupt, K. Porogen formulations for obtaining molecularly imprinted polymers with optimized binding properties. *Anal Chim Acta*. **2005**, *542*, 118–124.
17. Al Kobaisi, M.; Tate, M.; Rix, C.; Jakubov, T.; Mainwaring, D. The effect of molecular imprinting on the pore size distribution of polymers. *Adsorption*. **2007**, *13*, 15–321.
18. Songa, X.; Wanga, J.; Zhuc, J. Effect of porogenic solvent on selective performance of molecularly imprinted polymer for quercetin. *J. Mater Res*. **2009**, *12*, 299–304.
19. Djourelou, N.; Ates, Z.; Güven, O.; Misheva, M.; Suzuki, T. Positron annihilation lifetime spectroscopy of molecularly imprinted hydroxyethyl methacrylate based polymers. *Polymer*. **2007**, *48*, 2692–2699.
20. Parmpi, P.; Kofinas, P. Biomimetic glucose recognition using molecularly imprinted polymer hydrogels. *Biomaterials*. **2004**, *25*, 1969–1973.
21. Singh, B.; Chauhan, N. Molecular imprinted polymers for use as drug delivery devices: preliminary evaluation. *J Macromol Sci A*. **2008**, *45*, 776–784.
22. Bodugoz, H.; Güven, O.; Peppas, N. glucose recognition capabilities of hydroxyethyl methacrylate-based hydrogels containing poly(ethylene glycol) chains. *J. Appl. Polym. Sci*. **2007**, *103*, 432–441.
23. Yang, Y.; Yi, C.; Luo, J.; Liu, R.; Liu, J.; Jiang, J.; Liu, X. Glucose sensors based on electrodeposition of molecularly imprinted polymeric micelles: A novel strategy for MIP sensors. *Biosen Bioelectron*. **2011**, *26*, 2607–2612.
24. Seong, H.; Lee, H.; Park, K. Glucose binding to molecularly imprinted polymers. *J. Biomater. Sci. Polymer Edn*. **2002**, *13*, 637–649.
25. Karim, K.; Breton, F.; Rouillon, R.; Piletska, E.; Guerreiro, A.; Chianella, I.; Piletsky, S. How to find effective functional monomers for effective molecularly imprinted polymers?. *Adv Drug Deliv Rev*. **2005**, *57*, 1795–1808.
26. Mayes, A.; Whitcombe, M. Synthetic strategies for the generation of molecularly imprinted organic polymers. *Adv Drug Deliv Rev*. **2005**, *57*, 1742–1778.
27. Benito-Pena, E.; Navarro-Villoslada, F.; Carrasco, S.; Jockusch, S.; Ottaviani, M.; Moreno-Bondi, M. Experimental mixture design as a tool for the synthesis of antimicrobial selective molecularly imprinted monodisperse microbeads. *ACS Appl. Mater. Interfaces* **2015**, *7*, 10966–10976.
28. Chianella, Lotierzo, M.; Piletsky, S.; Tothill, I.E.; Chen, B.N.; Karim, K.; Turner, A.P.F. Rational design of a polymer specific for microcystin-LR using a computational approach. *Anal. Chem*. **2002**, *74*, 1288–1293.
29. Khan, M.; Wate, P.; Krupadam, R. Combinatorial screening of polymer precursors for preparation of benzo[α] pyrene imprinted polymer: an ab initio computational approach. *J Mol Model*. **2012**, *18*, 1969–1981.
30. Li, X.; Zhong, S.; Chen, L.; Whittaker, A. Computer simulation and preparation of molecularly imprinted polymer membranes with chlorogenic acid as template. *Polym Int*. **2011**, *60*, 592–598.

31. Monti, S.; Cappelli, C.; Bronco, S.; Giusti, P.; Ciardelli, G. Towards the design of highly selective recognition sites into molecular imprinting polymers: A computational approach. *Biosens Bioelectron.* **2006**, *22*, 153–163.
32. Farrington, K. The design and characterisation of biomimetic artificial receptors based on molecular imprinting technology. Ph.D. Thesis, Dublin City University, **2007**.
33. Nicholls, I.; Andersson, H.; Golker, K.; Henschel, H.; Karlsson, B.; Olsson, G.; Rosengren, A.; Shoravi, S.; Suriyanarayanan, S.; Wiklander, J.; Wikman, S. Rational design of biomimetic molecularly imprinted materials: theoretical and computational strategies for guiding nanoscale structured polymer development. *Anal Bioanal Chem.* **2011**, *400*, 1771–1786.
34. Dourado, E.; Herdes, C.; Tassel, P.; Sarkisov, L. Molecular recognition effects in atomistic models of imprinted polymer. *Int. J. Mol. Sci.* **2011**, *12*, 4781–4804.
35. Karlsson, B.; O'Mahony, J.; Karlsson, J.; Bengtsson, H.; Eriksson, L.; Nicholls, I. Structure and dynamics of monomer-template complexation: an explanation for molecularly imprinted polymer recognition site heterogeneity. *J. Am. Chem. Soc.* **2009**, *131*, 13297–13304.
36. Chianella, I.; Karim, K.; Piletska, E.; Preston, C.; Piletsky, S.A. Computational design and synthesis of molecularly imprinted polymers with high binding capacity for pharmaceutical applications-model case: Adsorbent for abacavir. *Anal Chim Acta.* **2006**, *559*, 73-78.
37. Dourado, E. Computer simulations of adsorption and molecular recognition phenomena in molecularly imprinted polymers. Ph.D. Thesis, University of Edinburgh, **2011**.
38. Yañez, F.; Chianella, I.; Piletsky, S.; Concheiro, A.; Alvarez-Lorenzo, C. Computational modeling and molecular imprinting for the development of acrylic polymers with high affinity for bile salts. *Anal Chim Acta.* **2010**, *659*, 178-185.
39. Piletsky, S.; Karim, K.; Piletska, E.V.; Day, C.J.; Freebairn, K.W.; Legge, C.; Turner, A. P. F. Recognition of ephedrine enantiomers by molecularly imprinted polymers designed using a computational approach. *Analyst.* **2001**, *126*, 1826–1830.
40. Pavel, D.; Lagowski, J. Computationally designed polymers for molecular imprinting of theophylline and its derivatives - Part IV. *Adv Res Pol Sci.* **2006**, 115-131.
41. Pavel, D.; Lagowski, J. Computationally designed polymers for molecular imprinting of theophylline and its derivatives - Part I. *Polymer.* **2005**, *46*, 7528–7542.
42. Henthorn, D.; Peppas, N. Molecular simulations of cognitive behavior of molecularly imprinted intelligent polymeric networks. *Ind. Eng. Chem. Res.* **2007**, *46*, 6084-6091.
43. Oral, E.; Peppas, N. A. Responsive and cognitive hydrogels using star polymers. *J. Biomed. Mater. Res.* **2004**, *68A*, 439-447.
44. Oral, E.; Peppas, N. A. Dynamic studies of molecular imprinting polymerizations. *Polymer.* **2004**, *45*, 6163-6173.
45. Carraher, Charles E. *Polymer Chemistry*, 7th ed.; Taylor & Francis: Florida, **2007**.
46. Teraoka, I. *Polymer Solutions: An Introduction to Physical Properties*. John Wiley & Sons, Inc: New York, **2002**.

47. Rostamizadeh, K.; Abdollahi, H.; Parsajoo, C. Synthesis, optimization, and characterization of molecularly imprinted nanoparticles. *Int Nano Lett.* **2013**, *3*, 20-28.
48. Dubois, M.; Gilles, K.A.; Hamilton, J.K.; Rebers, P.A.; Smith, F. Colorimetric method for determination of sugars and related substances. *Anal. Chem.* **1956**, *28*(3), 350-356.
49. Kryscio, D.; Shi, Y.; Ren, P.; Peppas, N. Molecular docking simulations for macromolecularly imprinted polymers. *Ind Eng Chem Res.* **2011**, *50*(24), 13877-13884.
50. Nicholls, I.; Andersson, H.; Charlton, C.; Henschel, H.; Karlsson, B.; Karlsson, J.; O'Mahony, J.; Rosengren, A.; Rosengren, K.; Wikman, S. Theoretical and computational strategies for rational molecularly imprinted polymer design. *Biosens Bioelectron.* **2009**, *25*, 543-552.
51. Gunther, J.; Bergner, A.; Hendlich, M.; Klebe, J. Utilising structural knowledge in drug design strategies: applications using Relibase. *J Mol Biol.* **2003**, 326, 621.
52. Turner, N. W.; Piletska, E. V.; Karim, K.; Whitcombe, M.; Malecha, M.; Magan, N.; Baggiani, C.; Piletsky, S. Effect of the solvent on recognition properties of molecularly imprinted polymer specific for ochratoxin A. *Biosens Bioelectron.* **2004**, *20*, 1060.
53. Cela-Perez, M.C.; Lasagabaster-Latorre, A.; Abad-Lopez, M.J.; Lopez-Vilariño, J.M.; Gonzalez-Rodriguez, M.V. A study of competitive molecular interaction effects on imprinting of molecularly imprinted polymers. *Vibrational Spectroscopy.* **2013**, *65*, 74-83.
54. Holland, N.; Frisby, J.; Owens, E.; Hughes, H.; Duggan, P.; McLoughlin, P. The influence of polymer morphology on the performance of molecularly imprinted polymers. *Polymer*, **2010**, *51*, 1578-1584.
55. Kempe, H.; Pujolràs, A.; Kempe, M. Molecularly imprinted polymer nanocarriers for sustained release of erythromycin. *Pharm Res.* **2015**, *32*, 375-388.
56. Priego-Capote F.; Ye, L.; Shakil, S.; Shamsi, S.; Nilsson, S. Monoclonal behavior of molecularly imprinted polymer nanoparticles in capillary electrochromatography. *Anal Chem.* **2008**, *80*(8), 2881-2887.
57. Wulff, G.; Chong, B.; Kolb, U. Soluble single-molecule nanogels of controlled structure as a matrix for efficient artificial enzymes. *Angew. Chem. Int. Ed.* **2006**, *45*, 2955-2958.
58. Mirmohseni, A.; Shojaei, M.; Pourata, R. Experimental design and multi-objective optimization of molecularly imprinted polymers for monosaccharides. *RSC Adv.*, **2014**, *4*, 20177.